

C–H ACTIVATION BY A TUNGSTEN TRIMETHYLSILYLALLYL COMPLEX

by

Catherine Chow

B.Sc. (Hons), The University of British Columbia, 2009

A THESIS SUBMITTED IN PARTIAL FULFILLMENT OF
THE REQUIREMENTS FOR THE DEGREE OF

MASTER OF SCIENCE

in

THE FACULTY OF GRADUATE STUDIES

(Chemistry)

THE UNIVERSITY OF BRITISH COLUMBIA

(Vancouver)

July 2012

© Catherine Chow, 2012

Abstract

Thermolysis of $\text{Cp}^*\text{W}(\text{NO})(\text{Np})(\eta^3\text{-CH}_2\text{CHCHSiMe}_3)$ generates a 16-electron allene intermediate complex that selectively activates hydrocarbons at their methyl groups. In the case of linear alkanes, only terminal activation is observed. This selectivity persists in the presence of an ether functionality, but not of other oxygen-containing substrates such as aldehydes and alcohols. With these latter substrates, oxidation of the complex to $\text{Cp}^*\text{W}(\text{O})_2\text{Np}$ has been noted. The existence of the allene intermediate has been verified by two thermolytic experiments, and kinetic studies show that $\text{Cp}^*\text{W}(\text{NO})(\text{Np})(\eta^3\text{-CH}_2\text{CHCHSiMe}_3)$ is consumed according to pseudo-first-order kinetics during C–H bond activation. The neopentyl ligand can be functionalized by reaction with CO, and the resulting acyl complexes undergo chemical exchange on a slow timescale. The congeneric Mo complex has also been synthesized, and although this complex is equally capable of generating the η^2 -allene intermediate, its preferred mode of reactivity is coupling of the allyl and alkyl ligands. As a result, the Mo complex is inferior to the W system for C–H activation.

The thermolysis of $\text{Cp}^*\text{W}(\text{NO})(\text{Np})(\eta^3\text{-CH}_2\text{CHCHSiMe}_3)$ in benzene has been studied since the major products of this reaction each contain a 1,3-disubstituted allyl ligand which might reduce reactivity at the allyl ligand in subsequent chemistry. In thermolytic conditions, the resulting disubstituted allyl hydride complex undergoes no apparent reaction with alkanes, but with deuterobenzene, deuterium incorporation into the allyl ligand is observed. In addition to H/D exchange, the hydride ligands in these complexes can also

migrate onto the allyl ligand, forming an η^2 -olefin complex that can be trapped as the pyridine adduct.

The activation of fluorobenzenes by $\text{Cp}^*\text{W}(\text{NO})(\text{Np})(\eta^3\text{-CH}_2\text{CHCHSiMe}_3)$ was also studied, and in these substrates, exclusive activation of the C–H bond is observed. Migration of the newly formed aryl ligands onto the allyl ligand does not occur when there is a fluorine atom in the *ortho* position, which is probably due to the reduced nucleophilicity of the ligand relative to the unfluorinated phenyl ligand. Selectivity in the activation of C–H bonds in fluorobenzenes appears to be determined by sterics.

Preface

Some of the results presented in this thesis are the result of collaboration with other researchers. Collection, solution, and refinement of X-ray diffraction data for most solid-state molecular structures in this thesis was done primarily by the author (Catherine Chow) with the assistance of Dr. Michelle Thibault and Dr. Brian Patrick. The solution of the solid-state molecular structures of **3.1b** and **4.3** was done primarily by Dr. Brian Patrick.

Table of Contents

Abstract.....	ii
Preface.....	iv
Table of Contents	v
List of Tables	x
List of Figures.....	xi
List of Schemes.....	xiv
List of Abbreviations	xvi
Acknowledgements	xx
Dedication	xxii
Chapter 1: Introduction	1
1.1 C–H bond activation and functionalization	1
1.1.1 Historical perspective on C–H activation	3
1.1.2 Mechanisms and examples of C–H activation.....	4
1.1.3 C–H functionalization.....	6
1.2 Cp*W(NO)(alkyl)(η^3 -allyl) systems for C–H activation.....	6
1.3 Motivation.....	9
1.4 Scope of this thesis.....	10
1.5 Format of this thesis.....	10
1.5.1 Allyl nomenclature.....	11
1.6 General experimental procedures	11
Chapter 2: Chemistry of Cp*W(NO)(Np)(η^3-CH₂CHCHSiMe₃).....	14

2.1	Introduction	14
2.2	Results and discussion	14
2.2.1	Synthesis of $\text{Cp}^*\text{W}(\text{NO})(\text{Np})(\eta^3\text{-CH}_2\text{CHCHSiMe}_3)$	14
2.2.2	C–H activation	20
2.2.2.1	Alkanes	20
2.2.2.2	Arenes	24
2.2.2.3	Other functional groups	25
2.2.3	Mechanistic studies	27
2.2.3.1	Reaction with PMe_3	28
2.2.3.2	Reaction with cyclohexene	32
2.2.3.3	Kinetics of C–H activation by 2.1	35
2.2.4	Carbonylation of $\text{Cp}^*\text{W}(\text{NO})(\text{Np})(\eta^3\text{-CH}_2\text{CHCHSiMe}_3)$	39
2.2.5	Congeneric Mo system	47
2.2.5.1	Synthesis and structure of $\text{Cp}^*\text{Mo}(\text{NO})(\text{Np})(\eta^3\text{-CH}_2\text{CHCHSiMe}_3)$	48
2.2.5.2	Trapping experiment: PMe_3	50
2.2.5.3	Thermolysis of 2.12 in benzene	52
2.2.5.4	Thermolysis of 2.12 in other solvents	54
2.2.5.5	Investigation into the reaction pathways of 2.12	55
2.2.5.6	Attempted derivatization with CO	59
2.3	Experimental procedures	60
2.3.1	Preparation of $\text{Cp}^*\text{W}(\text{NO})(\text{Np})(\eta^3\text{-CH}_2\text{CHCHSiMe}_3)$ (2.1).	60
2.3.2	Preparation of $\text{Cp}^*\text{W}(\text{NO})((\text{CH}_2)_4\text{CH}_3)(\eta^3\text{-CH}_2\text{CHCHSiMe}_3)$ (2.2).	61
2.3.3	Preparation of $\text{Cp}^*\text{W}(\text{NO})(\eta^3\text{-CH}_2\text{CHCHSiMe}_3)(\text{CH}_2\text{Cy})$ (2.3).	62

2.3.4	Competition study for the activation of pentane and cyclohexane by 2.1.	62
2.3.5	Preparation of $\text{Cp}^*\text{W}(\text{NO})(\text{Me})(\eta^3\text{-CH}_2\text{CHCHSiMe}_3)$ (2.4).	63
2.3.6	Preparation of $\text{Cp}^*\text{W}(\text{NO})(\text{Et})(\eta^3\text{-CH}_2\text{CHCHSiMe}_3)$ (2.5).	63
2.3.7	Preparation of $\text{Cp}^*\text{W}(\text{NO})(\text{CH}_2\text{-3,5-Me}_2\text{C}_6\text{H}_3)(\eta^3\text{-CH}_2\text{CHCHSiMe}_3)$ (2.6)..	64
2.3.8	Preparation of $\text{Cp}^*\text{W}(\text{NO})(\text{CH}_2\text{SiMe}_3)(\eta^3\text{-CH}_2\text{CHCHSiMe}_3)$ (2.7).	65
2.3.9	Preparation of $\text{Cp}^*\text{W}(\text{NO})(\text{CH}_2\text{CH}_2\text{OCH}_2\text{CH}_3)(\eta^3\text{-CH}_2\text{CHCHSiMe}_3)$ (2.8). 65	
2.3.10	Thermolyses of 2.1 in <i>n</i> PrOH and 1-butyraldehyde.	66
2.3.11	Preparation of $\text{Cp}^*\text{W}(\text{NO})(\text{PMe}_3)(\eta^2\text{-CH}_2=\text{C}=\text{CHSiMe}_3)$ (2.9).	66
2.3.12	Preparation of $\text{Cp}^*\text{W}(\text{NO})(\text{H})(\eta^3\text{-CH}_2\text{C(3-cyclohexenyl)CHSiMe}_3)$ (2.10)..	67
2.3.13	Monitoring the thermolytic consumption of 2.1 by ^1H NMR spectroscopy...	68
2.3.14	Attempted carbonylation of 2.2.	68
2.3.15	Preparation of $\text{Cp}^*\text{W}(\text{NO})(\eta^1\text{-C(=O)Np})(\eta^3\text{-CH}_2\text{CHCHSiMe}_3)$ (2.11).	69
2.3.16	Monitoring the conversion of 2.1 to 2.11 by ^1H NMR spectroscopy.	70
2.3.17	Preparation of $\text{Cp}^*\text{Mo}(\text{NO})(\text{Np})(\eta^3\text{-CH}_2\text{CHCHSiMe}_3)$ (2.12).	70
2.3.18	Preparation of $\text{Cp}^*\text{Mo}(\text{NO})(\eta^2\text{-CH}_2=\text{C}=\text{CHSiMe}_3)(\text{PMe}_3)$ (2.13).	71
2.3.19	Thermolysis of 2.12 in benzene.	72
2.3.20	Monitoring the thermolytic consumption of 2.12 by ^1H NMR spectroscopy. 72	
2.3.21	X-ray crystallography	73
Chapter 3: Chemistry of $\text{Cp}^*\text{W}(\text{NO})(\eta^3\text{-Me}_3\text{SiCHCHCHPh})(\text{H})$.....		76
3.1	Introduction.....	76
3.2	Results and discussion	77
3.2.1	Attempts to synthesize $\text{Cp}^*\text{W}(\text{NO})(\text{Np})(\eta^3\text{-1,3-(SiMe}_3)_2\text{C}_3\text{H}_3)$	77
3.2.2	The $\text{Cp}^*\text{W}(\text{NO})(\eta^3\text{-Me}_3\text{SiCHCHCHPh})(\text{H})$ system	77

3.2.2.1	Synthesis and structure of $\text{Cp}^*\text{W}(\text{NO})(\eta^3\text{-Me}_3\text{SiCHCHCHPh})(\text{H})$	77
3.2.2.2	Formation of $\text{Cp}^*\text{W}(\text{NO})(\text{H})(\eta^3\text{-CH}_2\text{CHC}(\text{SiMe}_3)\text{Ph})$	87
3.2.2.3	Thermolysis of other $\text{Cp}^*\text{W}(\text{NO})(\eta^3\text{-CH}_2\text{CHCHSiMe}_3)(\text{R})$ complexes	88
3.2.3	Reactivity of $\text{Cp}^*\text{W}(\text{NO})(\eta^3\text{-Me}_3\text{SiCHCHCHPh})(\text{H})$	89
3.2.3.1	Reaction with PMe_3	89
3.2.3.2	Reaction with pyridine	90
3.2.3.3	Reaction with deuterobenzene	92
3.2.3.4	Thermolysis of 3.1 in alkanes	98
3.3	Experimental procedures	99
3.3.1	Preparation of $\text{Cp}^*\text{W}(\text{NO})(\text{H})(\eta^3\text{-Me}_3\text{SiCHCHCHPh})$ (3.1).	99
3.3.2	Extended thermolysis of 2.7	100
3.3.3	Extended thermolysis of 2.6	101
3.3.4	Thermolysis of 3.1 in PMe_3	101
3.3.5	Preparation of $\text{Cp}^*\text{W}(\text{NO})(\eta^2\text{-PhCH=CHCH}_2\text{SiMe}_3)(\text{py})$ (3.2).....	101
3.3.6	Thermolysis of 3.1 in C_6D_6	102
3.3.7	Thermolysis of 3.1 in C_6D_6 and pyridine.....	102
3.3.8	Thermolysis of 3.1 in C_6D_{12}	103
3.3.9	X-ray crystallography	103
Chapter 4: Reactivity of $\text{Cp}^*\text{W}(\text{NO})(\text{Np})(\eta^3\text{-CH}_2\text{CHCHSiMe}_3)$ with Fluorobenzenes		
.....		105
4.1	Introduction.....	105
4.2	Results and discussion	105
4.2.1	Introduction of C_6F_5 groups	105

4.2.2	Reactions of $\text{Cp}^*\text{W}(\text{NO})(\text{Np})(\eta^3\text{-CH}_2\text{CHCHSiMe}_3)$ with fluorobenzenes ..	107
4.2.2.1	Pentafluorobenzene	107
4.2.2.2	<i>p</i> -Difluorobenzene	110
4.2.2.3	<i>o</i> -Difluorobenzene	115
4.3	Experimental procedures	120
4.3.1	Preparation of $\text{Cp}^*\text{W}(\text{NO})(\text{C}_6\text{F}_5)(\eta^3\text{-CH}_2\text{CHCHSiMe}_3)$ (4.1).....	120
4.3.2	Preparation of $\text{Cp}^*\text{W}(\text{NO})(2,5\text{-F}_2\text{C}_6\text{H}_3)(\eta^3\text{-CH}_2\text{CHCHSiMe}_3)$ (4.2).	121
4.3.3	Thermolysis of 4.2.	121
4.3.4	Thermolysis of 2.1 in <i>o</i> -difluorobenzene.....	122
4.3.5	X-ray crystallography	123
Chapter 5: Conclusion		125
5.1	Summary of thesis work	125
5.2	Future work.....	127
References.....		129
Appendix.....		134
Appendix A X-ray crystallographic data		134

List of Tables

Table 2.1. Rate constants for the loss of 2.1 during thermolysis in C ₆ D ₆	37
Table 2.2. Selected ¹ H NMR data for the products of C ₆ H ₆ activation by 2.12	53
Table 2.3. Selected ¹ H NMR signals from the products of the thermolysis of 2.12 in pentane.	55
Table 2.4. Comparison of the rate constants for the consumption of 2.12 under thermolytic conditions.....	57
Table 2.5. Comparison of the Eyring parameters for the thermolysis of 2.12 in C ₆ D ₆ and C ₆ D ₁₂	59
Table 3.1. Comparison of solid-state structural and solution spectroscopic properties of 3.1a and 3.1b	85
Table 3.2. ³¹ P NMR spectroscopic data for the product mixture arising from thermolysis of 3.1a and 3.1b in PMe ₃	90
Table 4.1. ¹ H NMR chemical shifts and coupling constants of selected signals from the mixture of products arising from the thermolysis of 2.1 in <i>o</i> -difluorobenzene.....	115

List of Figures

Figure 1.1. Oxidative addition of C–H bonds to metal centres includes both (a) σ -donation from ligand to metal and (b) π backdonation from metal to ligand.	4
Figure 1.2. σ -Bond metathesis.	5
Figure 1.3. Generic σ -CAM mechanism.	5
Figure 1.4. Graphical representation of allyl nomenclature used in this thesis.	11
Figure 2.1. Solid-state molecular structure of 2.1 with 50% probability thermal ellipsoids.	17
Figure 2.2. Expansion of the ^{13}C APT NMR spectrum of complex 2.2 (400 MHz, C_6D_6). ..	22
Figure 2.3. Expansion of the $^{31}\text{P}\{^1\text{H}\}$ NMR (121 MHz, C_6D_6) spectrum of complex 2.9 (and minor product).	29
Figure 2.4. Solid-state molecular structure of 2.9 with 50% probability thermal ellipsoids.	30
Figure 2.5. Solid-state molecular structure of 2.10 with 50% probability thermal ellipsoids.	33
Figure 2.6. Monitoring loss of starting material through integration of the area under the peak at 1.30 ppm (Np Me) during the thermolysis of 2.1 in C_6D_6 by ^1H NMR spectroscopy at 75 °C.	35
Figure 2.7. First-order kinetics plot of the consumption of 2.1 when heated at 75 °C in C_6D_6	36
Figure 2.8. Eyring plot for the thermolysis of 2.1 in C_6D_6	37
Figure 2.9. Arrhenius plot of the thermolysis of 1.1 in C_6D_6	39
Figure 2.10. Solid-state molecular structure of one isomer of 2.11 with 50% probability thermal ellipsoids.	42

Figure 2.11. Stack plot of an expansion (3.80 to 5.35 ppm) of the ^1H NMR spectrum (300 MHz, C_6D_6) during the course of carbonylation of 2.1 to form 2.11	45
Figure 2.12. Expansions of the ROESY spectrum (600 MHz, C_6D_6) of 2.11 , focusing on the cross-peaks of the signal at 3.90 ppm between 2.5 and 5.5 ppm on the F1 axis.	47
Figure 2.13. Solid-state molecular structure of 2.12 with 50% probability thermal ellipsoids.	49
Figure 2.14. Solid-state molecular structure of 2.13 with 50% probability thermal ellipsoids.	51
Figure 2.15. First-order kinetic plot of the thermolysis of 2.12 in C_6D_6 at 45 °C.	56
Figure 2.16. Monitoring loss of starting material and product formation during the thermolysis of 2.12 in C_6D_6 by ^1H NMR spectroscopy.	58
Figure 3.1. ^1H NMR spectrum (300 MHz) of the final reaction mixture of 2.1 thermolyzed in C_6D_6	80
Figure 3.2. Product distribution during the thermolysis of 2.1 in C_6D_6 at 75 °C as monitored by ^1H NMR spectroscopy.	82
Figure 3.3. Solid-state molecular structure of 3.1a with 50% probability thermal ellipsoids.	83
Figure 3.4. Solid-state molecular structure of 3.1b with 50% probability thermal ellipsoids.	84
Figure 3.5. Possible products arising from the thermolysis of 3.1 in PMe_3	90
Figure 3.6. Expansion (−1.5 to +6.0 ppm) of the ^1H NMR spectrum (300 MHz) of 3.1 thermolyzed in C_6D_6 (2 d, 75 °C) with ten equivalents of pyridine demonstrating deuterium incorporation on the <i>meso</i> proton of the allyl ligand.	95

Figure 3.7. Comparison of the M^+ peaks for the product of the reaction of **3.1** in a) neat pyridine; b) pyridine and C_6D_6 ; c) neat C_6D_6 . The M^+ peak of **3.1** is found at m/z 539 (^{184}W).

..... 96

Figure 4.1. Solid-state molecular structure of **4.1** with 50% probability thermal ellipsoids.

..... 108

Figure 4.2. Expansion (4.1 to 5.1 ppm) of the 1H NMR spectrum (300 MHz, C_6D_6) of the products of the thermolysis of **2.1** in *p*-difluorobenzene. 111

Figure 4.3. Solid-state molecular structure of one of the isomers of complex **4.2** with 50% probability thermal ellipsoids. 113

Figure 4.4. Solid-state molecular structure of **4.3** with 50% probability ellipsoids. 117

List of Schemes

Scheme 1.1. Alkane activation by $\text{Cp}^*\text{Ir}(\text{PMe}_3)(\text{H})_2$.	3
Scheme 1.2. Reactivity of $\text{Cp}^*\text{W}(\text{NO})(\text{Np})(\eta^3\text{-CH}_2\text{CHCMe}_2)$.	7
Scheme 1.3. Reactivity of $\text{Cp}^*\text{W}(\text{NO})(\text{Np})(\eta^3\text{-CH}_2\text{CHCHMe})$.	8
Scheme 1.4. Reactivity of $\text{Cp}^*\text{W}(\text{NO})(\text{Np})(\eta^3\text{-CH}_2\text{CHCHPh})$.	9
Scheme 2.1. Synthesis of 2.1 .	15
Scheme 2.2. Activation of alkanes by 2.1 .	21
Scheme 2.3. Activation of gaseous alkanes by 2.1 .	24
Scheme 2.4. Activation of tetramethylsilane by 2.1 .	26
Scheme 2.5. Activation of diethyl ether by 2.1 .	26
Scheme 2.6. Attempted activation of aldehydes and alcohol by 2.1 .	27
Scheme 2.7. General mechanism for C–H activation by 2.1 .	27
Scheme 2.8. Formation of the PMe_3 adduct of the 16e intermediate responsible for C–H activation by 2.1 .	28
Scheme 2.9. Rationalization for allyl isomerization after C–H activation by 2.1 .	32
Scheme 2.10. Mechanism for the formation of 2.10 .	34
Scheme 2.11. Carbonylation of 2.1 .	41
Scheme 2.12. Mechanism for the <i>endo</i> , <i>syn</i> to <i>exo</i> , <i>anti</i> shift of the allyl ligand during the carbonylation of 2.1 .	44
Scheme 2.13. Reactivity of various $\text{Cp}^*\text{Mo}(\text{NO})(\text{alkyl})(\eta^3\text{-allyl})$ systems.	48
Scheme 2.14. Selected products of benzene activation by 2.12 .	53
Scheme 2.15. Proposed products for the thermolysis of 2.12 in pentane.	54

Scheme 3.1. Proposed C–H activation chemistry by complexes containing 1,3-disubstituted allyl ligands.	76
Scheme 3.2. Reaction of 2.1 in benzene.	78
Scheme 3.3. Reaction of 3.1a and 3.1b in pyridine.	91
Scheme 3.4. Reactivity of 3.1b with deuterobenzene and pyridine.	93
Scheme 3.5. Proposed mechanism for deuterium incorporation into 3.1b	98
Scheme 4.1. Activation of pentafluorobenzene by 2.1	107
Scheme 4.2. Activation of <i>p</i> -C ₆ F ₂ H ₄ by 2.1	112
Scheme 4.3. C–H activation of <i>o</i> -C ₆ F ₂ H ₄ by 2.1	116

List of Abbreviations

\ddagger	transition state
α	the position once removed from a reference point
β	the position twice removed from a reference point
ϵ	molar absorptivity coefficient
Δ	heat
η	ligand hapticity
ν	stretching frequency
\AA	angstrom, 10^{-10} m
abs	absorption
Anal.	analysis
APT	attached proton test
arb. units	arbitrary units
br	broad
Calcd.	calculated
coeff	coefficient
COSY	correlation spectroscopy
Cp	cyclopentadienyl, C_5H_5^-
Cp*	pentamethylcyclopentadienyl, C_5Me_5^-
cryst	crystal
Cy	cyclohexyl, C_6H_{11}
d	doublet (spectral); days (time)

D, <i>d</i>	deuterium, ^2H
DFT	density functional theory
diff.	diffraction
diTMS	bis(trimethylsilyl)allyl; $(\text{Me}_3\text{Si})_2\text{C}_3\text{H}_3$
e	electron
Et	ethyl; CH_3CH_2
FT	Fourier transform
<i>G</i>	Gibbs free energy
h	hours
<i>H</i>	enthalpy
$\{^1\text{H}\}$	proton-decoupled
hν	light energy
HMBC	heteronuclear multiple bond correlation
HREI	high-resolution electron impact
HSQC	heteronuclear single quantum coherence
IR	infrared
$^nJ_{\text{AB}}$	scalar coupling constant (Hz) between atoms A and B, <i>n</i> bonds apart
<i>k</i>	rate constant
LREI	low-resolution electron impact
m	multiplet or medium (spectral)
M	molarity; mol L^{-1}
M^+	parent molecular ion
<i>m/z</i>	mass-to-charge ratio

Me	methyl; CH ₃
measd	measured
min	minutes
MS	mass spectrometry
<i>n</i> Bu	<i>n</i> -butyl; CH ₃ CH ₂ CH ₂ CH ₂
NMR	nuclear magnetic resonance
NOE	nuclear Overhauser effect
Np	neopentyl; CH ₂ CMe ₃
<i>o</i>	<i>ortho</i>
ORTEP	Oak Ridge Thermal Ellipsoid Program
<i>p</i>	<i>para</i>
Ph	phenyl, C ₆ H ₅
ppm	parts per million
psig	pounds per square inch (gauge)
py	pyridine, C ₅ H ₅ N
reflns	reflections
ROE	rotating frame nuclear Overhauser effect
ROESY	rotating frame nuclear Overhauser effect spectroscopy
RT	room temperature
<i>S</i>	entropy
s	singlet or strong (spectral); seconds (time)
t	triplet (spectral); time
<i>t</i> Bu	<i>tert</i> -butyl; CMe ₃

THF	tetrahydrofuran
TMEDA	<i>N,N,N',N'</i> -tetramethylethylenediamine, $\text{Me}_2\text{NCH}_2\text{CH}_2\text{NMe}_2$
Tp	hydrido trispyrazoylborate
UV/Vis	ultraviolet/visible
XRD	x-ray diffraction
xs	excess

Acknowledgements

My gratitude to those I wish to thank for their support and aid throughout the course of this thesis work cannot be adequately expressed by the written word, so I can only hope this small token reflects the depth of my sentiments.

Professor Peter Legzdins has been the best chemical father I could have asked for, right from the time I was a fresh-faced, dewy-eyed, knee-high-to-a-grasshopper undergraduate asking to join his group for the summer term. Four years later, I'm getting ready to spread my wings and leave the nest for good, and I will always be grateful for his guidance and wisdom, which have led me to this point.

To Legzdins group members, past and present: thank you. Rhett Baillie, for your sharp mind and sharper NMR skills. Monica Shree, for your super friendship, your tea, and the East Van classiness you brought to the lab. Travis Nagle, for your fabulousness and fastidiousness. Kaity Lalonde, for your laughter and cheer. Tommy Tran, for showing me being a cowboy wasn't just about style. Dr. Michelle Thibault, for knowing everything, even when you said you didn't. Shawn Postle, for getting stuff off the top shelf and reminding me to have a snack once in a while.

Our various Dow collaborators have been immensely helpful as well as generous with their time and resources. It has been a pleasure to work with them. Thank you to Drs. Bill Tenn, David Graf, Peter Nickias, Brandon Rodriguez, and Devon Rosenfeld.

The technical staff at UBC have much of my gratitude for their aid in the preparation of this thesis, in particular Marshall Lapawa of the microanalytical facility and Dr. Brian

Patrick of the X-ray crystallography lab. Thank you all for having patience with my many, many questions and getting me out of some tight spots.

Finally, I extend my heartfelt thanks to my family and friends for continuing with me on this journey through graduate school. Your inexhaustible love, support, and care have seen me through to the end.

„Sie sind so jung, so vor allem Anfang, und ich möchte Sie, so gut ich es kann, bitten, lieber Herr, Geduld zu haben gegen alles Ungelöste in Ihrem Herzen und zu versuchen, die Fragen selbst liebzuhaben wie verschlossene Stuben und wie Bücher, die in einer sehr fremden Sprache geschrieben sind.“ – Rainer Maria Rilke, Briefe an einen jungen Dichter

“You are so young, so much before all beginning, and I would like to beg you, dear Sir, as well as I can, to have patience with everything unresolved in your heart and to try to love the questions themselves as if they were locked rooms or books written in a very foreign language.” (trans. Stephen Mitchell)

to my parents Jack and Diana, and my little brother Michael

Chapter 1: Introduction

The use of transition metals for the activation of small molecules is almost as ubiquitous as the small molecules themselves. Nitrogen fixation represents a prime example. Although dinitrogen makes up over 78% of the Earth's atmosphere, the incorporation of nitrogen from this source into fine chemicals remains an extremely difficult task. This is due in no small part to the strength of the N–N triple bond. Without transition metals (e.g, the Mo/Fe combination in many nitrogenases, or the Fe or Ru catalyst in Haber-Bosch processes), this transformation would not be possible.¹ Interest in the activation of this and other small molecules (CO, CO₂, CH₄, *inter alia*) is a rapidly-expanding field. As in the example of nitrogen activation, these questions are interesting not only from a fundamental perspective, but also have the potential to revolutionize current industrial processes for the manufacture of chemicals.

The work in this thesis is concerned with the activation of C–H bonds, in particular those of alkanes, by a tungsten trimethylsilylallyl complex.

1.1 C–H bond activation and functionalization

C–H activation, in the most general sense, is the cleavage of a carbon–hydrogen bond. C–H bonds are considered relatively inert, and introduction of functionality is a desirable goal for the synthesis of both fine and industrial chemicals.² However, traditional methods for introducing functionality into aliphatic substrates often involve forcing conditions such as radical chemistry, which lead to low selectivity and mixtures of products.³ Selectivity in the activation of C–H bonds is much sought-after, especially for linear alkanes,

in which functionalization at the terminal position to form derivatives such as alcohols or aldehydes is of particular interest. Thus, organometallic systems have been the subject of much study, as the reactions they facilitate are often regioselective. Additionally, such systems are often able to tolerate the presence of other functional groups in the molecule, reducing the need for additional steps in protecting and deprotecting reactive sites. Finally, the use of homogeneous catalysts can afford precise knowledge of the mechanism of the transformation, which is not always possible for heterogeneous catalysts. If the mechanism of the transformation is known, then the rational design of a catalyst becomes a much more viable goal. Organometallic catalysts are already used in many transformations, ranging from the palladium catalysts used on the bench for cross-coupling reactions⁴ to the iridium catalysts used in the large-scale production of acetic acid.⁵

C–H activation represents the first step in the more ambitious goal of C–H functionalization, which is important to investigate as the world’s supply of easily accessible heavy petrochemicals continues to dwindle. C–H functionalization offers the possibility of elaborating light alkanes into longer-chain products, which could lead to their incorporation into industrial feedstocks, ultimately facilitating a more efficient exploitation of this resource. Functionalization of gaseous alkanes such as methane and ethane may also reduce the inconvenience and hazards of moving large quantities of gas from remote gas fields to their destinations by transforming these gases into liquids.^{6, 7} However, the efficient use of methane, the most abundant light alkane, is hampered by the fact that over-oxidation to CO and CO₂ is extremely facile. For this reason, most methane intended for synthesis (as opposed to energy) is first converted to synthesis gas, a mixture of CO and H₂, before being subjected to the Fischer-Tropsch process to form liquid hydrocarbons.⁸

The interest in selective C–H functionalization is not limited to industry, of course; as the field matures it has also captured the attention of synthetic organic⁹ and biological chemists,¹⁰ among others. Nowhere is the broad applicability of this process more apparent than in a recent issue of *Chemical Reviews*, whose focus topic is C–H functionalization.¹¹

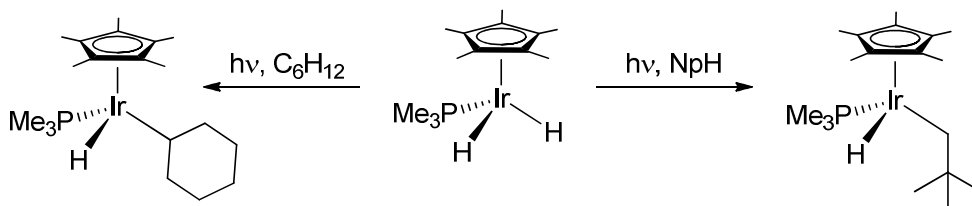
Let us first consider C–H activation, as this step remains the first obstacle *en route* to C–H functionalization.

1.1.1 Historical perspective on C–H activation

The first examples of C–H bond activation by transition-metal complexes were activations of aromatic C–H bonds, with both intramolecular¹² and intermolecular¹³ variants known. Despite the greater strength of C_{aryl}–H bonds compared to C_{alkyl}–H bonds, arene activation is generally favoured over alkane activation since the resulting metal–aryl bonds are stronger than metal–alkyl bonds.⁶

Intermolecular alkane activation was first observed in 1982 by Bergman using Cp*Ir(PMe₃)(H)₂. Upon photolysis in cyclohexane or neopentane, this complex reductively eliminates H₂ and forms an alkyl hydride complex by activating a C–H bond (Scheme 1.1).¹⁴

Scheme 1.1. Alkane activation by Cp*Ir(PMe₃)(H)₂.



In the same year, Graham reported similar results with $\text{Cp}^*\text{Ir}(\text{CO})_2$,¹⁵ and in 1983, Jones reported the first example of C–H activation of a linear alkane: $\text{Cp}^*\text{Rh}(\text{PMe}_3)(\text{H})_2$ activates propane at $-55\text{ }^\circ\text{C}$ upon irradiation.¹⁶

Although these early examples all involve metals from Group 9, in the present day, intermolecular C–H activation is known for elements from every group of the *d*-block transition series, and several mechanisms for this transformation have been proposed.

1.1.2 Mechanisms and examples of C–H activation

The classic mechanism for C–H activation is oxidative addition to an unsaturated metal centre. In many ways this parallels the activation of dihydrogen; the σ bond donates electron density into an empty *d* orbital on the metal centre, while the filled metal *d* orbitals can backdonate into the σ^* anti-bonding orbital (Figure 1.1). These two interactions reinforce one another, leading ultimately to the cleavage of the bond in question as the bond order in the ligand becomes progressively more reduced. This is the presumed mechanism of the Group 9 systems cited above.

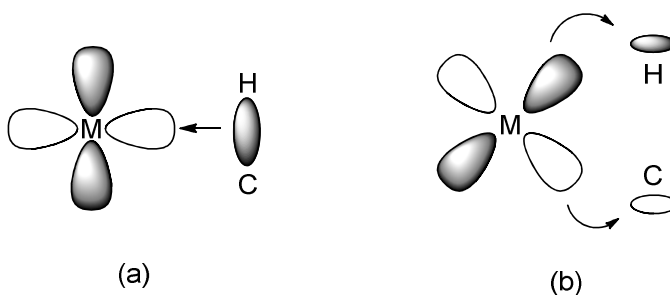


Figure 1.1. Oxidative addition of C–H bonds to metal centres includes both (a) σ -donation from ligand to metal and (b) π backdonation from metal to ligand.

However, C–H activation has also been observed for early transition metals with d^0 configurations, for which oxidative addition is impossible. Instead, these transformations are proposed to occur *via* σ -bond metathesis, which does not require a change in the metal's oxidation state (Figure 1.2).^{17, 18}

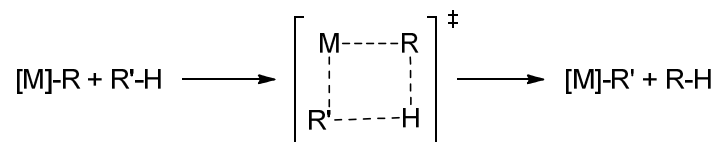


Figure 1.2. σ -Bond metathesis.

Perutz and Sabo-Etienne have recently suggested a mechanism called σ -complex assisted metathesis (σ -CAM), in which the oxidation state of the metal remains unchanged. Instead, transient—but discrete— η^2 -C–H σ -complexes are invoked to facilitate exchange of hydrides between ligands without formal scission of the C–H bond by the metal centre (Figure 1.3).¹⁹ The net transformation is therefore C–H activation. With experimental evidence for transition-metal alkane σ -complexes mounting,^{20, 21} this mechanism should be kept in mind as an alternative to previously-established ones.

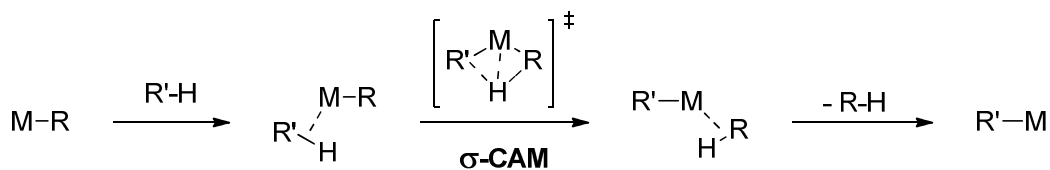


Figure 1.3. Generic σ -CAM mechanism.

1.1.3 C–H functionalization

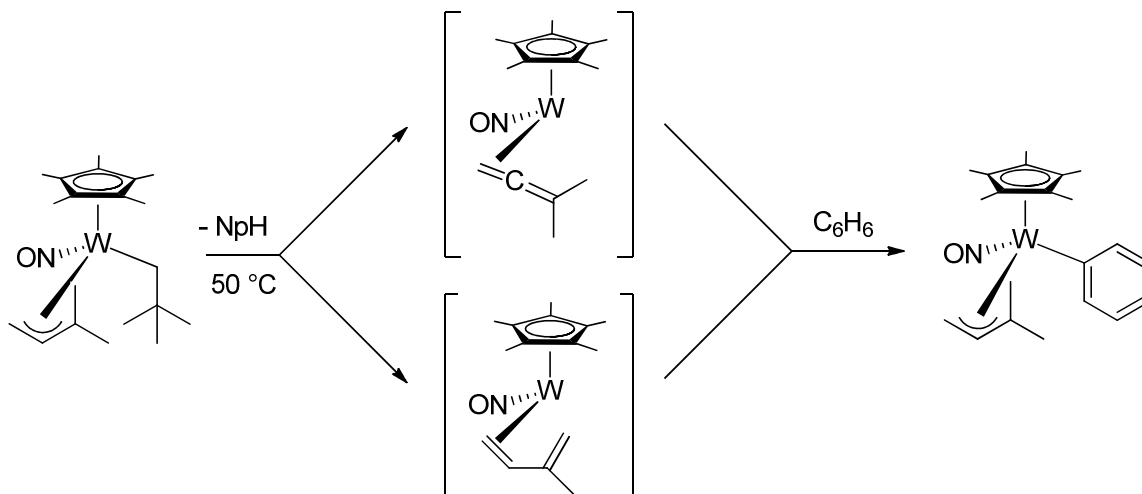
Having discussed C–H activation, we now turn our attention to the transformation of the newly-formed alkyl ligand. Despite the advances that have been made in C–H activation, the functionalization and release of the alkyl ligand, especially in a catalytic manner, have proven to be fraught with difficulties. One strategy that does not rely on the incorporation of an external functionalizing reagent into the alkyl ligand is the dehydrogenation of *n*-alkanes by Ir pincer complexes. Instead, the hydrogen atoms from the *n*-alkane are transferred onto an olefinic sacrificial acceptor. Unfortunately, the terminal olefins which are the initial products of this reaction can still react with the catalyst, leading to a variety of internal olefins.²² Functionalization with other reagents is also challenging, since alkyl hydride complexes often release alkane when reacted with these substances.⁶ To date only several truly catalytic systems have been developed; among these are systems which convert methane to methanol,²³ methane to methyl bisulphate,²⁴ and alkanes to alkyl boronates.^{25, 26} Regrettably, the wider application of these systems has been limited due to either the harsh acidic conditions required for conversion or to the somewhat unusual nature of the products generated.

1.2 Cp*W(NO)(alkyl)(η^3 -allyl) systems for C–H activation

For the last decade, the Legzdins group has investigated the use of Cp*W(NO)(alkyl)(η^3 -allyl) complexes as systems for C–H activation with the ultimate goal of developing these systems as catalysts for C–H functionalization.

These systems were initially researched as potential intermediates in C–H activation by $\text{Cp}^*\text{W}(\text{NO})(\text{Np})_2$. The first such system studied was $\text{Cp}^*\text{W}(\text{NO})(\text{Np})(\eta^3\text{-CH}_2\text{CHCMe}_2)$,²⁷ and the reactivity of this complex is summarized in Scheme 1.2.

Scheme 1.2. Reactivity of $\text{Cp}^*\text{W}(\text{NO})(\text{Np})(\eta^3\text{-CH}_2\text{CHCMe}_2)$.

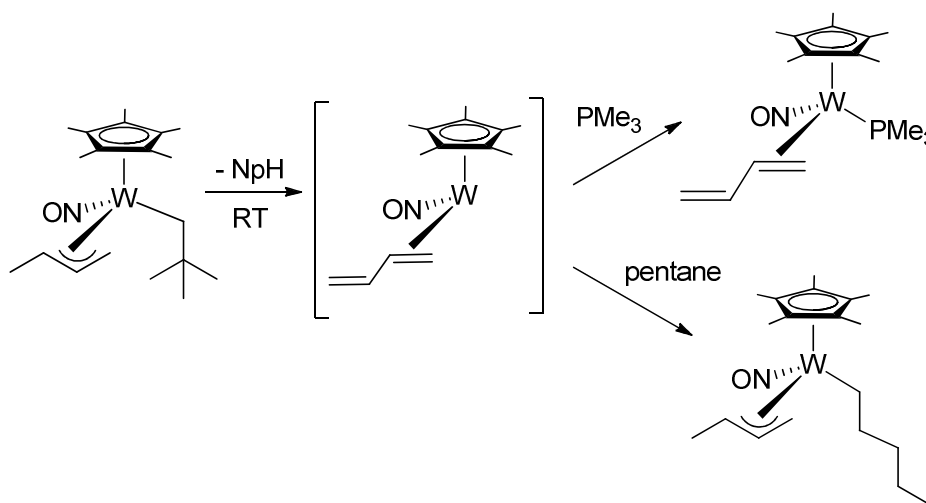


This complex loses neopentane by abstracting a hydrogen atom from the allyl ligand. If the central *meso* hydrogen is abstracted, an η^2 -allene intermediate is formed; if a hydrogen is instead abstracted from one of the terminal methyl groups, then an η^2 -diene intermediate is formed. Both of these intermediates are electronically and coordinatively unsaturated compared to the neopentyl precursor, so in order to restore an 18e configuration, this complex oxidatively adds an aromatic C–H bond to generate an allyl-aryl complex.

$\text{Cp}^*\text{W}(\text{NO})(\text{Np})(\eta^3\text{-CH}_2\text{CHCMe}_2)$ can also activate benzylic C–H bonds to give the analogous allyl-benzyl complexes, but shows a preference for aromatic C–H bonds when these are sterically accessible. However, when reacted with alkanes, the complex appears to activate multiple C–H bonds, usually giving allyl hydride products.

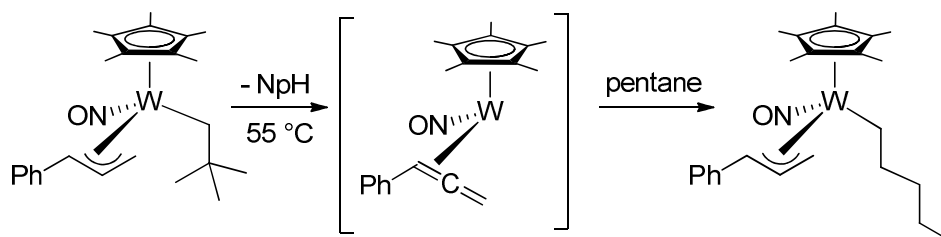
This preference for aromatic *vs* aliphatic C–H activation is reversed for $\text{Cp}^*\text{W}(\text{NO})(\text{Np})(\eta^3\text{-CH}_2\text{CHCHMe})$, which activates only the terminal C–H bond of pentane at room temperature to form the *n*-pentyl complex.²⁸ While this complex could, in principle, generate the η^2 -allene intermediate through abstraction of the *meso* hydrogen on the allyl ligand, in practice only the diene intermediate is observed (Scheme 1.3).

Scheme 1.3. Reactivity of $\text{Cp}^*\text{W}(\text{NO})(\text{Np})(\eta^3\text{-CH}_2\text{CHCHMe})$.



In light of these observations, it was proposed that the nature of the 16e intermediate (allene *vs* diene) was responsible for the selectivity of the subsequent C–H activation chemistry. However, this assumption proved incorrect when $\text{Cp}^*\text{W}(\text{NO})(\text{Np})(\eta^3\text{-CH}_2\text{CHCHPh})$ was shown to activate the terminal bonds of alkanes at $55\text{ }^\circ\text{C}$ ²⁹ (Scheme 1.4).

Scheme 1.4. Reactivity of $\text{Cp}^*\text{W}(\text{NO})(\text{Np})(\eta^3\text{-CH}_2\text{CHCHPh})$.



Since $\text{Cp}^*\text{W}(\text{NO})(\text{Np})(\eta^3\text{-CH}_2\text{CHCHPh})$ cannot form a diene intermediate, allene intermediates must also be capable of selectively activating aliphatic C–H bonds.

The newly formed alkyl ligands can be released by treatment with I_2 , but this reagent also reacts with the allyl ligand, giving $\text{Cp}^*\text{W}(\text{NO})\text{I}_2$ as the organometallic product along with the halogenated hydrocarbons.²⁸ Subsequent functionalization and release of the new alkyl ligand has also been somewhat hampered by the tendency of the releasing agents to react with the allyl ligand rather than the alkyl ligand.³⁰

1.3 Motivation

With this knowledge in mind, we turned our attention to other possible allyl ligands to use in these systems. In order to decrease the likelihood of reaction at the allyl ligand once a C–H bond has been activated, the effect of increasing the steric bulk on the ligand by using a trimethylsilyl group has been investigated. In addition to changing the steric demand of the allyl ligand, silicon's low electronegativity imparts a slight δ^- charge on the α carbon of the allyl ligand, thereby subtly changing its electronics.

In addition, there is a slowly-growing body of literature on the use of bis(trimethylsilyl)allyl ligands in stabilizing otherwise unstable complexes,³¹ and the

possibility of installing a 1,3-disubstituted allyl ligand to reduce the reactivity at the allyl ligand was also investigated.

1.4 Scope of this thesis

After this introductory chapter, this thesis is divided into four chapters concerned with the following topics.

Chapter 2 explores the characteristic chemistry of the title $\text{Cp}^*\text{W}(\text{NO})(\text{Np})(\eta^3\text{-CH}_2\text{CHCHSiMe}_3)$ (**2.1**) complex. The scope and mechanism of its C–H activation chemistry as well as attempts to derivatize the alkyl ligand through carbonylation are discussed. In addition, the chemistry of the related molybdenum complex is also considered.

Chapter 3 examines in detail the reaction of $\text{Cp}^*\text{W}(\text{NO})(\text{Np})(\eta^3\text{-CH}_2\text{CHCHSiMe}_3)$ with benzene, and the chemistry of the resulting disubstituted allyl hydride complexes.

Chapter 4 discusses the C–H activation of fluorobenzenes by **2.1** and the subsequent reactivity of the fluoroaryl complexes.

Chapter 5 provides a summary of the research presented in the three preceding chapters, discusses its possible implications, and offers perspectives on the possibilities of future work in this area.

1.5 Format of this thesis

Within Chapters 2–4 of this thesis, there are three major sections: Introduction, Results and Discussion, and Experimental Procedures. There is one set of references for the whole thesis. Complexes are assigned numbers based on their order of appearance in a

chapter; for example, the complexes in Chapter 2 are numbered **2.1**, **2.2**, **2.3**, etc. Figures, Schemes, and Tables are similarly numbered within their respective categories.

General experimental procedures are detailed in Section 1.6, and apply for all manipulations performed during the course of this research. X-ray crystallography tables for all solid-state molecular structures appearing in this thesis are presented in Appendix A.

1.5.1 Allyl nomenclature

Faller's nomenclature is used to describe the stereochemistry of the allyl ligand in this thesis.³² Allyl complexes are designated as *endo* or *exo* depending on whether the central *meso* hydrogen points towards or away from the Cp* ring. Terminal substituents are placed either *syn* or *anti* with respect to the *meso* hydrogen. These terms are summarized in Figure 1.4.

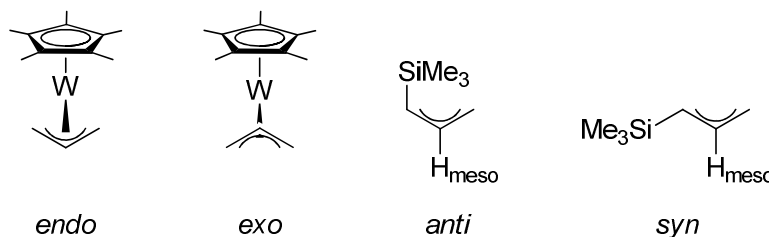


Figure 1.4. Graphical representation of allyl nomenclature used in this thesis.

1.6 General experimental procedures

Except where noted, all reactions and subsequent manipulations involving organometallic reagents were performed under anhydrous and anaerobic conditions, either on double-manifold Schlenk lines or in Innovative Technologies LabMaster 100 and MS-130 BG dual-station gloveboxes equipped with freezers maintained at $-30\text{ }^{\circ}\text{C}$. Purification of dinitrogen and argon was achieved by passing these gases first through a column containing

MnO and then a column of activated 4 Å molecular sieves. Small-scale reactions were conducted in J. Young NMR tubes equipped with Kontes greaseless stopcocks. Larger-scale thermolysis reactions were performed in thick-walled glass reaction vessels equipped with Kontes greaseless stopcocks. Reactions with gases were performed in either a specially made stainless steel pressure reactor or a Parr pressure reactor equipped with a sampling arm. Pentane, diethyl ether (Et₂O), benzene, cyclohexane, methylcyclohexane, mesitylene, and tetrahydrofuran (THF) were dried over sodium/benzophenone ketyl and freshly distilled prior to use. All other solvents were dried according to standard procedures.³³ Cp*Mo(NO)(Np)Cl and Cp*W(NO)(Np)Cl were prepared according to slight modifications of the published procedure.³⁴ All other chemicals were ordered from commercial suppliers and used as received.

All IR samples were prepared as Nujol mulls sandwiched between NaCl plates, and their spectra were recorded on a Thermo Nicolet Model 4700 FT-IR spectrometer. NMR spectra were recorded at room temperature (except where noted) on Bruker AV-300, AV-400, or AV-600 instruments, and all chemical shifts and coupling constants are reported in ppm and in Hz, respectively. ¹H NMR spectra were referenced to either the residual C₆D₅H present in C₆D₆ (7.16 ppm) or C₆D₁₁H (1.38 ppm) in C₆D₁₂. ¹³C NMR spectra were referenced to C₆D₆ (128.4 ppm) or C₆D₁₂ (26.4 ppm). ¹⁹F NMR spectra were externally referenced to CFCl₃. ³¹P NMR spectra were externally referenced to 85% H₃PO₄. When necessary, ¹H-¹H COSY, ¹H-¹³C HSQC, and ¹H-¹³C HMBC experiments were carried out to correlate and assign ¹H and ¹³C NMR signals. UV/Vis spectra were recorded on an Agilent Cary 5000 spectrophotometer in single-beam mode using a quartz cuvette with a 1.0 cm path length. Low-resolution mass spectra (EI, 70 eV) were recorded by Mr. Marshall Lapawa of

the UBC mass spectrometry facility using a Kratos MS-50 spectrometer. Elemental analyses were performed by Mr. David Wong and Mr. Derek Smith of the UBC microanalytical facility. X-ray crystallographic data collection, solution, and refinement were performed at the UBC X-ray Crystallography facility with the assistance of Dr. Brian Patrick and Dr. Michelle Thibault.

Chapter 2: Chemistry of $\text{Cp}^*\text{W}(\text{NO})(\text{Np})(\eta^3\text{-CH}_2\text{CHCHSiMe}_3)$

2.1 Introduction

Alkanes represent a particular challenge in C–H activation because they contain only unactivated C–H bonds.^{35, 36} In addition, not all the C–H bonds in a linear alkane are of equal value for functionalization; introducing functionality at the terminal positions is often more desirable than at internal ones.³⁷ Thus, the challenge to develop a selective and catalytic system for the functionalization of alkanes continues.

The initial inspiration for this research project was the possibility of synthesizing and installing 1,3-disubstituted allyl ligands on the $\text{Cp}^*\text{W}(\text{NO})(\text{alkyl})(\eta^3\text{-allyl})$ complexes. Trimethylsilylallyl ligands were investigated due to the possibility of straightforward derivatization. However, investigation into the chemistry of the monosubstituted trimethylsilylallyl ligand was also necessary to provide a baseline for comparison. In addition, the trimethylsilylallyl ligand is the first allyl ligand in the $\text{Cp}^*\text{W}(\text{NO})(\text{alkyl})(\eta^3\text{-allyl})$ family of complexes to contain a heteroatom.

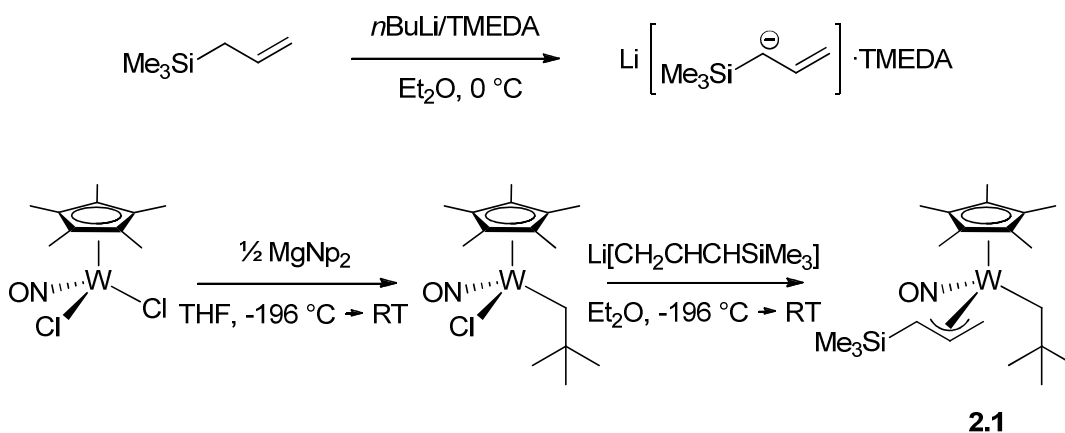
2.2 Results and discussion

2.2.1 Synthesis of $\text{Cp}^*\text{W}(\text{NO})(\text{Np})(\eta^3\text{-CH}_2\text{CHCHSiMe}_3)$

Various routes to piano-stool complexes containing allyl ligands exist. Pannell and Lappert installed a monohapto $\text{CH}_2\text{CHCHSiMe}_3$ ligand *via* salt metathesis onto $\text{Na}[\text{CpW}(\text{CO})_3]$; subsequent photolysis displaced CO, allowing the allyl ligand to shift from

an η^1 to an η^3 coordination mode.³⁸ $\text{Cp}^*\text{Cr}(\text{NO})(\text{CO})(\eta^2\text{-CH}_2\text{CHCH}_2\text{SiMe}_3)$, a related η^2 -olefin complex, has also been synthesized by photolysis of $\text{Cp}^*\text{Cr}(\text{NO})(\text{CO})_2$ in the presence of the allyl silane.³⁹ Syntheses of the Legzdins family of $\text{Cp}^*\text{M}(\text{NO})(\text{alkyl})(\eta^3\text{-allyl})$ ($\text{M} = \text{Mo}, \text{W}$) complexes all proceed in a similar fashion: from the dichloro starting material, $\text{Cp}^*\text{M}(\text{NO})\text{Cl}_2$, the alkyl and allyl ligands are installed sequentially *via* salt metathesis from MgR_2 reagents.⁴⁰ However, for the trimethylsilylallyl ligand, neither the Grignard reagent $\text{XMgCH}_2\text{CHCHSiMe}_3$ ($\text{X} = \text{Cl}, \text{Br}$) nor the binary magnesium reagent $\text{Mg}(\text{CH}_2\text{CHCHSiMe}_3)_2$ has been reported in the literature. Conversely, the allyl chloride starting material for these reagents has been synthesized by several methods previously.⁴¹⁻⁴³ In order to simplify the synthesis by reducing the number of steps required, $\text{Li}[\text{CH}_2\text{CHCHSiMe}_3]\cdot\text{TMEDA}$ was used as the allylating reagent for the $\text{Cp}^*\text{W}(\text{NO})(\text{Np})\text{Cl}$ precursor (Scheme 2.1).

Scheme 2.1. Synthesis of **2.1**.



Previous synthetic efforts towards $\text{CpW}(\text{NO})\text{Me}_2$ *via* $\text{CpW}(\text{NO})\text{Cl}_2$ and MeLi have suggested that the Li^+ ion could coordinate to the NO ligand due to lithium's high

oxophilicity.⁴⁴ Fortunately, this behaviour has not been observed in the preparation of $\text{Cp}^*\text{W}(\text{NO})(\text{Np})(\eta^3\text{-CH}_2\text{CHCHSiMe}_3)$ (**2.1**), and the procedure proved successful in producing moderate yields of the desired complex. The solid-state molecular structure of **2.1** is shown in Figure 2.1.

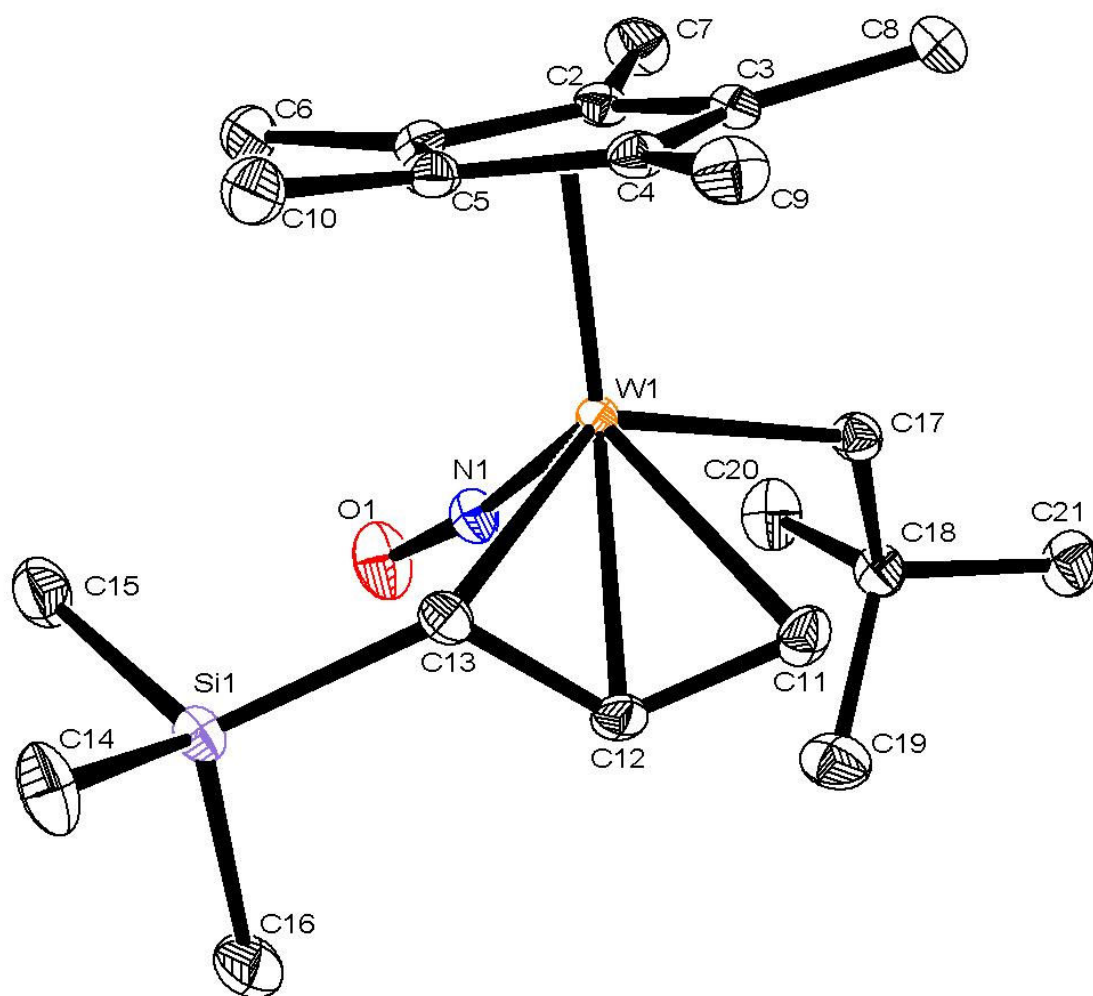


Figure 2.1. Solid-state molecular structure of **2.1** with 50% probability thermal ellipsoids.

Selected interatomic distances (Å) and angles (deg): C(11)–W(1) = 2.4081(17); C(12)–W(1) = 2.3340(17); C(13)–W(1) = 2.2934(17); C(11)–C(12) = 1.387(2); C(12)–C(13) = 1.438(2); N(1)–W(1) = 1.7846(15); N(1)–O(1) = 1.227(2); C(11)–C(12)–C(13) = 119.96(17); O(1)–N(1)–W(1) = 172.04(14).

The metrical parameters of the solid-state molecular structure (W–N–O bond angle: 172°; N–O bond length: 1.227 Å) provide strong evidence for the NO ligand being bound in a linear fashion. The ν_{NO} observed in IR spectroscopy (1589 cm^{-1}) is low for a linear NO ligand,⁴⁵ but is perfectly consistent with other data for this family of complexes, and is the result of the strong backbonding from the electron-rich W centre.

Also consistent with other members of the $\text{Cp}^*\text{M}(\text{NO})(\text{alkyl})(\eta^3\text{-allyl})$ family of complexes is the σ - π distortion in the allyl ligand of **2.1**; that is, its C–C bond lengths are unequal. Thus, the bonding of the allyl ligand to the metal is closer to the enyl form, rather than the pure trihapto mode, where the bond lengths would be equal. In the enyl formulation, the allyl ligand can be considered to be σ -bound to the W centre at the carbon with more sp^3 character (in **2.1**, at C(13)), and the partial double bond between the other two carbon atoms is π -coordinated. In addition, the σ -bound carbon is also slightly closer to the W centre than the other two carbon atoms (2.2934 Å vs 2.4081, 2.3340 Å). Distorted allyl ligands like these have been previously observed in electronically asymmetric environments.^{32, 46, 47} This feature is a consequence of the presence of NO, which is a strong π -acceptor ligand, in contrast to the Np ligand, which has no π -bonding capabilities. Through synergic backbonding, NO withdraws electron density from the metal, which reduces its ability to π bond to the ligand *trans* to NO—in this case, the double-bond end of the allyl ligand. In contrast, π backbonding between the W centre and the C(12)–C(13) unit is unaffected, leading to a reduced bond order and shorter W–C distances.

The allyl ligand in **2.1** is bound to the metal in an *endo* fashion, with the central *meso* proton pointing away from the Cp^* ring, rather than in an *exo* mode. The SiMe_3 group is found in the *syn* position. The *endo*, *syn* mode of allyl binding is probably favoured for steric

reasons, rather than electronic ones; Jia has used DFT calculations to show that the energy differences between *endo* and *exo* $\text{CpMo}(\text{CO})_2(\eta^3\text{-C}_3\text{H}_5)$ are very small.⁴⁸

This solid-state structure agrees with solution NMR spectroscopic data. In particular, the signals due to the four hydrogen atoms on the allyl ligand have markedly different chemical shifts in the ^1H NMR (C_6D_6) spectrum of **2.1**: CHSiMe_3 , 0.21 ppm; CH_2 , 2.02 and 4.09 ppm; and CH_{meso} , 5.20 ppm. This is due in part to the chemical environments within the allyl ligand itself—the α hydrogen to the SiMe_3 will be more shielded as a result of its proximity to the electropositive silicon atom—but coordination to the metal centre also reinforces these differences. In addition, the NMR spectroscopic data indicate the presence of a single isomer in solution. This is in contrast to $\text{Cp}^*\text{W}(\text{NO})(\text{Np})(\eta^3\text{-CH}_2\text{CHCHMe})$, which exists as two isomers in solution, with the methyl group on the allyl ligand occupying positions either proximal or distal to the NO ligand.²⁸ The absence of similar isomers for **2.1** is probably due to the steric crowding that would result from placing the SiMe_3 substituent proximal to the Np ligand, as $\text{Cp}^*\text{W}(\text{NO})(\text{Np})(\eta^3\text{-CH}_2\text{CHCHPh})$ exhibits similar behaviour.²⁹ In contrast, the less sterically-congested $\text{Cp}^*\text{Cr}(\text{CO})(\text{NO})(\eta^2\text{-CH}_2\text{CH=CHSiMe}_3)$ exists as a mixture of diastereomers.³⁹ The signals in the ^1H NMR spectrum of **2.1** are also well resolved (in particular the characteristic ddd splitting pattern for the *meso* proton on the allyl ligand), meaning that **2.1** is stereochemically rigid.

The final 18e product is fairly air-stable as a solid, but not in solution. Storage of the complex at room temperature in a benzene solution exposed to the atmosphere leads to its decomposition to $\text{Cp}^*\text{W}(\text{O})_2(\text{Np})$ and free $\text{CH}_2\text{CHCHSiMe}_3$ over 2 days.

2.2.2 C–H activation

From early studies of the $\text{Cp}^*\text{W}(\text{NO})(\text{alkyl})(\eta^3\text{-allyl})$ systems, we speculated that the nature of the 16e intermediate responsible for C–H activation dictated the type of product formed. Allene intermediates were thought to activate only sp^2 C–H bonds cleanly, while diene intermediates were believed to activate only sp^3 C–H bonds cleanly. This hypothesis proved to be invalid when $\text{Cp}^*\text{W}(\text{NO})(\text{Np})(\eta^3\text{-CH}_2\text{CHCHPh})$, which forms an allene intermediate after losing neopentane, was shown to activate linear alkanes at 55 °C.²⁹

As the allyl ligand in complex **2.1**, $\text{Cp}^*\text{W}(\text{NO})(\text{Np})(\eta^3\text{-CH}_2\text{CHCHSiMe}_3)$, does not contain a terminal methyl group, it should react *via* a pathway similar to $\text{Cp}^*\text{W}(\text{NO})(\text{Np})(\eta^3\text{-CH}_2\text{CHCHPh})$: i.e., generation of a 16e allene intermediate complex through loss of the *meso* hydrogen on the allyl ligand, followed by activation of a C–H bond to regenerate an alkyl allyl complex and an 18e configuration.

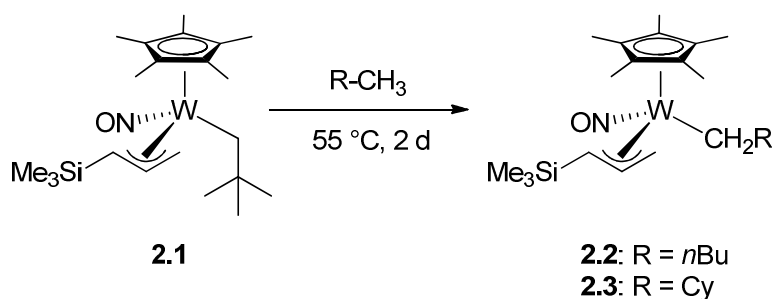
Substrates which are liquids at room temperature are easiest to study, because C–H activations can be effected simply by heating the appropriate solution of **2.1**. Unlike $\text{Cp}^*\text{W}(\text{NO})(\text{Np})(\eta^3\text{-CH}_2\text{CHCHMe})$, for which activations occur at room temperature,²⁸ heating is necessary to effect these C–H activations by **2.1**. A moderate temperature, 55 °C, was chosen for most experiments in order to strike a balance between temperatures too low to effect activations in a timely manner and those high enough to possibly cause decomposition of the starting material or its products.

2.2.2.1 Alkanes

Both pentane and methylcyclohexane (representative alkanes containing methyl groups) can be activated in this fashion, affording $\text{Cp}^*\text{W}(\text{NO})(n\text{-pentyl})(\eta^3\text{-$

CH₂CHCHSiMe₃) (**2.2**) and Cp*W(NO)(CH₂Cy)(η³-CH₂CHCHSiMe₃) (**2.3**), respectively (Scheme 2.2); in both cases only activation at the methyl group is observed. Unfortunately, neither of these complexes formed crystals of sufficient quality for X-ray diffraction analysis, but the NMR spectroscopic evidence unambiguously points to the formation of these products.

Scheme 2.2. Activation of alkanes by **2.1**.



¹H NMR spectroscopy is of limited utility to determine the site of C–H activation due to the many overlapping signals from the aliphatic protons. Fortunately, the ¹³C APT NMR experiment provides the necessary data. This experiment gives information about the number of hydrogen atoms attached to a given carbon atom: signals from quaternary and methylene carbons are phased oppositely from signals from methine and methyl carbon atoms. The ¹³C APT NMR spectrum of **2.2** in Figure 2.2 shows four signals pointing up and one pointing down in the region corresponding to *sp*³-hybridized carbon atoms; this indicates that only terminal activation of pentane has occurred. This selectivity for primary C–H bonds is probably a result of the increased steric accessibility of the terminal C–H bonds over internal ones.²⁶ Calculations on the activation of propane by the CpW(NO)(η²-methylallene)

fragment have demonstrated that terminal activation is favoured over internal activation by a ratio of 68:1.²⁹

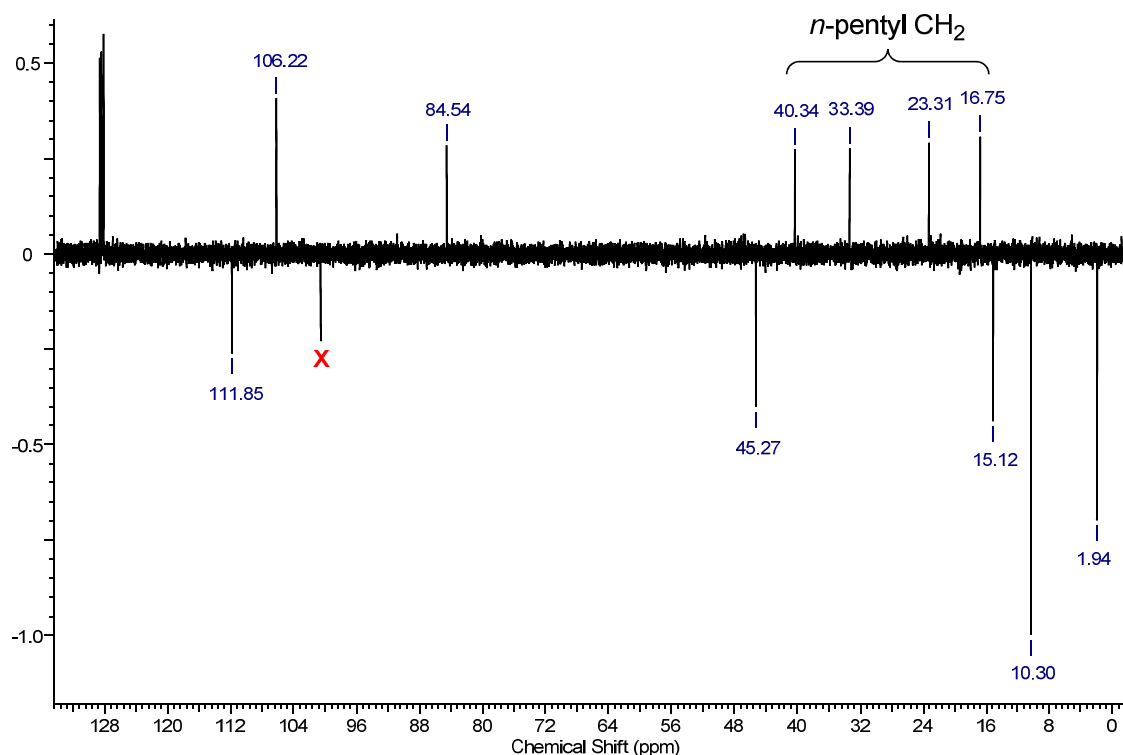


Figure 2.2. Expansion of the ^{13}C APT NMR spectrum of complex **2.2** (400 MHz, C_6D_6).

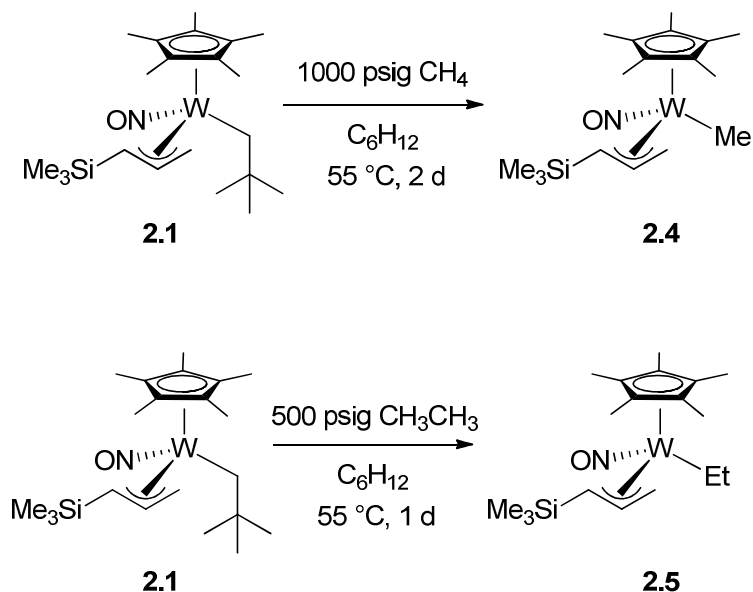
The apparent signal at approximately 100 ppm (marked by a red “X”) is a centre glitch from the NMR processing software and does not correspond to a carbon atom in the complex.

Though the activation of heavier alkanes is useful for determining the selectivity of the C–H activation process, the activation of gaseous alkanes is even more interesting from an industrial point of view due to their abundance and low cost. However, they present a greater challenge in terms of experimental design, since an inert solvent must be found which will dissolve both the W complex and the substrate to be activated. Cyclohexane has been previously shown to perform well as a non-reactive solvent for these kinds of activations,²⁸

but a complication arises in the case of $\text{Cp}^*\text{W}(\text{NO})(\text{Np})(\eta^3\text{-CH}_2\text{CHCMe}_2)$. This complex, which like **2.1** forms the η^2 -allene intermediate, activates cyclohexane at multiple positions to form the cyclohexenyl hydride $\text{Cp}^*\text{W}(\text{NO})(\eta^3\text{-C}_6\text{H}_9)(\text{H})$, losing the dimethylallyl ligand in the process.²⁷ As a matter of fact, this product is identifiable by ^1H NMR spectroscopy in the final reaction mixture after the thermolysis of **2.1** in cyclohexane (among a number of other organometallic products). Fortunately, a competition experiment shows that **2.1** prefers to activate primary sp^3 C–H bonds rather than secondary ones: when complex **2.1** is thermolyzed in an equimolar mixture of cyclohexane and pentane, only the *n*-pentyl complex **2.2** is observed to form.

Both methane and ethane are activated by complex **2.1** to give the corresponding methyl ($\text{Cp}^*\text{W}(\text{NO})(\text{Me})(\eta^3\text{-CH}_2\text{CHCHSiMe}_3)$, **2.4**) and ethyl ($\text{Cp}^*\text{W}(\text{NO})(\text{Et})(\eta^3\text{-CH}_2\text{CHCHSiMe}_3)$, **2.5**) complexes (Scheme 2.3). Higher pressures of methane than ethane are necessary to observe activation of the substrate, which may be due to the lower solubility of methane in cyclohexane.⁴⁹

Scheme 2.3. Activation of gaseous alkanes by **2.1**.



These activations are also air- and moisture-sensitive, unlike the carbonylations carried out in cyclohexane (*vide infra*). Unless the reaction is carried out under rigorously air-free conditions, the primary organometallic product produced is the $\text{Cp}^*\text{W}(\text{O})_2(\text{Np})$ dioxo decomposition species.

Unlike the neopentyl starting material **2.1**, which is isolable as an orange solid, the majority of **2.2–2.5** exist as oils, making their further derivatization more complex than for **2.1**. However, these complexes, in particular **2.4** and **2.5**, represent key intermediates in the possible functionalization of these light alkanes, having overcome the first barrier in this process: breaking the C–H bond.

2.2.2.2 Arenes

Thermolysis of **2.1** in benzene leads to three organometallic products resulting from the activation of benzene and migration of the newly-formed phenyl ligand onto the allyl

ligand, and is treated in detail in Chapter 3. The reaction of **2.1** with fluorobenzenes is discussed in Chapter 4.

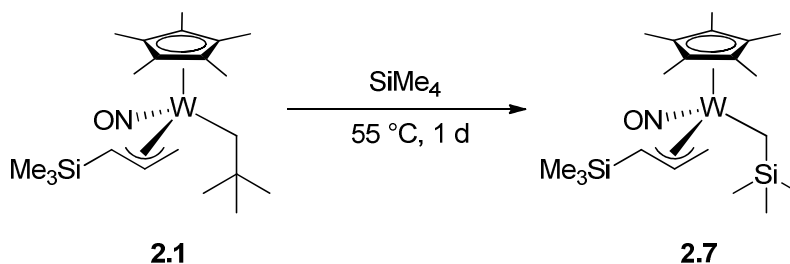
Thermolysis of **2.1** in mesitylene leads only to activation at the methyl group, yielding $\text{Cp}^*\text{W}(\text{NO})(\text{CH}_2\text{-3,5-Me}_2\text{C}_6\text{H}_3)(\eta^3\text{-CH}_2\text{CHCHSiMe}_3)$, **2.6**. In this case, the selective activation is due to the steric bulk of the methyl groups hindering access to the aromatic C–H bonds of the substrate. A brief study of the thermolysis of **2.1** in toluene-*d*₈ reveals that activation can occur at both the *sp*² and *sp*³ C–H bonds in these mixed systems.

2.2.2.3 Other functional groups

Other substrates have also been screened to ascertain the tolerance of the C–H activation chemistry of **2.1** for other functional groups. While such a range of studies has been performed on $\text{Cp}^*\text{W}(\text{NO})(\text{Np})(\eta^3\text{-CH}_2\text{CHCHMe})$,²⁸ this screening has not been as extensive for complexes which activate C–H bonds *via* an η^2 -allene intermediate.

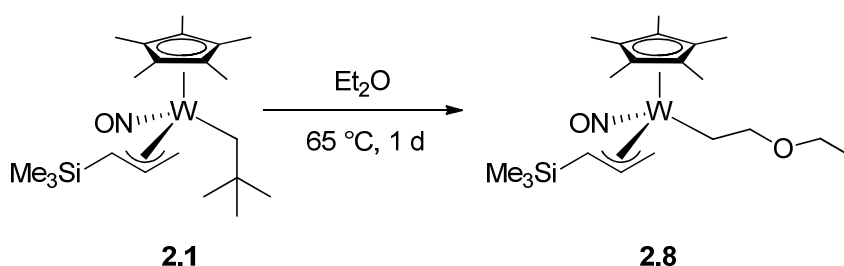
Tetramethylsilane is activated cleanly to give $\text{Cp}^*\text{W}(\text{NO})(\text{CH}_2\text{SiMe}_3)(\eta^3\text{-CH}_2\text{CHCHSiMe}_3)$, **2.7** (Scheme 2.4), the silyl neopentyl analogue of the parent complex **2.1**. As has been the case for other complexes synthesized by members of the Legzdins group,⁵⁰ this complex (**2.7**) shows diminished reactivity compared to the neopentyl version; prolonged thermolysis of this complex in deuterobenzene at elevated temperatures leads only to recovery of the starting material.

Scheme 2.4. Activation of tetramethylsilane by **2.1**.



The activation of diethyl ether proceeds in the same manner as for pentane: the only C–H bond activated is that of the terminal methyl group, affording $\text{Cp}^*\text{W}(\text{NO})(\text{CH}_2\text{CH}_2\text{OCH}_2\text{CH}_3)(\eta^3\text{-CH}_2\text{CHCHSiMe}_3)$, **2.8** (Scheme 2.5). Despite the presence of Lewis basic lone pairs on the substrate, no coordination of the oxygen atom to the metal centre is observed. The regiospecific activation precludes a possible pre-coordination of O to the W centre selecting the C–H bonds α to the oxygen atom for activation.

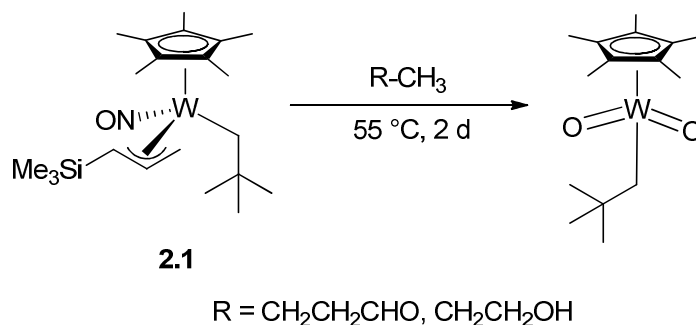
Scheme 2.5. Activation of diethyl ether by **2.1**.



In contrast, activation of other oxygen-containing substrates such as aldehydes and alcohols has been unsuccessful. In all cases, this leads to formation of the $\text{Cp}^*\text{W}(\text{O})_2(\text{Np})$ dioxo species (Scheme 2.6), identified from its signature ^1H NMR spectrum.⁵¹ In both of

these substrates the oxygen atom is more sterically accessible than in diethyl ether; this may be the factor responsible for the decomposition of the starting material.

Scheme 2.6. Attempted activation of aldehydes and alcohol by **2.1**.

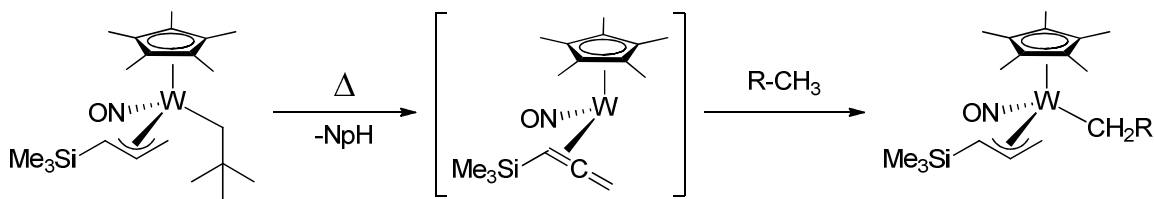


The reaction of **2.1** with cyclohexene (as a representative alkene) is examined in detail in Section 2.2.3.2 as part of a mechanistic study.

2.2.3 Mechanistic studies

C–H activation by **2.1** occurs *via* a coordinatively and electronically unsaturated η^2 -allene intermediate which is formed following abstraction of the allyl *meso* hydrogen by the neopentyl ligand and loss of neopentane (Scheme 2.7). Support for the existence of this intermediate has been established by two thermolytic experiments.

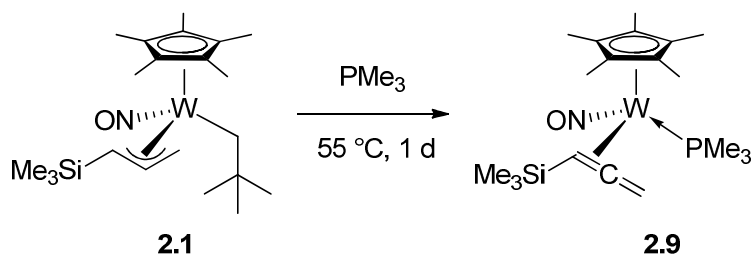
Scheme 2.7. General mechanism for C–H activation by **2.1**.



2.2.3.1 Reaction with PMe₃

Thermolysis of **2.1** in the presence of PMe₃ (either neat or in benzene solution) leads to the formation of a single product, Cp*W(NO)(η^2 -CH₂=C=CHSiMe₃)(PMe₃) (**2.9**), formally the Lewis-base adduct of the 16e η^2 -allene complex (Scheme 2.8).

Scheme 2.8. Formation of the PMe₃ adduct of the 16e intermediate responsible for C–H activation by **2.1**.



The ³¹P{¹H} NMR spectrum of **2.9** (Figure 2.3) displays the expected ¹⁸³W satellites arising from direct phosphorus coordination to tungsten. The main peak for the product appears at –9.5 ppm, but a minor signal is also present at –12.1 ppm. Because the quantity of this minor product is very small (< 7%), its precise identity remains to be elucidated. However, on the basis of the similar chemical shifts of the signals arising from these two products, it is reasonable to assume that they are isomers differing in the orientation of the allene ligand.

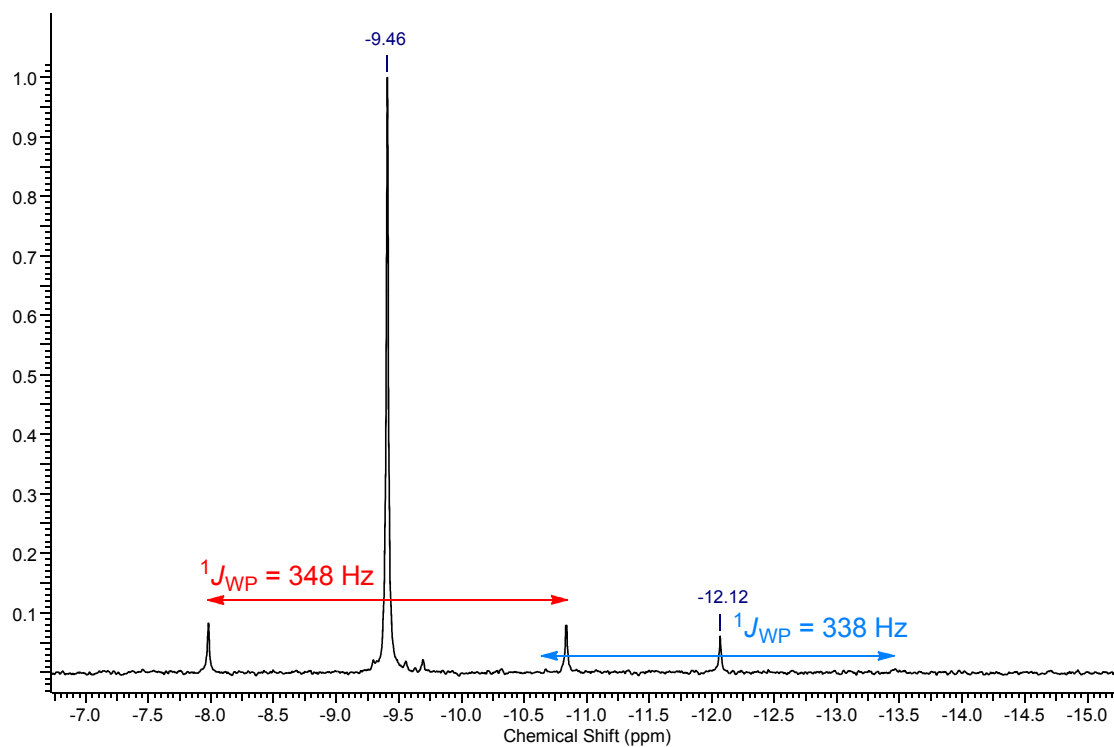


Figure 2.3. Expansion of the $^{31}\text{P}\{^1\text{H}\}$ NMR (121 MHz, C_6D_6) spectrum of complex **2.9** (and minor product).

The ORTEP diagram of the solid-state molecular structure of **2.9** is shown in Figure 2.4.

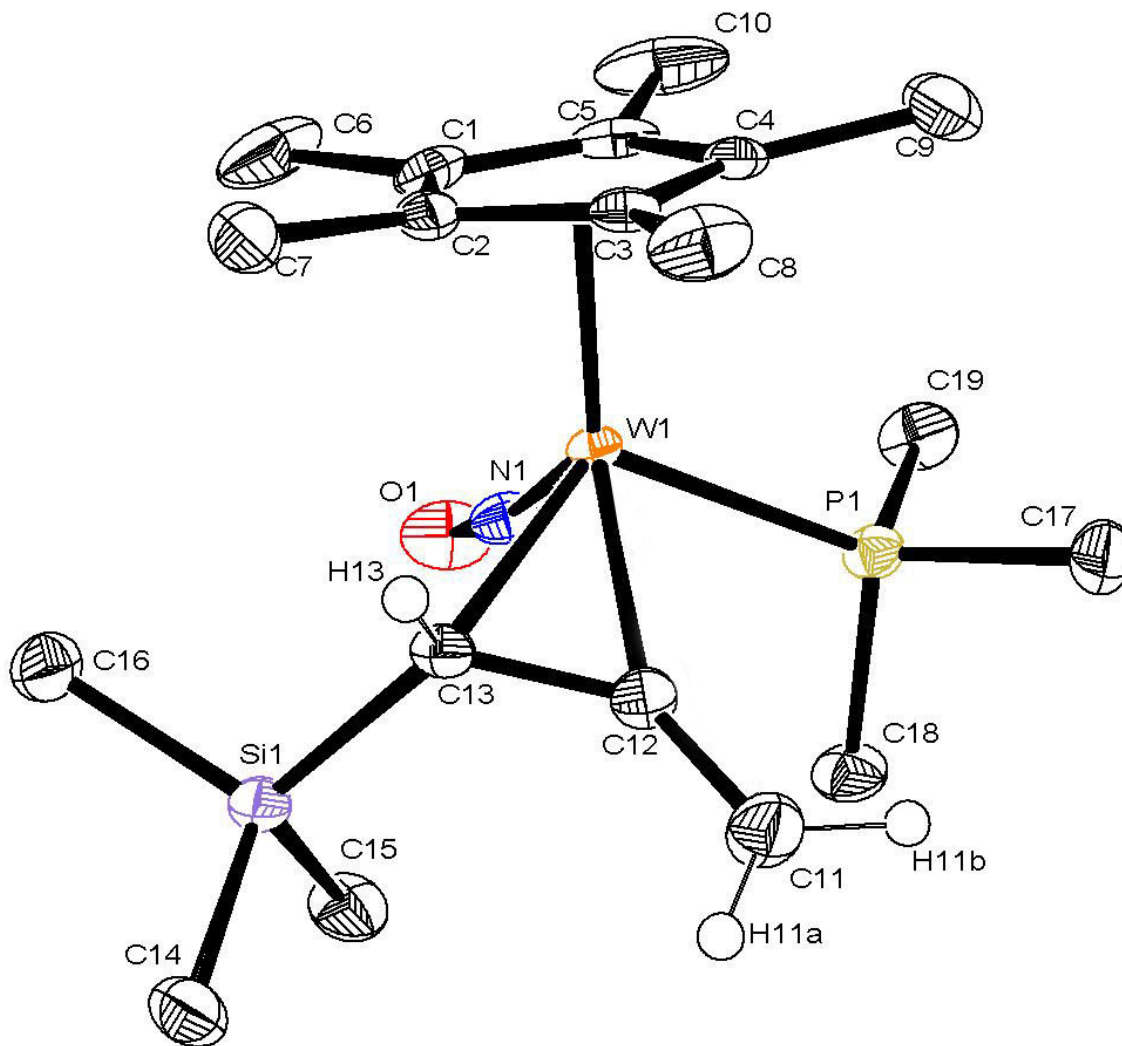


Figure 2.4. Solid-state molecular structure of **2.9** with 50% probability thermal ellipsoids.

Selected interatomic distances (Å) and angles (deg): C(11)–C(12) = 1.322(4); C(12)–C(13) = 1.435(4); C(12)–W(1) = 2.154(3); C(13)–W(1) = 2.204(3); N(1)–O(1) = 1.235(3); N(1)–W(1) = 1.779(2); P(1)–W(1) = 2.4490(9); C(11)–C(12)–C(13) = 135.9(3); O(1)–N(1)–W(1) = 169.7(2); Si(1)–C(13)–H(13) = 113.5(18).

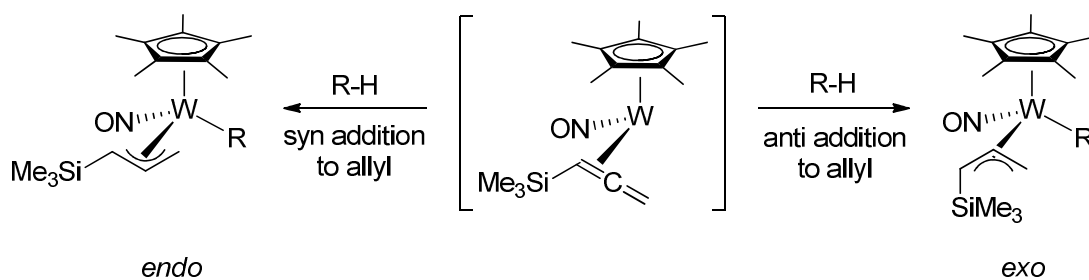
The allene ligand in complex **2.9** displays several interesting characteristics. Firstly, its structure is distorted from the simplest allene, $\text{H}_2\text{C}=\text{C}=\text{CH}_2$. The angle between the three carbon atoms is not 180° , but 136° . Nor are the two C–C bonds of equal length: C(12)–C(13)

is 0.11 Å longer than C(11)–C(12). Two effects working in concert cause this phenomenon, which is the result of the allene's coordination to W. First, coordination to W drains electron density from the allene's filled π orbital. Second, backdonation from the W centre to the C(12)–C(13) unit lengthens the C–C bond. Conversely, the bond between C(11) and C(12) is relatively unaffected due to its distance from the W centre and thus retains more of its double-bond character.

While the solid-state structure of **2.9** shares the above features with the PMe_3 adducts of the other allene intermediates,^{27, 29} it differs from them in one major aspect: the carbon atoms coordinated to the metal center are the ones closest to, rather than furthest from, the substituted end of the ligand. The chemical shifts of the methylene hydrogens (5.53, 6.85 ppm) in the ^1H NMR spectrum of **2.9** are consistent with this formulation, as they are found in a range typical for olefinic protons, rather than being shifted upfield due to coordination to the metal centre. In contrast, the hydrogen α to the Si atom is shifted upfield (0.06 ppm) relative to free trimethylsilyllallene (4.80 ppm).⁵² The origin of the preference for this coordination mode may be the silicon atom, whose electropositive nature could make the bond between C(12) and C(13) a better electron donor than the bond between C(11) and C(12).

Notably, the central carbon of the allene ligand is the closest to the W centre; this feature is typical for transition-metal allene complexes.⁵³ The positioning of this atom could provide a rationale for the allyl ligand's *endo* to *exo* conversion as observed in the activation of pentafluorobenzene, for example (Chapter 4). The hydrogen atom from the activated C–H bond could add either *syn* or *anti* relative to the SiMe_3 on the allyl ligand, affording the *endo*, *syn* and *exo*, *anti* isomers respectively (Scheme 2.9).

Scheme 2.9. Rationalization for allyl isomerization after C–H activation by **2.1**.



2.2.3.2 Reaction with cyclohexene

A second experiment has been performed to verify the identity of this intermediate, as well as to probe the reactivity of the complex with an olefinic substrate. Reactions with cyclohexene have been used to confirm the nature of the C–H activating intermediate in other systems.²⁷ Upon thermolysis in of **2.1** in cyclohexene, a single tractable organometallic product can be isolated: $\text{Cp}^*\text{W}(\text{NO})(\text{H})(\eta^3\text{-CH}_2\text{C(3-cyclohexenyl)CHSiMe}_3)$ (**2.10**). Its solid-state molecular structure is presented in Figure 2.5.

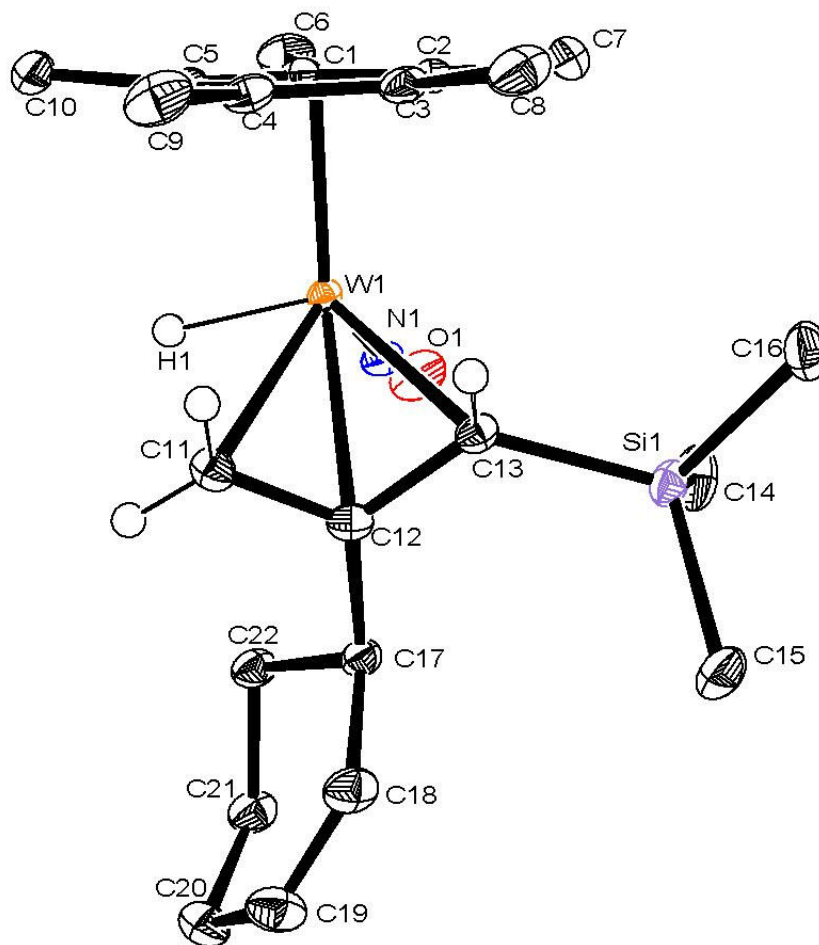


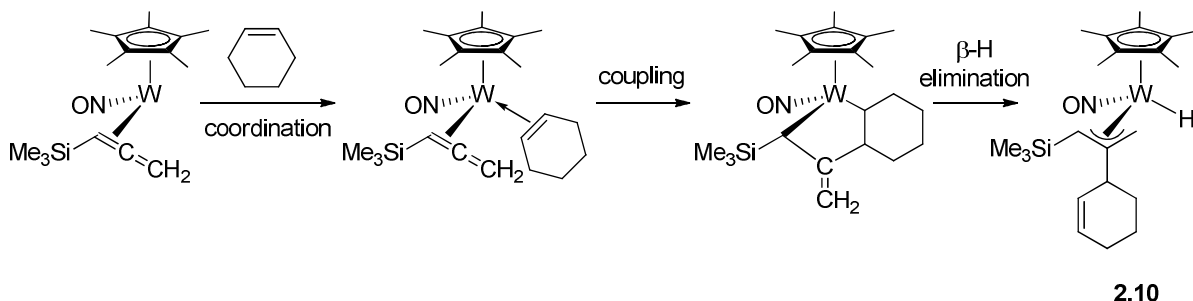
Figure 2.5. Solid-state molecular structure of **2.10** with 50% probability thermal ellipsoids.

Selected interatomic distances (Å) and angles (deg): C(11)–C(12) = 1.388(3); C(12)–C(13) = 1.444(3); C(17)–C(18) = 1.522(3); C(18)–C(19) = 1.322(3); N(1)–O(1) = 1.229(2); N(1)–W(1) = 1.7813(16); W(1)–H(1) = 1.58(3); C(11)–C(12)–C(13) = 117.04(18); O(1)–N(1)–W(1) = 168.49(14).

This hydride results from the formal exchange of the allyl *meso* proton and the cyclohexenyl ligand, probably by a mechanism such as the one presented in Scheme 2.10. In contrast to aryl ligands (Chapters 3 and 4), the cyclohexenyl group migrates not onto the terminal carbon of the allyl ligand but onto the *meso* carbon of the allyl ligand. The key step

of this transformation must therefore involve the η^2 -allene species rather than the η^3 -allyl complex.

Scheme 2.10. Mechanism for the formation of **2.10**.



This complex appears to exist as a single isomer both in the solid state and in solution. Ultimately, this observation can be rationalized by two facts: first, the starting material itself does not display isomerism, and secondly, having the SiMe₃ group of the allene and the coordinated cyclohexene ligand cisoid to each other is probably prevented by the steric bulk of these two substituents. Isomeric forms of this complex may exist, since replacing the neopentyl ligand by a hydride relieves the crowding in the metal's coordination sphere.

These two experiments confirm the existence of the allene intermediate, as well as suggest that substrates containing multiple bonds are less prone to undergo C–H activation, since they likely coordinate to the metal centre and couple with the allene ligand before C–H activation can be effected.

2.2.3.3 Kinetics of C–H activation by 2.1

Kinetic studies of the C–H activation effected by **2.1** have been performed to understand more fully the mechanism and to compare its thermodynamic parameters to other members of the $\text{Cp}^*\text{W}(\text{NO})(\text{alkyl})(\eta^3\text{-allyl})$ family. Such parameters are interesting from a fundamental point of view, illustrating how changes in the ligand set can modify the reactivity of a complex. A fuller understanding of these properties can lead to a rational design of a complex for C–H activation and functionalization. Small-scale reactions have been carried out using benzene- d_6 as the substrate to facilitate monitoring by ^1H NMR spectroscopy.

The results of a representative thermolysis are presented in Figure 2.6.

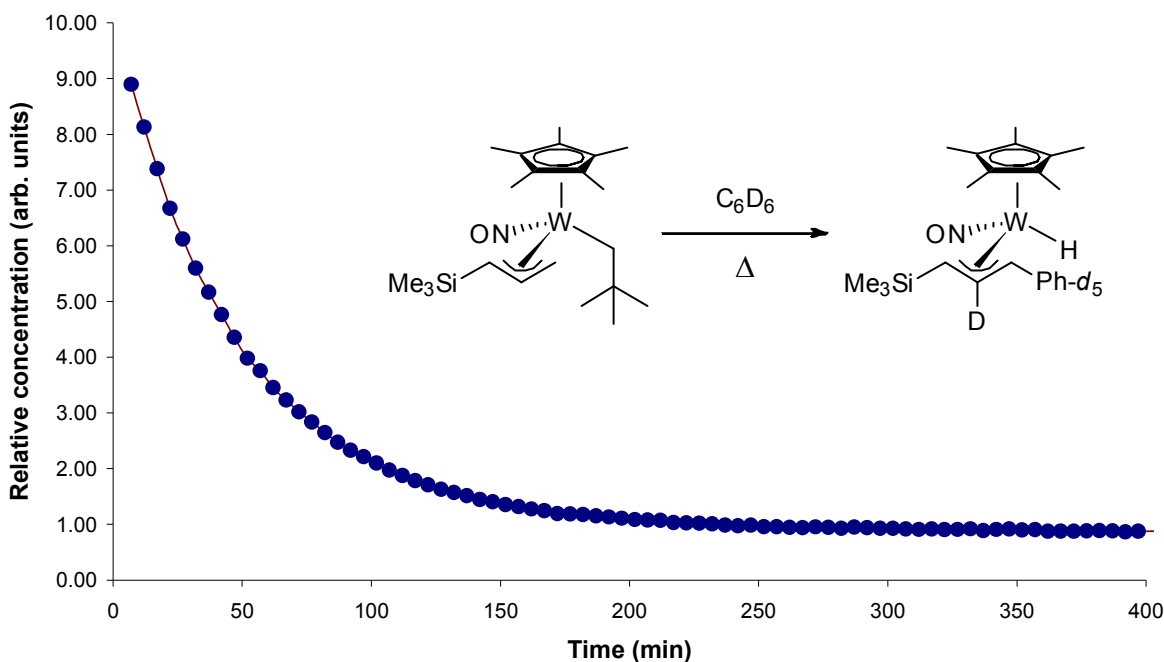


Figure 2.6. Monitoring loss of starting material through integration of the area under the peak at 1.30 ppm (Np Me) during the thermolysis of **2.1** in C_6D_6 by ^1H NMR spectroscopy at 75 °C.

At 75 °C, virtually all the starting material is consumed in 250 min. **2.1** is consumed according to pseudo first-order kinetics (Figure 2.7), which is consistent with the rate-determining step in C–H activation being unimolecular.

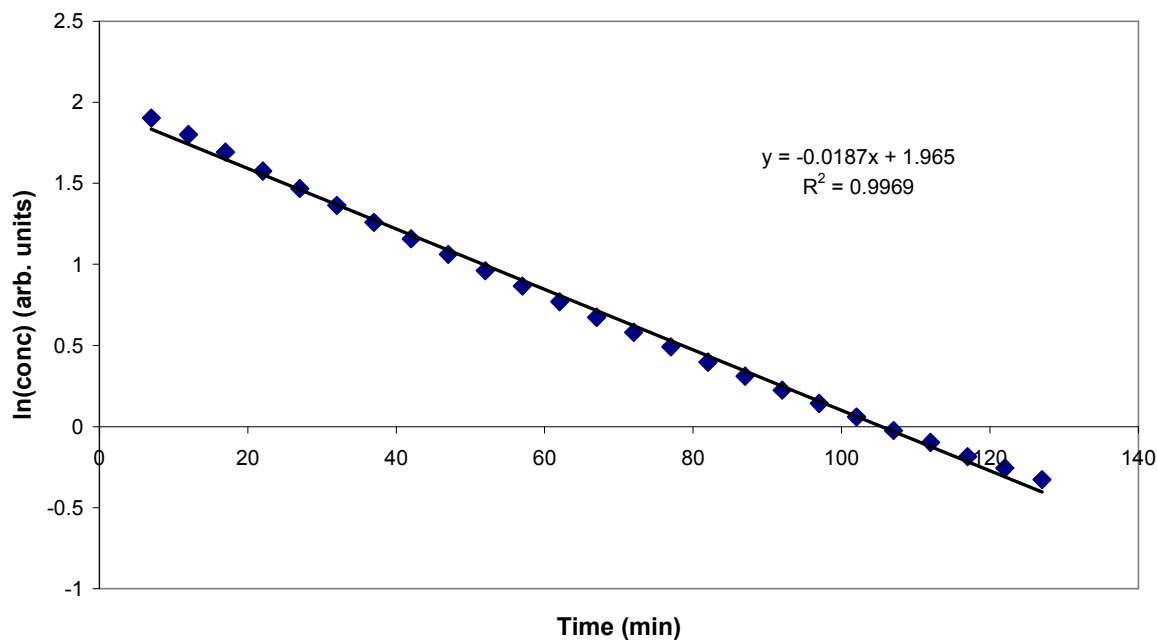


Figure 2.7. First-order kinetics plot of the consumption of **2.1** when heated at 75 °C in C₆D₆.

The rate constant for the decomposition of **2.1** has been measured at several different temperatures, and it increases with increasing temperature (Table 2.1).

Table 2.1. Rate constants for the loss of **2.1** during thermolysis in C₆D₆.

Temperature (°C)	Rate constant, (s ⁻¹)
45.5	$(5.57 \pm 0.01) \times 10^{-6}$
55.3	$(2.81 \pm 0.01) \times 10^{-5}$
65.0	$(9.93 \pm 0.07) \times 10^{-5}$
75.1	$(3.11 \pm 0.04) \times 10^{-4}$

From this data, an Eyring plot (Figure 2.8) can be generated to determine the enthalpy (ΔH^\ddagger) and entropy (ΔS^\ddagger) of activation.

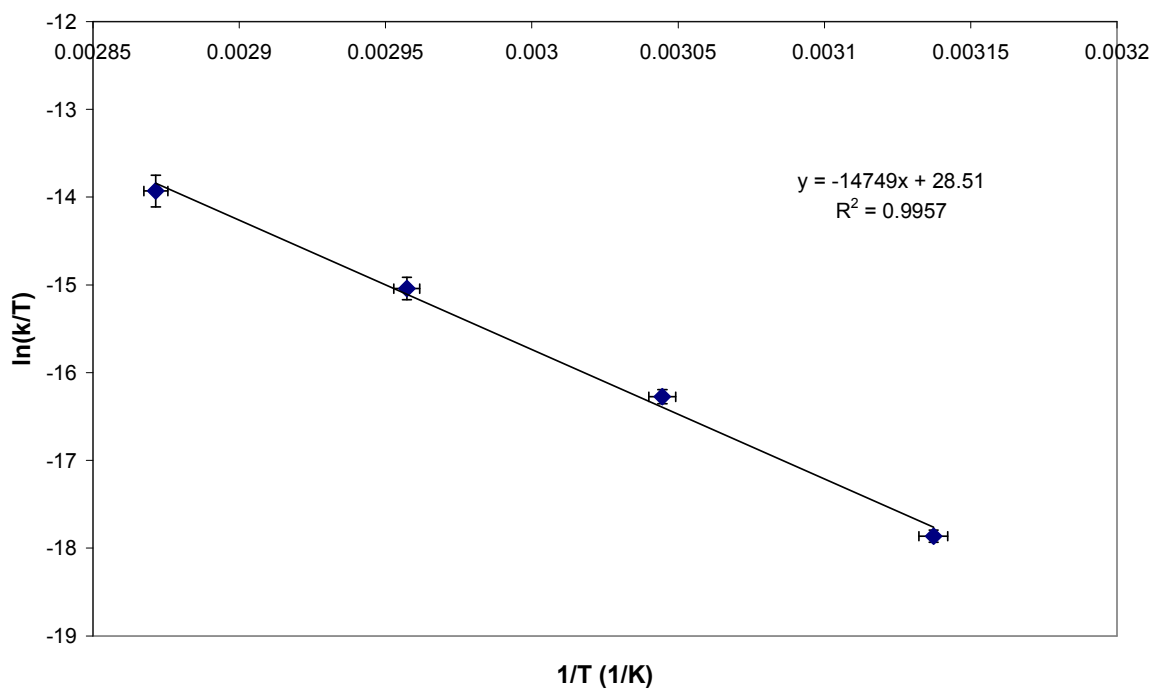


Figure 2.8. Eyring plot for the thermolysis of **2.1** in C₆D₆.

Both the values for the enthalpy and entropy of activation ($+122.6 \text{ kJ mol}^{-1}$ and $+39.4 \text{ J K}^{-1} \text{ mol}^{-1}$) support loss of neopentane as the first step in C–H activation. Positive values of ΔH^\ddagger imply bonds are breaking to form the transition state: in this case the enthalpic contribution of breaking the allyl C–H bond and W–C bond more than offset the enthalpic cost of C–H bond formed in making neopentane. In a similar vein, positive values of ΔS^\ddagger indicate that the conversion from starting material to transition state is entropically favoured, which is equally consistent, as two molecules are being formed from one.

Finally, using the Arrhenius equation and the following plot (Figure 2.9), the activation energy (E_a) for the process can be calculated to be $125.4 \text{ kJ mol}^{-1}$. This is significantly higher than the 79.1 kJ mol^{-1} reported for $\text{Cp}^*\text{W}(\text{NO})(\text{Np})(\eta^3\text{-CH}_2\text{CHCHMe})$,⁵⁴ which is consistent with the room temperature stability of **2.1**. In contrast, $\text{Cp}^*\text{W}(\text{NO})(\text{Np})(\eta^3\text{-CH}_2\text{CHCHMe})$ is unstable at ambient temperature.

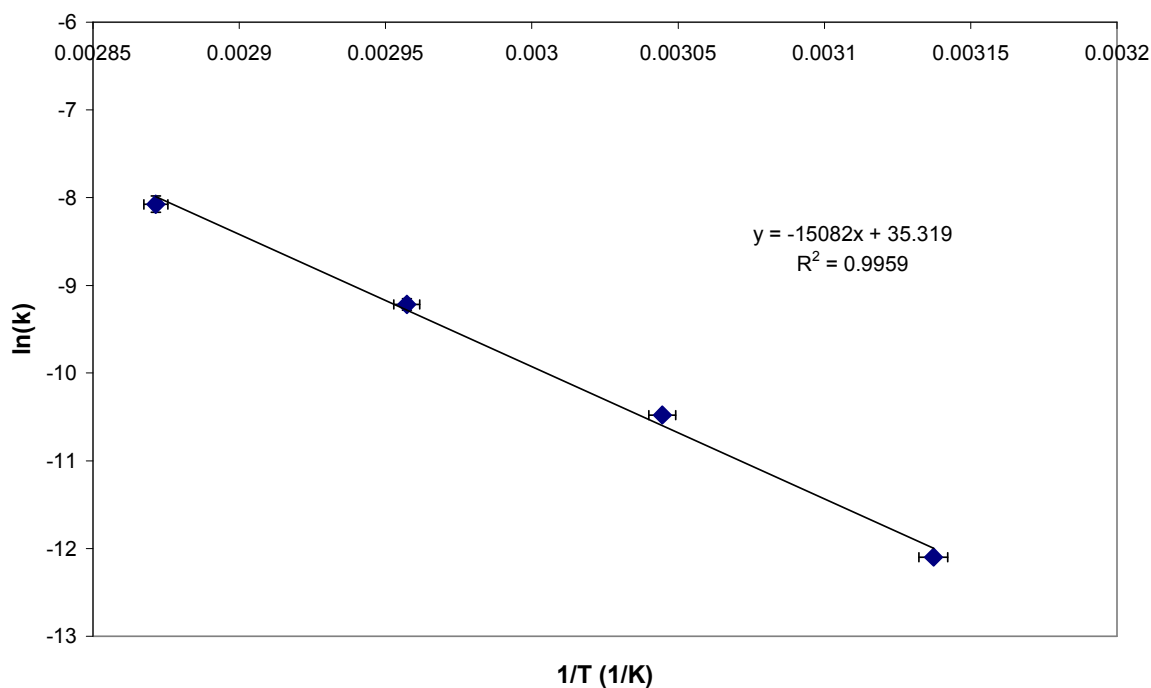


Figure 2.9. Arrhenius plot of the thermolysis of **1.1** in C₆D₆.

The evidence presented in this section supports the presumed mechanism for C–H activation by **2.1**: namely, that the initial (and rate-determining) step is probably the loss of neopentane from the metal's coordination sphere *via* hydrogen abstraction by the neopentyl ligand from the allyl ligand to form the η^2 -allene intermediate. This is followed by oxidative addition of a C–H bond onto the metal centre. The putative hydride thus formed can migrate onto the central carbon of the allene in a reversal of the first step to regenerate the allyl ligand.

2.2.4 Carbonylation of Cp*W(NO)(Np)(η^3 -CH₂CHCHSiMe₃)

To date, the cleanest and most facile route to derivatize the alkyl ligand on the W centre is to carbonylate the complex under CO pressure to generate products of the type

$\text{Cp}^*\text{W}(\text{NO})(\eta^3\text{-allyl})(\eta^1\text{-acyl})$.³⁰ However, this process presents several obstacles for these systems, some more easily overcome than others. Not only must an inert solvent (incapable of being subjected to C–H activation) be found, but both the temperature and pressure of the reaction must be carefully selected in order to avoid the formation of unwanted products, e.g., $\text{Cp}^*\text{W}(\text{NO})(\eta^1\text{-allyl})(\eta^1\text{-acyl})(\text{CO})$ or $\text{Cp}^*\text{W}(\text{NO})(\text{CO})_2$.

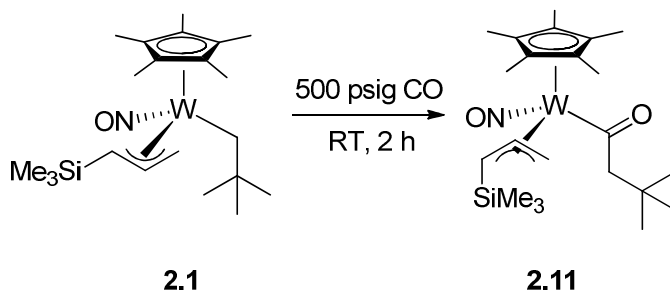
The parent neopentyl allyl complex **2.1** was used as a model complex for carbonylation, since the use of this complex has several advantages over one containing a different alkyl ligand. First, it is generally true that CO insertion into the neopentyl ligand happens more quickly than for other ligands such as methyl, which is likely a consequence of steric congestion favouring the insertion upon CO coordination.⁵⁵ Second, undesirable byproducts involving the incorporation of more than one equivalent of CO have never been observed during the carbonylation of the W neopentyl complexes containing other allyl ligands. Finally, the methyl groups on the neopentyl ligand provide a convenient NMR handle for future acyl release studies.

These principles are best illustrated by an example. The feasibility of carbonylating other alkyl ligands has been briefly explored using the *n*-pentyl complex, **2.2**, as a substrate. Under identical conditions to those employed for the neopentyl complex (C_6H_{12} solvent, 500 psig CO, room temperature), no conversion of the starting material is observed. An increase in the temperature of the reaction to 35 °C causes a small amount of conversion to a new product. Further increasing the temperature to 55 °C leads to more conversion, with ^1H NMR spectroscopic data indicating approximately a 4:3 ratio of starting material to product. IR spectroscopy of aliquots taken at this higher temperature reveals bands attributable to both acyl C=O (1689 cm^{-1}) and terminal carbonyl (1960 cm^{-1}) stretches. ^{13}C NMR spectroscopy

reveals downfield resonances at 211.8 and 226.2 ppm, both likely corresponding to carbonyl groups. Finally, mass spectral data show peaks corresponding both to the expected product $\text{Cp}^*\text{W}(\text{NO})(\text{C}(=\text{O})\text{pentyl})(\eta^3\text{-CH}_2\text{CHCHSiMe}_3)$ (m/z 561, ^{184}W) as well as this product with an additional CO ligand (m/z 589, ^{184}W). As a result of the difficulty of isolating the desired product, investigations were focused on the carbonylation product of the neopentyl complex.

In contrast, the reaction of **2.1** with CO leads to the clean formation of $\text{Cp}^*\text{W}(\text{NO})(\eta^1\text{-C}(=\text{O})\text{Np})(\eta^3\text{-CH}_2\text{CHCHSiMe}_3)$ (**2.11**) at room temperature under 500 psig CO (Scheme 2.11).

Scheme 2.11. Carbonylation of **2.1**.



In the solid state, a single isomer is observed, and its structure is presented in Figure 2.10.

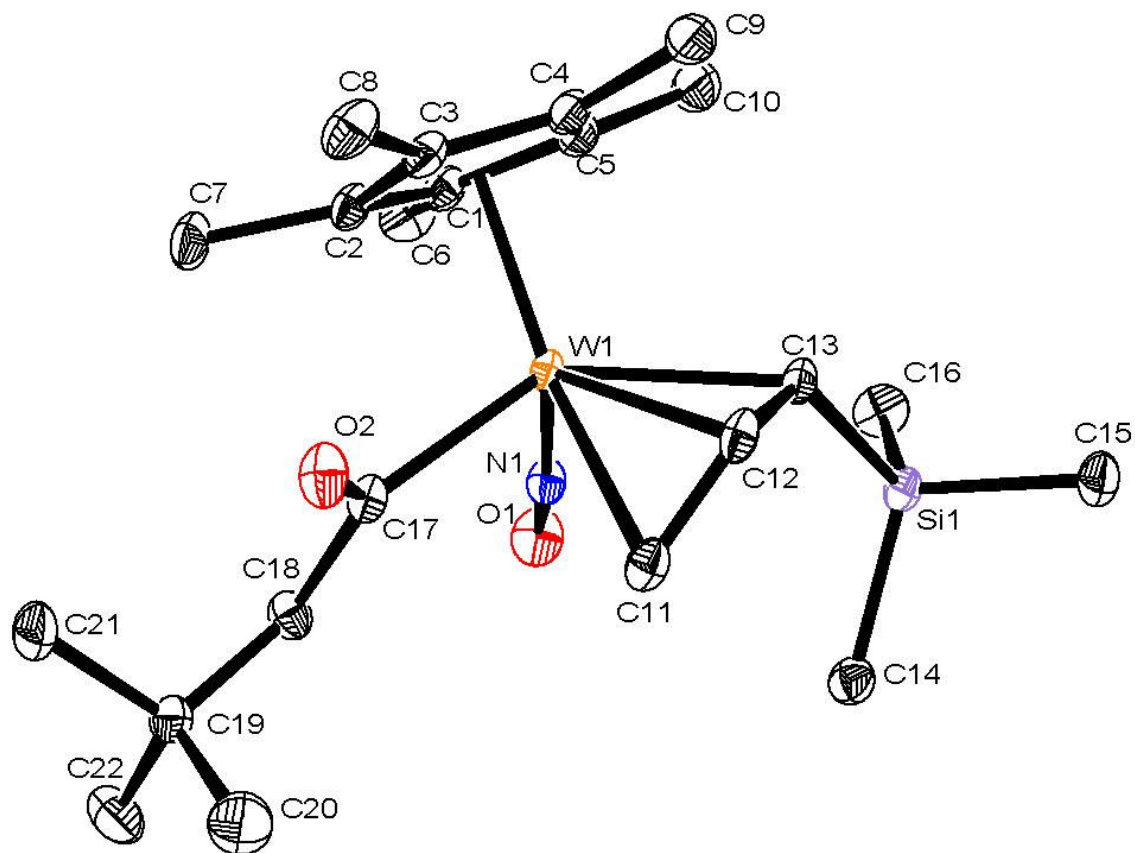


Figure 2.10. Solid-state molecular structure of one isomer of **2.11** with 50% probability thermal ellipsoids.

Selected interatomic distances (Å) and angles (deg): C(11)–W(1) = 2.4043(18); C(12)–W(1) = 2.2855(17); C(13)–W(1) = 2.3096(16); C(17)–W(1) = 2.2099(17); C(11)–C(12) = 1.392(3); C(12)–C(13) = 1.424(3); C(17)–O(2) = 1.221(2); N(1)–O(1) = 1.2188(19); N(1)–W(1) = 1.7784(14); C(11)–C(12)–C(13) = 122.10(16); O(1)–N(1)–W(1) = 170.48(14); O(2)–C(17)–W(1) = 121.61(13).

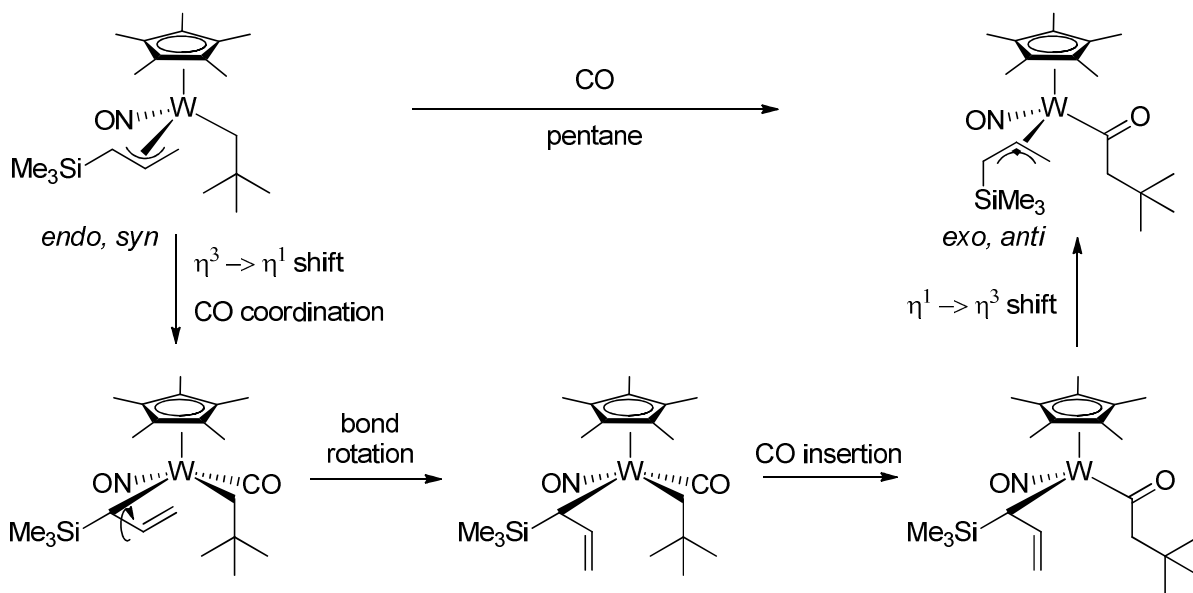
The η^1 -acyl formulation is well-supported by the metrical parameters of the solid-state molecular structure: the distance between W(1) and O(2) is 3.03 Å, significantly longer than the W(1)–C(17) bond at 2.2099 Å, and the O(2)–C(17)–W(1) angle is very close to

120°. If the acyl ligand in this complex were instead coordinated in an η^2 fashion through the C=O bond, one would expect the W–C and W–O bond lengths to be closer in value, and the O–C–W bond angle to be considerably less than 120°. This η^2 bonding mode has appeared in $\text{Cp}^*\text{Mo}(\text{NO})(\eta^2\text{-C(=O)Np})\text{Cl}$, which is electron deficient for an acyl ligand bound in an η^1 fashion (the η^2 binding mode brings the complex up to an 18e configuration.)³⁴ Additionally, the IR spectrum of **2.11** displays bands corresponding to NO and CO stretching frequencies at 1588 and 1633 cm^{-1} , respectively; the latter band is consistent with other complexes of this type.³⁰

Interestingly, the allyl ligand in complex **2.11** has shifted to an *exo, anti* coordination mode from its initial *endo, syn* mode in the starting material. This transformation is all the more unique for being the sole $\text{Cp}^*\text{W}(\text{NO})(\eta^3\text{-allyl})(\eta^1\text{-acyl})$ complex to exhibit an *exo, anti* allyl ligand in the solid state.³⁰ The *endo* to *exo* shift in bonding mode has been observed for some C–H activations by **2.1**, in particular those of fluorobenzenes (Chapter 4); however, a different mechanism must be responsible for the change in the allyl ligand upon carbonylation of the complex, since the *meso* hydrogen is not lost during this process.

The changing hapticity of the allyl ligand the most probable rationalization for the change in the allyl's coordination mode (Scheme 2.12). The *exo, anti* mode is likely favoured for steric reasons, since this allows the bulky SiMe_3 group to be placed as far from the Cp^* ring as possible.

Scheme 2.12. Mechanism for the *endo, syn* to *exo, anti* shift of the allyl ligand during the carbonylation of **2.1**.



Monitoring of the reaction by ¹H NMR spectroscopy (Figure 2.11) indicates that starting material is completely consumed in 75 minutes. The chemical shift of the resonance due to the *meso* proton on the allyl ligand shifts upfield upon carbonylation, reflecting the change in the electronic environment resulting from the formation of the acyl ligand.

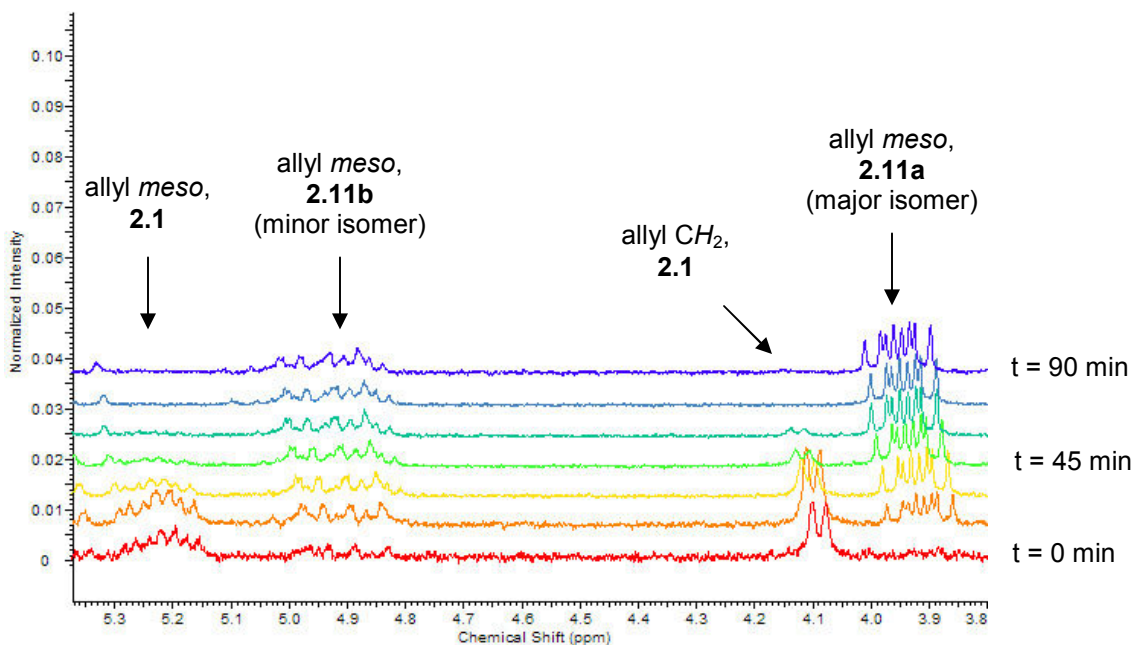


Figure 2.11. Stack plot of an expansion (3.80 to 5.35 ppm) of the ^1H NMR spectrum (300 MHz, C_6D_6) during the course of carbonylation of **2.1** to form **2.11**.

A sample was taken every 15 minutes.

Solution NMR spectra of the acyl complex indicate the existence of two products (**2.11a** and **2.11b**); these are likely isomers, as the ^1H NMR spectrum of a single crystal of **2.11** dissolved in C_6D_6 also shows this characteristic. A ROESY experiment has been conducted in order to assign the structure of the isomers based on the through-space correlation of protons close to one another. Regrettably, the complex also appears to be unstable in solution; upon standing at room temperature in a solution of C_6D_6 , some decomposition to an insoluble red residue occurs. Despite this transformation, sufficient amounts of **2.11a** remain in solution such that ROE crosspeaks between the signal arising from the allyl *meso* proton and the Cp^* Me groups as well the allyl CHSiMe_3 proton can be

observed. Together, these signals provide evidence for the major isomer in solution having the same structure as in the solid state.

However, crosspeaks in the ROESY spectrum also suggest that the isomers interconvert in solution, albeit on a slow enough timescale that they appear as two separate species in the ^1H NMR spectrum at room temperature. In a ROESY spectrum, the phase of the crosspeaks determines whether the cross-peak arises from a chemical exchange, ROE, or COSY correlation. In this case, a crosspeak at (3.90, 4.85) in the ROESY spectrum has the same phase relative to the diagonal (Figure 2.12a), confirming that the allyl *meso* protons in the two isomers are undergoing chemical exchange. The signal at 3.90 ppm provides an interesting case since it also displays an anti-phase COSY interaction (Figure 2.12b) to a signal at 3.35 ppm (arising from the CH_2 protons on the allyl), and an oppositely-phased ROE crosspeak (Figure 2.12c) at 1.57 ppm (arising from the Cp^* Me groups).

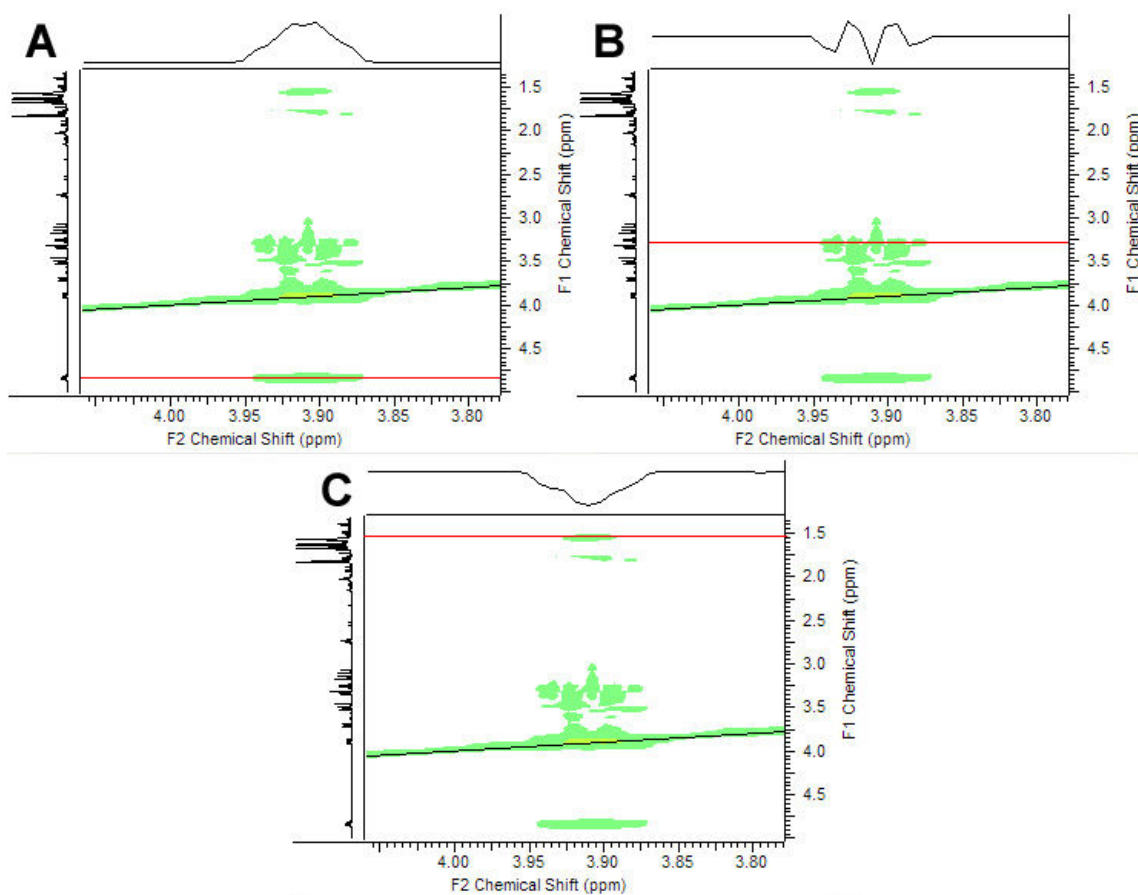


Figure 2.12. Expansions of the ROESY spectrum (600 MHz, C₆D₆) of **2.11**, focusing on the cross-peaks of the signal at 3.90 ppm between 2.5 and 5.5 ppm on the F1 axis.

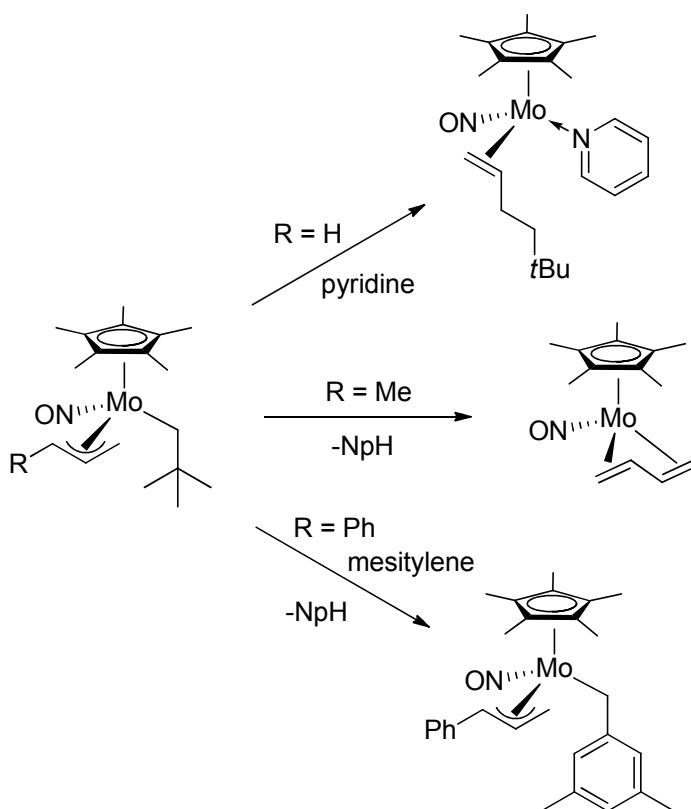
Along the F2 axis is displayed the horizontal slice of the ROESY NMR spectrum at the following F1 chemical shifts (highlighted in red): a) 4.85 ppm; b) 3.35 ppm; c) 1.57 ppm.

2.2.5 Congeneric Mo system

In order to investigate the effect of changing the metal centre on the reactivity of this complex, Cp*Mo(NO)(Np)(η^3 -CH₂CHCHSiMe₃) (**2.12**) has also been synthesized. Previous work (Scheme 2.13) has shown that the Mo congeners of the W systems exhibited limited C–H activating capability; instead, these systems have been observed to 1) couple the allyl and alkyl groups together in the presence of a Lewis base; 2) coordinate the other double bond of

a diene intermediate; and, 3) activate a benzylic C–H bond in low yield.^{29, 56} Since the only Cp*Mo(NO)(alkyl)(η^3 -allyl) complex which performed C–H activation would do so *via* a putative η^2 -allene intermediate,²⁹ similar to **2.1**, it was thought that the Mo congener of **2.1** would also be able to effect C–H activation. In addition, the change in the substituent on the allyl ligand might stabilize the reactive intermediate more than in the previously-investigated systems.

Scheme 2.13. Reactivity of various Cp*Mo(NO)(alkyl)(η^3 -allyl) systems.



2.2.5.1 Synthesis and structure of Cp*Mo(NO)(Np)(η^3 -CH₂CHCHSiMe₃)

The synthesis of **2.12**, Cp*Mo(NO)(Np)(η^3 -CH₂CHCHSiMe₃), proceeds fairly straightforwardly from Cp*Mo(NO)(Np)Cl and Li[CH₂CHCHSiMe₃]·TMEDA. Unlike its

yellow-orange W counterpart, the Mo complex is dull beige in colour. Fortunately, it appears to be stable in the solid state at room temperature, facilitating its isolation. A single-crystal X-ray crystallographic analysis has been performed, and the solid-state molecular structure of **2.12** is presented in Figure 2.13.

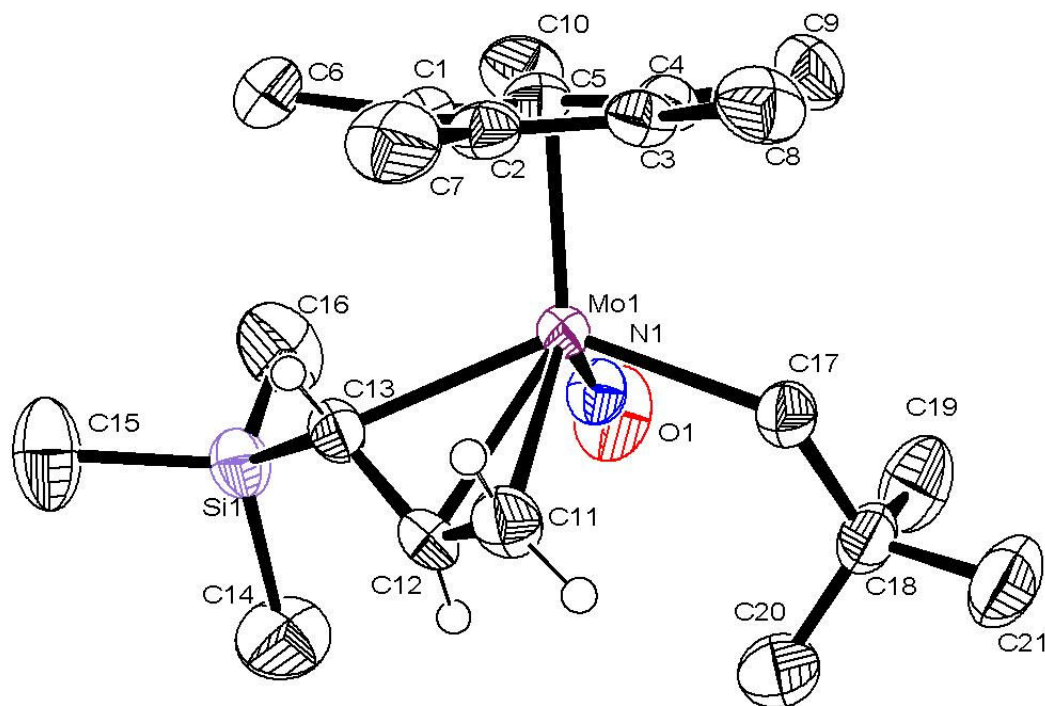


Figure 2.13. Solid-state molecular structure of **2.12** with 50% probability thermal ellipsoids.

Selected interatomic bond distances (Å) and angles (deg): C(11)–Mo(1) = 2.415(3); C(12)–Mo(1) = 2.329(2); C(13)–Mo(1) = 2.298(2); C(11)–C(12) = 1.362(4); C(12)–C(13) = 1.414(4); N(1)–O(1) = 1.210(3); N(1)–Mo(1) = 1.764(2); C(11)–C(12)–C(13) = 121.7(3); O(1)–N(1)–Mo(1) = 171.3(2).

This complex is isostructural with its W congener. Like the other members of the Cp*W(NO)(alkyl)(η^3 -allyl) family, it also displays a σ - π distortion in the allyl ligand. The C–

C bond lengths in the allyl ligand are slightly shorter than for the W analogue, which could indicate less backbonding from the Mo centre to the allyl ligand. In addition, the Mo centre appears to be more weakly backbonded to the NO ligand, judging from the increase in the ν_{NO} stretching frequency relative to the W compound (1604 cm^{-1} for Mo vs 1589 cm^{-1} for W). Finally, the metal–C_{allyl} bond lengths are shorter in the W congener than the Mo one. Taken together, these data suggest that the metal centre in the Mo congener is more electron-deficient than its W counterpart. Alternatively, these observations might also be explained by the decreased covalency of the Mo–C bond compared to the W–C bond.

2.2.5.2 Trapping experiment: PMe₃

In an attempt to trap the 16e intermediate implicated in C–H activation, **2.12** has been thermolyzed in neat PMe₃. Unlike the W systems, from which a single phosphorus-containing product can be isolated, the spectroscopic data for the Mo system indicate the presence of three organometallic products containing phosphorus. Column chromatography is only moderately successful at separating these three products; as a result, only one of them has been fully characterized. The product in question is the trapped η^2 -allene complex, Cp*Mo(NO)(η^2 -H₂C=C=CHSiMe₃)(PMe₃) (**2.13**), whose solid-state molecular structure is shown in Figure 2.14. Allene coordination to the Mo centre through the more substituted end of the ligand is supported both by the solid-state molecular structure as well as the ¹H NMR chemical shifts of the CH₂ protons (5.30 and 6.44 ppm), which fall in a downfield range typical for olefinic protons. This coordination mode is consistent with the observed solid-state structure for the W congener. Again, the relative electron deficiency of the Mo centre vs the W centre is evident from the ν_{NO} stretch, which is much higher in **2.13** than **2.9**, as well as

the bond length of the coordinated C–C bond, which is slightly shorter in **2.13** than **2.9**, both of which are indicative of less backbonding from the Mo centre.

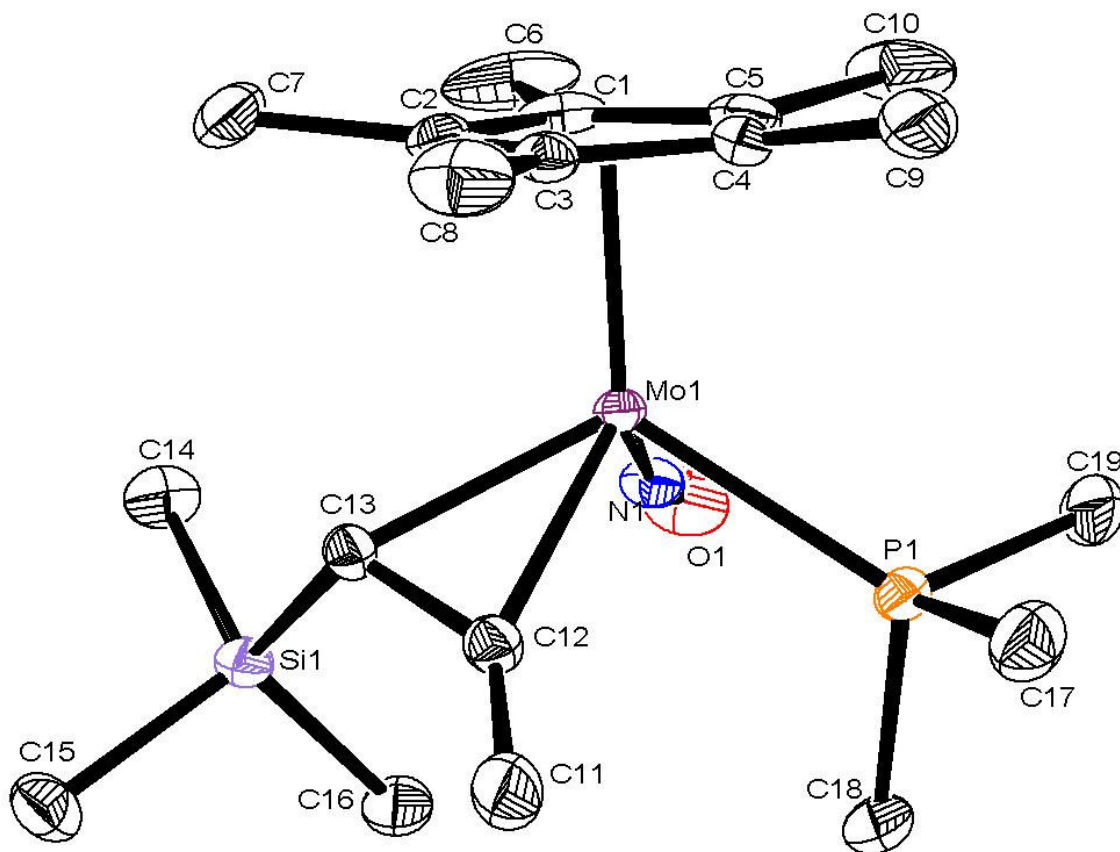


Figure 2.14. Solid-state molecular structure of **2.13** with 50% probability thermal ellipsoids.

Selected interatomic distances (Å) and angles (deg): C(12)–Mo(1) = 2.1808(14); C(13)–Mo(1) = 2.2261(13); P(1)–Mo(1) = 2.4588(4); C(11)–C(12) = 1.328(2); C(12)–C(13) = 1.423(2); N(1)–O(1) = 1.2234(17); N(1)–Mo(1) = 1.7871(13); C(11)–C(12)–C(13) = 137.65(15); O(1)–N(1)–Mo(1) = 168.88(12).

The identity of the other two products remains to be elucidated, but they could be the result of the allyl and neopentyl ligands coupling in the presence of a Lewis base, as was previously observed for $\text{Cp}^*\text{Mo}(\text{NO})(\text{Np})(\eta^3\text{-C}_3\text{H}_5)$.⁵⁶

2.2.5.3 Thermolysis of **2.12** in benzene

The trapping of the η^2 -allene intermediate indicates that **2.12** should be capable of C–H activation to regenerate an alkyl allyl complex. In order to establish the thermal chemistry of **2.12**, solutions of this complex in C_6D_6 have been heated and monitored by ^1H NMR spectroscopy. This complex reacts at or slightly above room temperature to give four organometallic hydrides after 2 hours. Unfortunately, since the NMR active isotopes of Mo have spin 5/2, molybdenum hydride resonances do not have the same characteristic satellites as hydrides of tungsten, whose NMR active isotope, ^{183}W , has spin 1/2. Their identification as hydride signals is therefore less certain than for the reaction with the W analogue; however, the upfield chemical shifts are fairly diagnostic for hydrides in these systems.

Having established the necessary conditions to effect complete conversion of **2.12**, this reaction has been repeated on a larger scale using C_6H_6 as solvent. A similar set of hydride peaks was observed in the upfield region below 0 ppm. While column chromatography proves ineffective at separating these products, two of the four products can be fractionally recrystallized from a pentane solution, facilitating their identification. Data from ^1H and COSY NMR experiments (Table 2.2) strongly suggest that the two products isolated in this way result from the activation of benzene and the migration of the phenyl ligand onto the allyl ligand, as depicted in Scheme 2.14. (A full discussion of this transformation for the tungsten congener is presented in Chapter 3.) Both low- and high-

resolution mass spectrometric data corroborate these conclusions; the low-resolution spectrum shows a $[M^+]$ signal at m/z 453 with a Mo isotope pattern, and the high-resolution measurement confirms the composition of $C_{22}H_{33}NOSi^{98}Mo$. Regrettably, these species are thermally unstable in solution, precluding their characterization by ^{13}C NMR spectroscopy.

Scheme 2.14. Selected products of benzene activation by **2.12**.

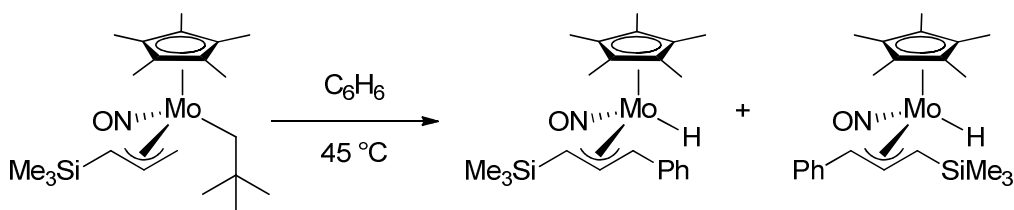


Table 2.2. Selected 1H NMR data for the products of C_6H_6 activation by **2.12**.

<i>Isomer 1</i>			<i>Isomer 2</i>		
δ (ppm)	Multiplicity, J (Hz)		δ (ppm)	Multiplicity, J (Hz)	
1.65	s	Cp* Me	1.58	s	
0.41	s	SiMe ₃	0.35	s	
-1.10	s	Mo-H	-0.68	s	
5.31	t, $J = 12.8$	Allyl <i>meso</i> H	4.22	dd, $J = 15.3, 11.9$	
0.49	d, $J = 12.8$	Allyl CHSiMe ₃	1.94	obscured	
2.69	d, $J = 13.1$	Allyl CHPh	5.03	d, $J = 15.4$	

Further characterization of the other products resulting from this reaction is difficult, as their purification remains challenging. Fortunately, thermolysis of **2.12** in other solvents provides some clues to the identity of these species.

2.2.5.4 Thermolysis of **2.12** in other solvents

The thermal chemistry of **2.12** with regards to alkanes has been assessed. Based on the results of the benzene experiments, it was found that heating for 2 h at 45 °C was sufficient to effect complete conversion of the starting material. That Mo complexes can perform the same chemistry as their W analogues under milder conditions has previously been established for complexes investigated by the Legzdins group.³⁴

In contrast to Cp*Mo(NO)(Np)(η^3 -CH₂CHCHPh), whose thermolysis in pentane leads to decomposition of the starting material,²⁹ **2.12** appears to form two hydrides. Comparison of the ¹H NMR spectra of these products with the four hydride products arising from the thermolysis of **2.12** in benzene reveals that these products have very similar chemical shifts to the two products not discussed in the preceding section (Table 2.3). Unlike the products resulting from the activation of benzene, these sets of signals each also includes a singlet around 1.0 ppm integrating to 9H that could be attributable to a neopentyl group. The second set of hydrides, therefore, could result from a migration of the neopentyl group onto the allyl ligand rather than the Ph group from activation of a molecule of benzene (Scheme 2.15).

Scheme 2.15. Proposed products for the thermolysis of **2.12** in pentane.

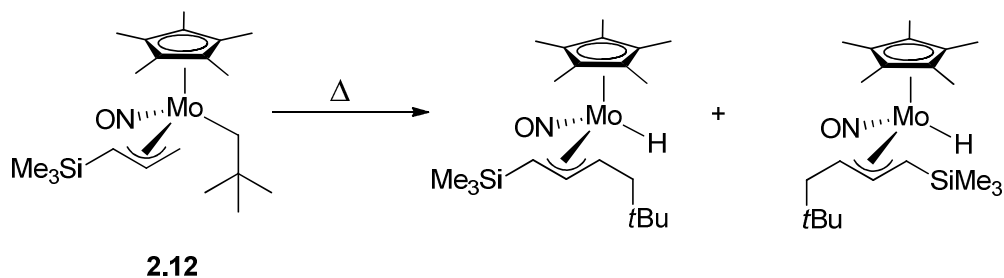


Table 2.3. Selected ^1H NMR signals from the products of the thermolysis of **2.12** in pentane.

<i>Product 1</i>		<i>Product 2</i>
δ (ppm)		δ (ppm)
1.74	$\text{Cp}^* \text{Me}$	1.69
0.39	SiMe_3	0.31
-1.71	Mo-H	-1.29
0.92	Np Me	1.04

Therefore, in **2.12**, migration of the neopentyl group competes with neopentane loss. In addition, the complex does not appear to activate aliphatic C-H bonds, as no evidence for a pentyl complex has been observed.

2.2.5.5 Investigation into the reaction pathways of **2.12**

Thermolysis of **2.12** in both benzene- d_6 and cyclohexane- d_{12} has been undertaken in order to compare the rates of benzene activation and the presumed neopentyl migration. Thermolysis of **2.12** in cyclohexane leads to the same hydride products as observed for pentane, lending credence to the hypothesis that these hydride products do not depend on the identity of the solvent and are probably the result of a self-reaction.

It has been previously established (Section 2.2.3.3) that the formation of the allene intermediate in the W congener **2.1** is a unimolecular reaction following pseudo-first-order kinetics. The rate-determining step in the formation of the other hydrides through migration of the neopentyl group (in essence an isomerization of the starting material) should also be first-order, since it is most likely an intramolecular reaction. Then, the rate law for the loss of

starting material is as follows, where $[Mo]$ is the concentration of **2.12**, and k_1 and k_2 are rate constants for the formation of the allene intermediate and the migration of the neopentyl ligand, respectively (Equation 2.1):

$$-\frac{d[Mo]}{dt} = (k_1 + k_2)[Mo] \quad (2.1)$$

Therefore, the pseudo-first-order rate constant k_{obs} for the consumption of **2.12** in benzene is composed of two components, k_1 and k_2 . This is borne out by tracking the loss of **2.12** when it is thermolyzed in benzene, which follows first-order kinetics consistent with Equation 2.1 (Figure 2.15).

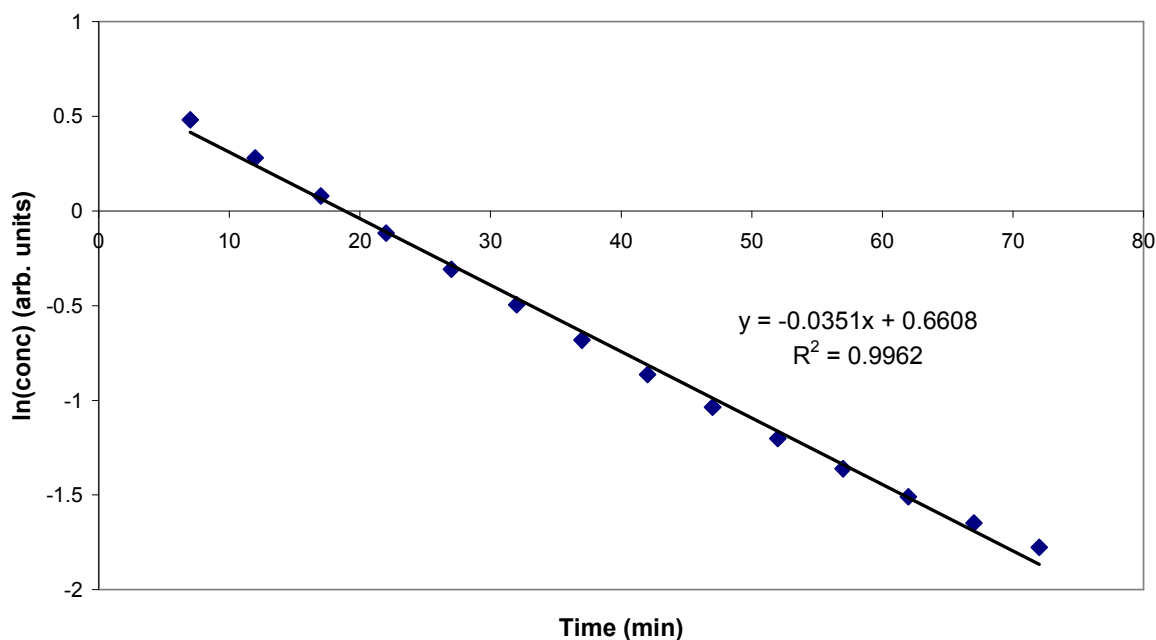


Figure 2.15. First-order kinetic plot of the thermolysis of **2.12** in C_6D_6 at 45 °C.

Because both routes are accessible when **2.12** is thermolyzed in benzene, the same experiments have been carried out in cyclohexane in order to measure k_2 alone. Table 2.4 presents the results of these experiments.

Table 2.4. Comparison of the rate constants for the consumption of **2.12** under thermolytic conditions.

Temperature (°C)	k_{obs} (s ⁻¹)	
	C ₆ D ₆	C ₆ D ₁₂
34.69	$(1.51 \pm 0.01) \times 10^{-4}$	$(1.13 \pm 0.03) \times 10^{-4}$
45.62	$(5.9 \pm 0.1) \times 10^{-4}$	$(3.8 \pm 0.1) \times 10^{-4}$

The k_{obs} for the consumption of **2.12** in C₆D₁₂ (which should represent k_2 only), is close to the value of k_{obs} in C₆D₆ (which is a sum of k_1 and k_2), implying that the neopentyl migration process is the favoured one—i.e., $k_2 > k_1$. This conclusion is consistent with the low overall yield for **2.13**, the PMe₃-trapped η^2 -allene complex. The traces in Figure 2.16, which present the relative distribution of products and starting material during the thermolysis of **2.12** in benzene, provide further evidence for this hypothesis. The major product from the thermolysis of **2.12** in benzene is the one in which the neopentyl ligand has migrated, and this is true for all timepoints: the product distribution remains fairly consistent over the course of the reaction.

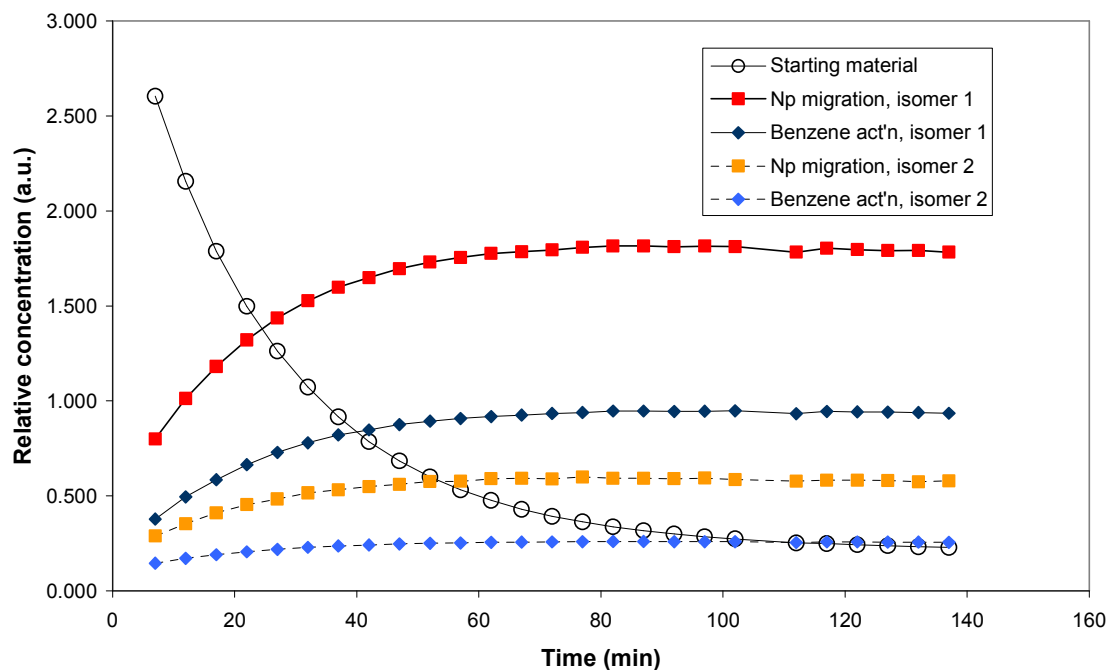


Figure 2.16. Monitoring loss of starting material and product formation during the thermolysis of **2.12** in C_6D_6 by 1H NMR spectroscopy.

Data from the timepoint at 107 minutes are omitted due to instrument error.

Examination of the Eyring parameters from these two sets of experiments also reveals some interesting contrasts. In particular, the entropy of activation, ΔS^\ddagger , is much more negative for the thermolysis in C_6D_{12} than C_6D_6 (Table 2.5); this is due to the difference in the transition state for the two transformations. The formation of the allene intermediate is entropically favoured due to the loss of neopentane; however, there is no such entropic driving force for the migration of the neopentyl ligand onto the allyl ligand. In fact, such a large negative value might even imply that the transition state is formed through an associative mechanism, but the kinetic data do not support second-order kinetics.

Table 2.5. Comparison of the Eyring parameters for the thermolysis of **2.12** in C₆D₆ and C₆D₁₂.

	C ₆ D ₆	C ₆ D ₁₂
ΔH^\ddagger (kJ mol ⁻¹)	101 ± 1	82 ± 3
ΔS^\ddagger (J mol ⁻¹ K ⁻¹)	10.3 ± 0.2	-53 ± 4
ΔG^\ddagger (kJ mol ⁻¹)	98 ± 1	98 ± 3

2.2.5.6 Attempted derivatization with CO

Finally, an attempt to derivatize the alkyl ligand with CO has been made, again using the neopentyl complex as a model for other alkyls. Because cyclohexane has been used successfully as an inert solvent for the carbonylation of **2.1** at room temperature, these conditions have been replicated in the attempted carbonylation of **2.13**. However, the assumption that the Mo system would react the same way as the W system in this case was incorrect. After two hours at room temperature under 400 psig CO pressure, only starting material is recovered, with no evidence of CO incorporation. This could be due to the more electron-deficient nature of the Mo systems compared to the W systems, as indicated by their relative ν_{NO} IR stretching frequencies (1604 cm⁻¹ for Mo vs 1589 cm⁻¹ for W). The conventional mechanism for carbonylation involves CO coordination followed by migratory insertion of an alkyl ligand. In order for CO to coordinate to the metal centre, there must be an empty coordination site on the metal; however, the Cp*M(NO)(alkyl)(η^3 -allyl) systems are both electronically and coordinatively saturated. Changing the allyl's coordination mode from η^3 to η^1 both frees up a coordination site and reduces the complex's formal electron

count from 18e to 16e. However, this also reduces electronic donation from the ligand to the metal centre, and it appears that in the case of Mo, this shift does not occur due to the intrinsic electron poverty at the metal centre.

2.3 Experimental procedures

2.3.1 Preparation of $\text{Cp}^*\text{W}(\text{NO})(\text{Np})(\eta^3\text{-CH}_2\text{CHCHSiMe}_3)$ (**2.1**).

$\text{Li}[\text{CH}_2\text{CHCHSiMe}_3]\cdot\text{TMEDA}$ was prepared by a method similar to that previously reported.⁵⁷ $\text{Me}_3\text{SiCH}_2\text{CHCH}_2$ (6.4 mL [40 mmol] in 10 mL Et_2O) was added to a mixture of $n\text{BuLi}\cdot\text{TMEDA}$ (6.0 mL TMEDA in 25 mL 1.6 M $n\text{BuLi}$ in hexanes) at 0 °C. The molarity of the resulting organolithium reagent was analyzed by titration with a standard solution of 0.1 M $s\text{BuOH}$ in toluene and 1,10-phenanthroline.

$\text{Cp}^*\text{W}(\text{NO})(\text{Np})\text{Cl}$ (2.49 g, 5.28 mmol) was dissolved in Et_2O (ca. 20 mL) to obtain a dark purple solution. This solution was frozen at -196 °C, and a solution of $\text{Li}[\text{CH}_2\text{CHCHSiMe}_3]\cdot\text{TMEDA}$ as prepared above (7.3 mL, 0.72 M, 5.26 mmol) was added by syringe. The reaction mixture was slowly warmed, and stirring was initiated as soon as it was feasible. The resulting orange-brown solution was stirred for 1.5 h at room temperature. The solvent was removed in vacuo to give a yellow solid. The solid was redissolved in 1:1 pentane/ Et_2O , and this solution was transferred onto an alumina column (3 x 7 cm). Elution of the column with the same solvent mixture produced a yellow-orange band which was collected. Removal of solvent from the eluate in vacuo afforded **2.1** as a yellow-orange solid (1.00 g, 35% yield). Single crystals suitable for X-ray diffraction were grown from an Et_2O solution maintained at -30 °C.

Characterization data for **2.1**: IR (cm^{-1}) 1589 (s, ν_{NO}). ^1H NMR (400 MHz, C_6D_6) δ 0.21 (d, 1H, $^3J_{\text{HH}} = 14.1$, CHSiMe_3), 0.35 (s, 9H, SiMe_3), 0.88 (d, 1H, $^2J_{\text{HH}} = 12.1$, Np CH_2), 1.30 (s, 9H, Np *Me*), 1.49 (s, 15H, Cp* *Me*), 1.72 (d, 1H, $^2J_{\text{HH}} = 12.1$, Np CH_2), 2.02 (d, 1H, $^3J_{\text{HH}} = 14.1$, allyl CH_2), 4.09 (d, 1H, $^3J_{\text{HH}} = 6.7$, allyl CH_2), 5.20 (td, 1H, $^3J_{\text{HH}} = 13.1$, 7.0, allyl *meso*). ^{13}C NMR (100 MHz, C_6D_6) δ 2.0 (SiMe_3), 10.3 (C_5Me_5), 27.4 (Np CH_2), 35.2 (Np *Me*), 39.7 (Np CMe_3), 43.6 (CHSiMe_3), 84.6 (allyl CH_2), 106.9 (C_5Me_5), 117.6 (allyl *meso* CH). MS (LREI, m/z , probe temperature 120 $^\circ\text{C}$) 533 [M^+ , ^{184}W]. Anal. Calcd for $\text{C}_{21}\text{H}_{39}\text{NOSiW}$: C, 47.28; H, 7.37; N, 2.63. Found: C, 47.64; H, 7.34; N, 2.28.

2.3.2 Preparation of $\text{Cp}^*\text{W}(\text{NO})((\text{CH}_2)_4\text{CH}_3)(\eta^3\text{-CH}_2\text{CHCHSiMe}_3)$ (**2.2**).

2.1 (280 mg, 0.525 mmol) was thermolyzed in pentane for 2 d at 55 $^\circ\text{C}$. The solvent was removed in vacuo to give an orange-brown oil, which was taken up in 4:1 pentane/ Et_2O and transferred onto a basic alumina column supported on a glass frit (2 x 5 cm). Elution of the column with this solvent mixture produced a peach-coloured band, from which the solvent was removed to leave **2.2** as an orange oil (185 mg, 66%).

Characterization data for **2.2**: IR (cm^{-1}) 1596 (s, ν_{NO}). ^1H NMR (400 MHz, C_6D_6) δ 0.25 (d, 2H, $^3J_{\text{HH}} = 12.1$, CHSiMe_3), 0.33 (s, 9H, SiMe_3), 1.01 (t, $^3J_{\text{HH}} = 7.0$, 3H, pentyl *Me*), 1.26 (m, 1H, metal-bound pentyl CH_2), 1.47 (m, 2H, pentyl CH_2), 1.50 (m, 2H, pentyl CH_2), 1.52 (s, 15H, Cp* *Me*), 1.54 (m, 2H, pentyl CH_2), 1.92 (dd, 1H, $^3J_{\text{HH}} = 13.9$, $^2J_{\text{HH}} = 1.0$, allyl CH_2), 2.00 (m, 1H, metal-bound pentyl CH_2), 3.62 (d, 1H, $^3J_{\text{HH}} = 7.0$, allyl CH_2), 5.04 (ddd, 1H, $^3J_{\text{HH}} = 13.7$, 11.9, 6.8, allyl *meso*). ^{13}C NMR (100 MHz, C_6D_6) δ 1.9 (SiMe_3), 10.3 (C_5Me_5), 15.1 (pentyl *Me*), 16.8 (pentyl CH_2), 23.3 (pentyl CH_2), 33.4 (pentyl CH_2), 40.3 (pentyl CH_2), 45.3 (CHSiMe_3), 84.5 (allyl CH_2), 106.2 (C_5Me_5), 111.8 (allyl *meso* CH). MS

(LREI, m/z , probe temperature 120 °C) 533 [M^+ , ^{184}W]; (HREI, m/z , ^{182}W) Calcd: 531.22832.

Found: 531.22815.

2.3.3 Preparation of $Cp^*W(NO)(\eta^3-CH_2CHCHSiMe_3)(CH_2Cy)$ (**2.3**).

2.1 (115 mg, 0.216 mmol) was thermolyzed in methylcyclohexane at 55 °C for 2 d.

2.3 was purified by the same procedure as **2.2** (17 mg, 14% yield).

Characterization data for **2.3**: IR (cm^{-1}) 1568 (s, ν_{NO}). 1H NMR (300 MHz, C_6D_6): δ 0.28 (obscured, 1H, $CHSiMe_3$), 0.34 (s, 9H, $SiMe_3$), 0.92 (obscured, 1H, CH_2Cy), 1.15 (obscured, 1H, CH_2Cy), 1.16 (obscured, 1H, Cy CH_2), 1.39 (br m, 2H, Cy CH_2), 1.40 (m, 1H, Cy CH), 1.48 (obscured, 2H, Cy CH_2), 1.50 (s, 15H, $Cp^* Me$), 1.68 (br m, 2H, Cy CH_2), 1.86 (br m, 3H, Cy CH_2), 1.94 (dd, 1H, $^3J_{HH} = 13.8$, $^4J_{HH} = 1.1$, allyl CH_2), 2.52 (d, 1H, $^2J_{HH} = 12.4$, Cy CH_2), 3.83 (d, 1H, $^3J_{HH} = 6.9$, allyl CH_2), 5.09 (ddd, 1H, $^3J_{HH} = 13.8$, 11.8, 7.0, allyl *meso*). ^{13}C NMR (75 MHz, C_6D_6) δ 1.2 ($SiMe_3$), 9.5 (C_5Me_5), 23.4 (CH_2Cy), 26.95 (CH_2), 27.03 (CH_2), 27.3 (CH_2), 36.8 (CH_2), 41.7 (CH_2), 43.9 (Cy CH), 44.8 ($CHSiMe_3$), 83.4 (allyl CH_2), 105.7 (C_5Me_5), 112.2 (allyl *meso*). MS (LREI, m/z , probe temperature 120 °C) 559 [M^+ , ^{184}W]; (HREI, m/z , ^{182}W) Calcd: 557.24397. Found: 557.24437.

2.3.4 Competition study for the activation of pentane and cyclohexane by **2.1**.

2.1 (50 mg, 0.094 mmol) was thermolyzed at 55 °C for 1 d in a 1:1 equimolar mixture of cyclohexane and pentane. Following removal of the solvent in vacuo, analysis of the crude reaction mixture by 1H NMR spectroscopy indicated that the primary organometallic product was the *n*-pentyl complex, **2.2**.

2.3.5 Preparation of Cp*W(NO)(Me)(η^3 -CH₂CHCHSiMe₃) (2.4).

2.1 (165 mg, 0.309 mmol) was dissolved in dry cyclohexane (ca. 100 mL) to obtain a yellow solution. The solution was transferred to a Parr pressure reactor and pressurized to 1000 psig CH₄ after three purge cycles with this gas. The reaction mixture was heated to 55 °C and stirred for 2 d. The solvent was subsequently removed in vacuo to give a brown oil. This oil was dissolved in a minimum of 4:1 pentane/Et₂O and transferred onto a silica column (2 x 5 cm) supported on a glass frit. A yellow band was eluted with 4:1 pentane/Et₂O, from which the solvent was removed in vacuo to give **2.4** as a yellow solid (65 mg, 44% yield).

Characterization data for **2.4**: IR (cm⁻¹) 1589 (s, ν_{NO}). ¹H NMR (300 MHz, C₆D₆): δ 0.20 (d, ³*J*_{HH} = 12.3, 1H, CHSiMe₃), 0.34 (s, 9H, SiMe₃), 0.39 (s, 3H, CH₃), 1.52 (s, 15H, Cp* Me), 1.88 (dd, 1H, ³*J*_{HH} = 13.8, ²*J*_{HH} = 1.3, allyl CH₂), 3.41 (d, 1H, ³*J*_{HH} = 7.0, allyl CH₂), 4.93 (ddd, 1H, ³*J*_{HH} = 13.8, 12.0, 6.9, allyl *meso*). ¹³C NMR (100 MHz, C₆D₆) δ 2.0 (SiMe₃), 3.8 (CH₃), 10.4 (C₅Me₅), 45.6 (CHSiMe₃), 84.4 (allyl CH₂), 106.2 (C₅Me₅), 111.2 (allyl *meso*). MS (LREI, *m/z*, probe temperature 120 °C) 477 [M⁺, ¹⁸⁴W]; (HREI, *m/z*, ¹⁸⁴W) Calcd: 477.16845. Found: 477.16816.

2.3.6 Preparation of Cp*W(NO)(Et)(η^3 -CH₂CHCHSiMe₃) (2.5).

2.1 (224 mg, 0.420 mmol) was dissolved in dry cyclohexane (ca. 100 mL) to obtain a yellow solution. The solution was transferred to a Parr pressure reactor and pressurized to 500 psig ethane after three purge cycles with this gas. The reaction mixture was stirred at 55 °C for 24 h before the solvent was removed in vacuo to give an orange-brown oil. After filtration through Celite, the remaining dark orange oil was dissolved in a minimum of 2:1

pentane/Et₂O and transferred onto a silica column (2 x 5 cm) supported on a frit. An orange band was eluted with 4:1 pentane/Et₂O, from which the solvent was removed under vacuum to give an orange solid, **2.5** (81 mg, 39% yield).

Characterization data for **2.5**: IR (cm⁻¹) 1596 (s, ν_{NO}). ¹H NMR (400 MHz, C₆D₆): δ 0.25 (d, 1H, ³*J*_{HH} = 11.7, CHSiMe₃), 0.33 (s, 9H, SiMe₃), 1.16 (q, 2H, ³*J*_{HH} = 7.4, CH₂CH₃), 1.51 (s, 15H, Cp* Me), 1.64 (t, 3H, ³*J*_{HH} = 7.3, CH₂CH₃), 1.89 (dd, 1H, ³*J*_{HH} = 13.7, ²*J*_{HH} = 1.2, allyl CH₂), 3.59 (d, 1H, ³*J*_{HH} = 6.8, allyl CH₂), 5.03 (ddd, 1H, ³*J*_{HH} = 13.7, 11.9, 6.8, allyl *meso*). ¹³C NMR (100 MHz, C₆D₆) δ 1.9 (SiMe₃), 8.7 (CH₂CH₃), 10.3 (C₅Me₅), 17.7 (CH₂CH₃), 45.3 (CHSiMe₃), 84.6 (allyl CH₂), 106.2 (C₅Me₅), 111.4 (allyl *meso*). MS (LREI, *m/z*, probe temperature 120 °C) 491 [M⁺, ¹⁸⁴W]; (HREI, *m/z*, ¹⁸⁴W) Calcd: 491.18410. Found: 491.18423.

2.3.7 Preparation of Cp*W(NO)(CH₂-3,5-Me₂C₆H₃)(η^3 -CH₂CHCHSiMe₃) (**2.6**).

2.1 (90 mg, 0.17 mmol) was thermolyzed in mesitylene (ca. 15 mL). After heating for 2 d at 55 °C, volatiles were removed from the reaction mixture to give an orange oil. Recrystallization from 1:1 pentane/Et₂O yielded an orange solid, **2.6** (30 mg, 31% yield).

Characterization data for **2.6**: IR (cm⁻¹) 1562 (m, ν_{NO}). ¹H NMR (400 MHz, C₆D₆): δ 0.23 (s, 9H, SiMe₃), 0.40 (d, 1H, ³*J*_{HH} = 12.1, CHSiMe₃), 1.52 (s, 15H, Cp* Me), 1.98 (d, 1H, ³*J*_{HH} = 14.1, allyl CH₂), 2.02 (d, 1H, ²*J*_{HH} = 9.0, aryl CH₂), 2.32 (s, 6H, aryl Me), 2.86 (d, 1H, ²*J*_{HH} = 9.0, aryl CH₂), 3.91 (d, 1H, ³*J*_{HH} = 6.7, allyl CH₂), 4.48 (td, 1H, ³*J*_{HH} = 12.7, 6.7, allyl *meso*), 6.66 (s, 1H, *para* CH), 7.20 (s, 2H, *ortho* CH). ¹³C NMR (100 MHz, C₆D₆) δ 1.6 (SiMe₃), 10.3 (C₅Me₅), 21.0 (aryl CH₂), 22.2 (aryl Me), 47.2 (CHSiMe₃), 88.1 (allyl CH₂), 106.6 (C₅Me₅), 114.3 (allyl *meso*), 125.8 (*para* CH), 127.5 (*ortho* CH), 136.8 (*meta* CMe),

152.8 (*ipso* C). MS (LREI, m/z , probe temperature 120 °C) 581 [M^+ , ^{184}W]; (HREI, m/z , ^{182}W) Calcd: 579.22832. Found: 579.22793. Anal. Calcd for $C_{25}H_{39}NOSiW$: C, 51.64; H, 6.76; N, 2.41. Found: C, 51.95; H, 6.87; N, 2.49.

2.3.8 Preparation of $Cp^*W(NO)(CH_2SiMe_3)(\eta^3-CH_2CHCHSiMe_3)$ (**2.7**).

Tetramethylsilane (ca. 25 mL) was added to **2.1** (170 mg, 0.319 mmol) to obtain an orange suspension. After heating for 1 d at 55 °C, the reaction mixture changed colour to a bright yellow solution. Volatiles were removed in vacuo to give an orange oil. This oil was taken up in Et_2O and filtered through silica; the solvent was removed from the orange filtrate to give an orange solid, **2.7** (136 mg, 78% yield).

Characterization data for **2.7**: IR (cm^{-1}) 1561 (m, ν_{NO}). 1H NMR (400 MHz, C_6D_6): δ -0.58 (d, 1H, $^2J_{HH} = 11.9$, CH_2SiMe_3), 0.03 (d, 1H, $^2J_{HH} = 11.9$, CH_2SiMe_3), 0.31 (obscured d, $^3J_{HH} = 12.3$, 1H, $CHSiMe_3$), 0.34 (s, 9H, allyl $SiMe_3$), 0.35 (s, 9H, CH_2SiMe_3), 1.49 (s, 15H, $Cp^* Me$), 1.99 (d, 1H, $^3J_{HH} = 14.1$, allyl CH_2), 3.81 (d, 1H, $^3J_{HH} = 7.0$, allyl CH_2), 5.27 (ddd, 1H, $^3J_{HH} = 13.8$, 12.2, 7.0, allyl *meso*). ^{13}C NMR (100 MHz, C_6D_6) δ -6.0 (CH_2SiMe_3), 2.0 (allyl $SiMe_3$), 4.3 (CH_2SiMe_3), 10.4 (C_5Me_5), 44.2 ($CHSiMe_3$), 84.3 (allyl CH_2), 106.9 (C_5Me_5), 116.3 (allyl *meso*). MS (LREI, m/z , probe temperature 120 °C) 549 [M^+ , ^{184}W]; (HREI, m/z , ^{182}W) Calcd: 547.20525. Found: 547.20534.

2.3.9 Preparation of $Cp^*W(NO)(CH_2CH_2OCH_2CH_3)(\eta^3-CH_2CHCHSiMe_3)$ (**2.8**).

2.1 (85 mg, 0.16 mmol) was dissolved in Et_2O (ca. 9 mL) to obtain an orange solution. The reaction mixture was heated at 65 °C for 24 h. Subsequently, the solvent was removed in vacuo, leaving **2.8** as a dark orange oil (80 mg, 94% yield).

Characterization data for **2.8**: IR (cm⁻¹) 1592 (s, ν_{NO}). ¹H NMR (400 MHz, C₆D₆): δ 0.16 (d, 1H, ³*J*_{HH} = 11.7, CHSiMe₃), 0.30 (s, 9H, SiMe₃), 1.26 (t, 3H, ³*J*_{HH} = 7.0, CH₂CH₃), 1.36 (m, 1H, CH₂CH₂O), 1.48 (s, 15H, Cp* Me), 1.53 (m, 1H, CH₂CH₂O), 1.85 (d, 1H, ³*J*_{HH} = 13.1, allyl CH₂), 3.32 (ddd, 1H, ²*J*_{HH} = 11.9, ³*J*_{HH} = 9.6, 4.0, CH₂CH₂O), 3.50 (overlapping q, 2H, ³*J*_{HH} = 7.0, CH₂CH₃), 3.77 (d, 1H, ³*J*_{HH} = 6.9, allyl CH₂), 3.98 (ddd, 1H, ²*J*_{HH} = 11.4, ³*J*_{HH} = 9.8, 5.6, CH₂CH₂O), 4.99 (ddd, 1H, ³*J*_{HH} = 13.8, 12.0, 6.9, allyl *meso*). ¹³C NMR (100 MHz, C₆D₆) δ 1.9 (SiMe₃), 10.3 (C₅Me₅), 14.3 (CH₂CH₂O), 16.6 (CH₂CH₃), 44.9 (allyl CHSiMe₃), 65.4 (CH₂CH₃), 76.3 (CH₂CH₂O), 84.1 (allyl CH₂), 106.7 (C₅Me₅), 113.0 (allyl *meso*). MS (LREI, *m/z*, probe temperature 120 °C) 535 [M⁺, ¹⁸⁴W]; (HREI, *m/z*, ¹⁸²W) Calcd: 533.20758. Found: 533.20784.

2.3.10 Thermolyses of 2.1 in *n*PrOH and 1-butyraldehyde.

2.1 (100 mg, 0.19 mmol) was thermolyzed in either neat *n*PrOH or 1-butyraldehyde (ca. 5 mL). After removal of solvent, the only organometallic product detected was Cp*W(O)₂(Np), which was identified by its characteristic ¹H NMR spectrum:^{51, 58} (300 MHz, C₆D₆) δ 1.34 (s, 9H, Np Me), 1.61 (s, 2H, Np CH₂), 1.65 (s, 15H, Cp* Me).

2.3.11 Preparation of Cp*W(NO)(PMe₃)(η^2 -CH₂=C=CHSiMe₃) (**2.9**).

2.1 (86 mg, 0.16 mmol) was dissolved in neat PMe₃ (ca. 5 mL) to obtain an orange solution. The reaction mixture was heated at 55 °C for 24 h. Subsequently, the volatiles were removed in vacuo, leaving an orange solid. This residue was taken up in 1:1 pentane/Et₂O and transferred to a silica column (0.5 cm x 4 cm). Elution with Et₂O produced an orange band, which was collected. An orange oil (30 mg, 35%) remained after removal of solvent

from the eluate. Single crystals suitable for X-ray diffraction were grown from a 1:1 pentane/Et₂O mixture maintained at −30 °C.

Characterization data for **2.9**: IR (cm^{−1}) 1525 (s, ν_{NO}), 1625 (m, $\nu_{\text{C}=\text{C}}$). ¹H NMR (300 MHz, C₆D₆): δ 0.06 (m, 1H, *CHSiMe₃*), 0.42 (s, 9H, *SiMe₃*), 1.25 (d, 9H, ²*J*_{HP} = 9.1, *PMe₃*), 1.67 (s, 15H, Cp* *Me*), 5.53 (dt, 1H, ²*J*_{HH} = 3.5, ⁴*J*_{HH} = 2.5, allene *CH₂*), 6.85 (m, 1H, allene *CH₂*). ¹³C NMR (75 MHz, C₆D₆): δ 1.7 (*SiMe₃*), 10.8 (*C₅Me₅*), 17.3 (d, ¹*J*_{CP} = 31, *PMe₃*), 33.4 (*CHSiMe₃*), 105.1 (d, ³*J*_{CP} = 8, allene *CH₂*), 105.3 (*C₅Me₅*), 184.0 (allene *C*). ³¹P{¹H} NMR (125 Hz, C₆D₆): δ −9.5 (¹*J*_{WP} = 348). MS (LREI, *m/z*, probe temperature 120 °C) 537 [*M*⁺, ¹⁸⁴W]; (HREI, *m/z*, ¹⁸²W) Calcd: 535.17961. Found: 535.17847.

2.3.12 Preparation of Cp*W(NO)(H)(η^3 -CH₂C(3-cyclohexenyl)CHSiMe₃) (**2.10**).

2.1 (0.118 g, 0.221 mmol) was dissolved in cyclohexene (ca. 8 mL) to obtain an orange solution. The reaction mixture was heated at 55 °C for 48 h. Subsequently, the solvent was removed in vacuo to give a brown oil. **2.10** was recrystallized from a 1:1 pentane/Et₂O mixture maintained at −30 °C as yellow crystals (30 mg, 25% yield).

Characterization data for **2.10**: IR (cm^{−1}) 1563 (s, ν_{NO}), 1925 (m, ν_{WH}). ¹H NMR (400 MHz, C₆D₆): δ −1.61 (s, 1H, ¹*J*_{WH} = 114, W−*H*), 0.11 (d, 1H, ⁴*J*_{HH} = 0.8, allyl *CHSiMe₃*), 0.48 (s, 9H, *SiMe₃*), 0.55 (s, 1H, allyl *CH₂*), 1.40 (m, 2H, cyclohexenyl *CH₂*), 1.63 (br s, 1H, cyclohexenyl *CH₂*), 1.78 (s, 15H, Cp* *Me*), 1.85 (br s, 2H, cyclohexenyl *CH₂*), 2.01 (d, 1H, ²*J*_{HH} = 12.3, cyclohexenyl *CH₂*), 3.08 (m, 1H, cyclohexenyl *CH*), 4.46 (t, 1H, *J* = 1.8, allyl *CH₂*), 5.74 (m, 1H, *CH=CH*), 6.10 (dd, 1H, ³*J*_{HH} = 10.1, ⁴*J*_{HH} = 1.7, *CH=CH*). ¹³C NMR (100 MHz, C₆D₆) δ 3.8 (*SiMe₃*), 11.4 (*C₅Me₅*), 23.4 (cyclohexenyl *CH₂*), 26.0 (cyclohexenyl *CH₂*), 26.9 (cyclohexenyl *CH₂*), 42.9 (cyclohexenyl *CH*), 50.9 (allyl *CHSiMe₃*), 56.1 (allyl *CH₂*),

105.0 (C_5Me_5), 127.4 ($CH=CH$), 130.2 (allyl *meso*), 135.4 ($CH=CH$). MS (LREI, m/z , probe temperature 120 °C) 543 [M^+ , ^{184}W]; (HREI, m/z , ^{184}W) Calcd: 543.21540. Found: 543.21506.

2.3.13 Monitoring the thermolytic consumption of **2.1** by 1H NMR spectroscopy.

A sample of **2.1** (10 mg, 0.019 mmol) was dissolved in C_6D_6 (ca. 700 μL) and transferred to a J. Young NMR tube. The NMR probe was heated to the desired temperature, and spectra were acquired every 5 minutes. The solvent signal at 7.16 ppm was used as an internal standard, and the decrease in the area of the signal at 1.30 ppm (corresponding to Np Me groups) was used to track the loss of the reactant. Errors in the rate constants were estimated from the standard error in the linear regression of the data. Errors in the temperature of the probe were estimated to be ± 0.5 °C.

2.3.14 Attempted carbonylation of **2.2**.

In a stainless steel Parr reactor, a solution of **2.2** (175 mg, 0.30 mmol) in cyclohexane (ca. 100 mL) was pressurized to 500 psig CO after three purge cycles with this gas. The reaction mixture was stirred at room temperature (approximately 22 °C) for 24 h, then heated at 35 °C and 55 °C for 24 h at each temperature. Aliquots of the reaction mixture were taken at various timepoints to determine the course of the reaction. After three days of reaction time, the solvent was removed in vacuo. One product was isolated by column chromatography on silica (2 x 5 cm), using 10:1 pentane/ Et_2O as eluent (56 mg). The product was not fully characterized but spectral evidence suggested the incorporation of two molecules of CO into **2.2**.

Partial characterization data: IR (cm^{-1}): 1603 (s, ν_{NO}), 1689 (m, ν_{CO}), 1960 (s, ν_{CO}). ^1H NMR (400 MHz, C_6D_6): δ 0.14 (s, 9H, SiMe_3), 1.75 (s, 15H, $\text{Cp}^* \text{Me}$), 3.05 (ddd, 1H, $^3J_{\text{HH}} = 18.4, 8.6, 5.7$, allyl *meso*). ^{13}C NMR (100 MHz, C_6D_6): δ 1.5 (SiMe_3), 10.4 (C_5Me_5), 105.3 (C_5Me_5), 211.8 (CO), 226.2 (CO). MS (LREI, m/z , probe temperature 120 °C) 589 [M^+ , (**2.2** + 2CO), ^{184}W], 561 [$\text{M}^+ - \text{CO}$, (**2.2** + CO), ^{184}W].

2.3.15 Preparation of $\text{Cp}^*\text{W}(\text{NO})(\eta^1\text{-C(=O)Np})(\eta^3\text{-CH}_2\text{CHCHSiMe}_3)$ (**2.11**).

2.1 (255 mg, 0.43 mmol) was dissolved in cyclohexane (ca. 100 mL) to obtain a yellow solution. This solution was transferred to a pressure reactor, which underwent three purge cycles with CO before being pressurized to 500 psig with this gas. The reaction mixture was stirred for 2 h at RT. Solvent was removed in vacuo to give an orange solid. Crystallization from 2:1 pentane/ Et_2O at -30 °C resulted in the deposition of **2.11** (160 mg, 60%) as orange crystals.

Characterization data for **2.11**: IR (cm^{-1}) 1588 (s, ν_{NO}), 1633 (m, ν_{CO}). ^1H NMR (400 MHz, C_6D_6): Major isomer, **2.11a**: δ 0.25 (s, 9H, SiMe_3), 1.22 (s, 9H, Np *Me*), 1.58 (s, 15H, $\text{Cp}^* \text{Me}$), 1.81 (dd, 1H, $^3J_{\text{HH}} = 10.8$, $^4J_{\text{HH}} = 2.0$, allyl CHSiMe_3), 3.14 (d, 1H, $^2J_{\text{HH}} = 18.6$, Np CH_2), 3.33 (d, 1H, $^3J_{\text{HH}} = 8.1$, allyl CH_2), 3.47 (d, 1H, $^2J_{\text{HH}} = 17.5$, Np CH_2), 3.51 (d, 1H, $^3J_{\text{HH}} = 14.7$, allyl CH_2), 3.91 (ddd, 1H, $^3J_{\text{HH}} = 14.9, 10.8, 8.2$, allyl *meso*). Minor isomer, **2.11b**: δ 0.31 (s, 9H, SiMe_3), 0.62 (d, 1H, $^3J_{\text{HH}} = 12.7$, allyl CHSiMe_3), 1.17 (s, 9H, Np *Me*), 1.64 (d, 1H, $^3J_{\text{HH}} = 10.1$, allyl CH_2), 1.69 (s, 15H, $\text{Cp}^* \text{Me}$), 2.53 (d, 1H, $^2J_{\text{HH}} = 17.5$, Np CH_2), 2.74 (d, 1H, $^2J_{\text{HH}} = 17.5$, Np CH_2), 3.63 (d, 1H, $^3J_{\text{HH}} = 6.5$, allyl CH_2), 4.84 (td, 1H, $^3J_{\text{HH}} = 13.2, 6.8$, allyl *meso*). ^{13}C NMR (100 MHz, C_6D_6) Major isomer only, **2.11a**: δ 2.1 (SiMe_3), 10.2 (C_5Me_5), 30.2 (Np *Me*), 32.0 (Np CMe_3), 55.5 (CHSiMe_3), 76.5 (allyl CH_2),

76.8 (Np CH₂), 107.4 (allyl *meso*), 107.5 (C₅Me₅), 265.2 (C(=O)). MS (LREI, *m/z*, probe temperature 120 °C) 561 [M⁺, ¹⁸⁴W]. Anal. Calcd for C₂₂H₃₉NO₂SiW: C, 47.06; H, 7.00; N, 2.49. Found: C, 47.18; H, 6.88; N, 2.81.

2.3.16 Monitoring the conversion of 2.1 to 2.11 by ¹H NMR spectroscopy.

The same procedure was followed as in Section 2.3.15, but aliquots (ca. 0.5 mL) were removed from the reaction mixture every 15 minutes. The solvent was removed from these samples under vacuum, and the remaining oil was dissolved in C₆D₆ and analyzed by ¹H NMR spectroscopy.

2.3.17 Preparation of Cp*Mo(NO)(Np)(η³-CH₂CHCHSiMe₃) (2.12).

A procedure similar to that for Cp*W(NO)(Np)(η³-CH₂CHCHSiMe₃) (Section 2.3.1) was followed, using Cp*Mo(NO)(Np)Cl (1.50 g, 4.08 mmol) and Li[CH₂CHCHSiMe₃] (5.7 mL, 0.72 M, 4.10 mmol). **2.12** was isolated as a pale tan solid after chromatography on basic alumina (0.22 g, 40% yield). Single crystals suitable for X-ray diffraction were grown from a pentane/Et₂O solution maintained at -30 °C.

Characterization data for **2.12**: IR (cm⁻¹) 1604 (s, ν_{NO}). ¹H NMR (400 MHz, C₆D₆) δ 0.49 (d, 1H, ³J_{HH} = 12.5, CHSiMe₃), 0.35 (s, 9H, SiMe₃), 1.03 (d, 1H, ²J_{HH} = 10.9, Np CH₂), 1.30 (s, 9H, Np Me), 1.46 (s, 15H, Cp* Me), 1.83 (d, 1H, ²J_{HH} = 11.2, Np CH₂), 1.90 (d, 1H, ³J_{HH} = 13.6, allyl CH₂), 4.15 (d, 1H, ³J_{HH} = 7.3, allyl CH₂), 5.10 (ddd, 1H, ³J_{HH} = 14.2, 12.7, 7.3, allyl *meso*); (400 MHz, C₆D₁₂) δ 0.17 (s, 9H, SiMe₃), 0.51 (d, 1H, ³J_{HH} = 12.7, CHSiMe₃), 0.95 (s, 9H, Np Me), 0.96 (obscured d, 1H, ²J_{HH} = 10.9, Np CH₂), 1.72 (s, 15H, Cp* Me), 1.77 (d, 1H, ²J_{HH} = 11.1, Np CH₂), 2.02 (dd, 1H, ³J_{HH} = 14.2, ²J_{HH} = 0.9, allyl

CH₂), 4.15 (d, 1H, ³J_{HH} = 7.2, allyl CH₂), 4.93 (ddd, 1H, ³J_{HH} = 14.1, 12.7, 7.2, allyl *meso*). ¹³C NMR (100 MHz, C₆D₁₂) δ 1.4 (SiMe₃), 10.4 (C₅Me₅), 34.6 (Np Me), 35.5 (Np CH₂), 39.3 (Np CMe₃), 51.0 (CHSiMe₃), 87.0 (allyl CH₂), 108.1 (C₅Me₅), 118.3 (allyl *meso* CH). MS (LREI, *m/z*, probe temperature 120 °C) 447 [M⁺, ⁹⁸Mo]; (HREI, *m/z*, ⁹⁸Mo) Calcd: 447.18550. Found: 447.18545. Anal. Calcd for C₂₁H₃₉NOSiMo: C, 56.60; H, 8.82; N, 3.14. Found: C, 56.80; H, 8.72; N, 3.13.

2.3.18 Preparation of Cp*Mo(NO)(η²-CH₂=C=CHSiMe₃)(PMe₃) (2.13).

A sample of **2.12** (140 mg, 0.313 mmol) was dissolved in neat PMe₃ (ca. 2 mL) to obtain an orange solution. The reaction mixture was heated at 45 °C for 2 h, and then the volatiles were removed in vacuo to leave a dark brown oil. This residue was taken up in pentane and transferred to a silica column (2 x 5 cm) supported on a medium porosity frit. An orange band was eluted with 4:1 pentane/Et₂O, which contained **2.13** (25 mg, 18%). A second yellow band was also eluted which contained three phosphorus-containing products. Single crystals of **2.13** suitable for X-ray diffraction were grown from a pentane solution maintained at -30 °C.

Characterization data for **2.13**: IR (cm⁻¹) 1575 (s, ν_{NO}), 1641 (w, ν_{C=C}). ¹H NMR (300 MHz, C₆D₆) δ 0.23 (m, 1H, allene CHSiMe₃), 0.40 (s, 9H, SiMe₃), 1.18 (d, 9H, ²J_{PH} = 8.7, PMe₃), 1.64 (s, 15H, Cp* Me), 5.30 (dt, 1H, ²J_{HH} = 3.8, ⁴J_{HH} = 2.0, allene CH₂), 6.44 (dt, 1H, ²J_{HH} = 3.4, ⁴J_{HH} = 1.7, allene CH₂). ¹³C NMR (75 MHz, C₆D₆) δ 1.4 (SiMe₃), 10.9 (C₅Me₅), 16.9 (CHSiMe₃, J_{CP} = 1.7), 17.5 (PMe₃, ¹J_{CP} = 27), 102.5 (allene CH₂, J_{CP} = 9.8), 106.3 (C₅Me₅), 186.3 (allene C, J_{CP} = 21.4). ³¹P {¹H} (121 MHz, C₆D₆) δ 18.0. MS (LREI, *m/z*,

probe temperature 120 °C) 451 [M^+ , ^{98}Mo]; (HREI, m/z , ^{98}Mo) Calcd: 451.13579. Found: 451.13615; (HREI, m/z , ^{92}Mo) Calcd: 445.13719. Found: 445.13741.

2.3.19 Thermolysis of 2.12 in benzene.

A sample of **2.12** (105 mg, 0.235 mmol), was dissolved in C_6H_6 (ca. 10 mL) and heated at 45 °C for 1.5 h. ^1H NMR spectroscopic analysis of the brown oil obtained after removal of solvent in vacuo showed the presence of four organometallic hydrides. Two molybdenum hydrides could be fractionally recrystallized from pentane (**2.14**); these are formulated as $\text{Cp}^*\text{Mo}(\text{NO})(\eta^3\text{-Me}_3\text{SiCHCHCHPh})(\text{H})$, and their characterization data is presented below.

Partial characterization data for **2.14**: ^1H NMR (300 MHz, C_6D_6): Primary isomer: δ -1.10 (s, 1H, Mo-*H*), 0.40 (s, 9H, SiMe_3), 0.49 (d, 1H, $^3J_{\text{HH}} = 12.8$, allyl CHSiMe_3), 1.65 (s, 15H, Cp^*Me), 2.69 (d, 1H, $^3J_{\text{HH}} = 13.0$, allyl CHPh), 5.30 (t, 1H, $^3J_{\text{HH}} = 12.8$, allyl *meso*), 7.02 (m, 1H, *para* CH), 7.11 (obscured, 2H, $^3J_{\text{HH}} = 7.7$, *meta* CH), 7.32 (d, 2H, $^3J_{\text{HH}} = 7.3$, *ortho* CH). Secondary isomer, selected signals: δ -0.69 (s, 1H, Mo-*H*), 1.98 (m, 1H, CHSiMe_3), 0.34 (s, 9H, SiMe_3), 1.57 (s, 15H, Cp^*Me), 4.22 (dd, 1H, $^3J_{\text{HH}} = 15.2$, 11.8, allyl *meso*), 5.03 (d, 1H, $^3J_{\text{HH}} = 15.4$, CHPh). ^{13}C NMR spectra could not be acquired due to the thermal instability of these complexes. MS (LREI, m/z , probe temperature 120 °C) 453 [M^+ , ^{98}Mo]; (HREI, m/z , ^{98}Mo) Calcd: 453.13855. Found: 453.13858.

2.3.20 Monitoring the thermolytic consumption of 2.12 by ^1H NMR spectroscopy.

The procedure employed was the same as that in Section 2.3.13. A sample of **2.12** was dissolved in either C_6D_6 (ca. 0.7 mL) or C_6D_{12} (ca. 0.65 mL) and transferred to a J.

Young NMR tube. The NMR probe was heated to the desired temperature (one of 45 °C, 35 °C, or 25 °C), and spectra were acquired every 5 minutes. The solvent signal at 7.16 ppm (for C₆D₆) or 1.40 ppm (for C₆D₁₂) was used as an internal standard, and the decrease in the area of the signal corresponding to Cp* Me groups was used to track the loss of the reactant. Errors in the rate constants were estimated from the standard error in the linear regression of the data. Errors in the temperature of the probe were estimated to be ± 0.5 °C.

2.3.21 X-ray crystallography

Data collection was carried out at $-173 (\pm 1)$ °C on a Bruker X8 diffractometer, using graphite-monochromated Mo K α radiation.

Data for **2.1** were collected to a maximum 2θ value of 60.4° in 0.5° oscillations with 0.5 s exposures. The structure was solved by direct methods⁵⁹ and expanded using Fourier techniques. All non-hydrogen atoms were refined anisotropically, and all hydrogen atoms were included in fixed positions. The final cycle of full-matrix least squares analysis was based on 6639 observed reflections and 237 variable parameters.

Data for **2.9** were collected to a maximum 2θ value of 55.9° in 0.5° oscillations with 5 s exposures. The structure was solved by direct methods⁵⁹ and expanded using Fourier techniques. All non-hydrogen atoms were refined anisotropically, and hydrogens H11a, H11b, and H13 were refined isotropically. All other hydrogen atoms were included in fixed positions. The final cycle of full-matrix least squares analysis was based on 5346 observed reflections and 240 variable parameters.

Data for **2.10** were collected to a maximum 2θ value of 60.2° in 0.5° oscillations. The structure was solved by direct methods⁵⁹ and expanded using Fourier techniques. All non-

hydrogen atoms were refined anisotropically, and hydrogens H1, H11a, H11b, H13, H18, H19, H20a, H20b, H21a, and H21b were refined isotropically. All other hydrogen atoms were included in fixed positions. The final cycle of full-matrix least squares analysis was based on 6757 reflections and 283 variable parameters.

Data for **2.11** were collected to a maximum 2θ value of 66.3° in 0.5° oscillations with 2 s exposures. The structure was solved by direct methods⁵⁹ and expanded using Fourier techniques. All non-hydrogen atoms were refined anisotropically, and hydrogens H11a, H11b, H12, and H13 were refined isotropically. All other hydrogen atoms were included in fixed positions. The final cycle of full-matrix least squares analysis was based on 8927 observed reflections and 271 variable parameters.

Data for **2.12** were collected to a maximum 2θ value of 60.3° in 0.5° oscillations with 40 s exposures. The structure was solved by direct methods⁵⁹ and expanded using Fourier techniques. All non-hydrogen atoms were refined anisotropically, and hydrogens H11a, H11b, H12, H13, H17a, and H17b were refined isotropically. All other hydrogen atoms were included in fixed positions. The final cycle of full-matrix least squares analysis was based on 6475 observed reflections and 261 variable parameters.

Data for **2.13** were collected to a maximum 2θ value of 71.2° in 0.5° oscillations with 20 s exposures. The structure was solved by direct methods⁵⁹ and expanded using Fourier techniques. All non-hydrogen atoms were refined anisotropically, and all hydrogen atoms were included in fixed positions. The final cycle of full-matrix least squares analysis was based on 10403 observed reflections and 228 variable parameters.

For each structure, neutral-atom scattering factors were taken from Cromer and Waber.⁶⁰ Anomalous dispersion effects were included in F_{calc} ;⁶¹ the values for $\Delta f'$ and $\Delta f''$

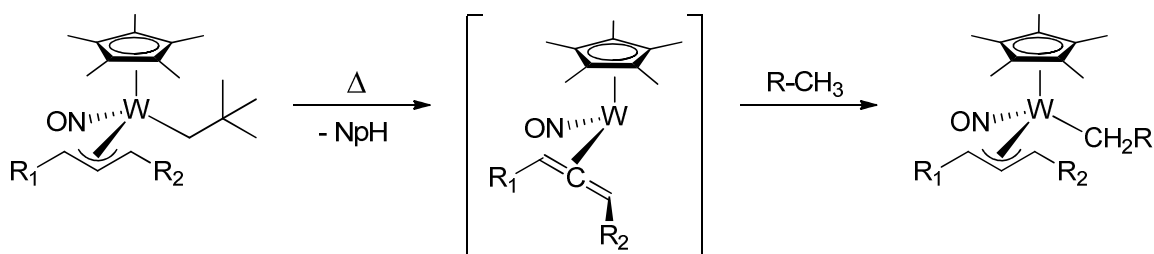
were those of Creagh and McAuley.⁶² The values for mass attenuation coefficients are those of Creagh and Hubbell.⁶³ All calculations were performed using SHELXL-97⁶⁴ *via* the WinGX interface.⁶⁵ X-ray crystallographic data for all structures are presented in Table A.1.

Chapter 3: Chemistry of $\text{Cp}^*\text{W}(\text{NO})(\eta^3\text{-Me}_3\text{SiCHCHCHPh})(\text{H})$

3.1 Introduction

The rationalization behind the investigation of the 1,3-disubstituted allyl ligands was simple: by placing a substituent on each end of the allyl ligand, coupling reactions between the allyl ligand and other ligands might be avoided. (This is especially salient when one considers that $\text{Cp}^*\text{Mo}(\text{NO})(\text{Np})(\eta^3\text{-C}_3\text{H}_5)$, a complex bearing an unsubstituted allyl ligand, undergoes coupling of the neopentyl and allyl ligands in the presence of a Lewis base.)⁵⁶ Such 1,3-disubstituted allyl species should, in principle, be able to access a 16e intermediate through a similar route to the monosubstituted allyl complexes, thus making them possible candidates for alkane activation and functionalization.

Scheme 3.1. Proposed C–H activation chemistry by complexes containing 1,3-disubstituted allyl ligands.



The structural features of metal complexes containing the 1,3-(SiMe₃)₂C₃H₃ (diTMS) allyl ligand have been extensively studied, due to the ability of these bulky disubstituted allyl ligands to stabilize homoleptic allyl complexes which are otherwise unstable.³¹ There have

also been some investigations into using $M(II)(diTMS)_2$ complexes as norbornene and ethylene polymerization catalysts in conjunction with methylaluminoxane or $B(C_6F_5)_3$.⁶⁶ However, in general, the use of transition metal-complexes containing the diTMS ligand for catalysis has been limited.

3.2 Results and discussion

3.2.1 Attempts to synthesize $Cp^*W(NO)(Np)(\eta^3-1,3-(SiMe_3)_2C_3H_3)$

Regrettably, the attempted direct synthesis of $Cp^*W(NO)(Np)(\eta^3-diTMS)$ from $Cp^*W(NO)(Np)Cl$ and appropriate organometallic reagents ($Li(diTMS)$, $Na(diTMS)$, $K(diTMS)$, $Mg(diTMS)_2$, $Me_3Sn(diTMS)$) leads to either decomposition of the starting material (in the case of the Group 1 and 2 reagents) or no reaction (in the case of the tin reagent). The bis(trimethylsilyl) allyl ligand may therefore be too sterically bulky for the $Cp^*W(NO)(Np)$ fragment. Very few $5d$ metal complexes of diTMS have been isolated, with one exception being $TaCl_4(diTMS)$.⁶⁷

3.2.2 The $Cp^*W(NO)(\eta^3-Me_3SiCHCHCHPh)(H)$ system

3.2.2.1 Synthesis and structure of $Cp^*W(NO)(\eta^3-Me_3SiCHCHCHPh)(H)$

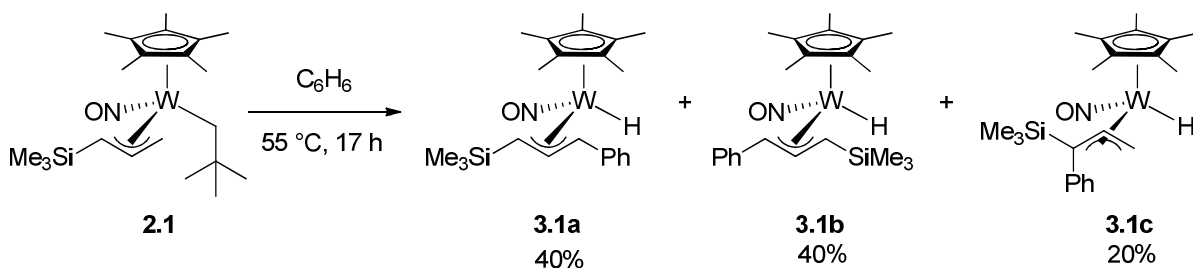
In spite of the difficulties encountered in the direct synthesis of $Cp^*W(NO)$ complexes containing 1,3-disubstituted allyl ligands, the reaction of benzene with the family of $Cp^*W(NO)(Np)(\eta^3-allyl)$ complexes provides an indirect route to related complexes. One might expect these complexes to form the $(\eta^3-allyl)(phenyl)$ derivatives through a route similar to sp^3 C–H activation. Instead, only $Cp^*W(NO)(Np)(\eta^3-1,1-CH_2CHCMe_2)$ forms the

phenyl compound cleanly;²⁷ the majority of the other Cp*W(NO)(Np)(η^3 -allyl) systems react with benzene to give complex mixtures.²⁸ In particular, migration of the phenyl group onto the allyl ligand is often observed, generating a 1,3-disubstituted (or, in some cases, 1,1-disubstituted) allyl ligand on a tungsten hydride complex.⁵⁴

Given the propensity for the phenyl ligands in these systems to migrate onto the allyl ligand, a secondary strategy for generating a 1,3-disubstituted allyl ligand on the metal centre presented itself: such a ligand could be created through activating benzene, although a hydride would take the place of an alkyl ligand on the metal centre. The allyl hydride systems are also of interest as potential C–H activation agents since DFT calculations on model CpW(NO)(diene) and CpW(NO)(allene) systems have shown that dihydrogen elimination from the metal's coordination sphere is only slightly more energetically demanding than alkane loss.⁶⁸ Therefore, these allyl hydride species should also be capable of generating an η^2 -allene intermediate for C–H activation.

Thermolysis of **2.1** in benzene generates three isomeric products, **3.1a**, **3.1b**, and **3.1c** (Scheme 3.2). These products are fairly air-stable and can be handled without recourse to inert atmosphere for short periods of time without noticeable degradation.

Scheme 3.2. Reaction of **2.1** in benzene.



The postulated intermediate in these transformations, namely $\text{Cp}^*\text{W}(\text{NO})(\eta^3\text{-CH}_2\text{CHCHSiMe}_3)(\text{Ph})$, has not been isolated, nor has it been directly observed by ^1H NMR spectroscopy. However, proof of its identity is provided by the thermolysis of **2.1** in benzene- d_6 . An expansion of the ^1H NMR spectrum of the final reaction mixture of this experiment is presented in Figure 3.1. The existence, however transient, of the phenyl complex can be inferred by three key pieces of evidence. First, the absence of the signal at 5.22 ppm in the ^1H NMR spectrum supports deuterium incorporation at the *meso* position of the allyl ligand, through C–D activation by the allene complex. Second, the signals for the other hydrogen atoms on the allyl ligand (0.68 and 2.25 ppm) have become singlets, rather than the doublets observed for the same reaction carried out in protio benzene; this is due to loss of the $^3J_{\text{HH}}$ coupling to the hydrogen at the *meso* position. Although a $^3J_{\text{HD}}$ coupling could be theoretically be observed, this value is expected to be around 2.2 Hz for the signal at 0.68 ppm by Equation 3.1,⁶⁹ where $(\gamma_{\text{H}}/\gamma_{\text{D}})$ is the ratio of the gyromagnetic ratios between these two nuclei.

$$^nJ_{\text{HH}} = (\gamma_{\text{H}}/\gamma_{\text{D}})^n J_{\text{HD}} \quad (3.1)$$

In addition, since ^2H is a quadrupolar nucleus, it is expected to have a very short T_1 relaxation, leading to broader signals of its coupling partners. This factor, together with the small magnitude of the coupling constant, means $^3J_{\text{HD}}$ may not be observable. Finally, the signal arising from the hydride integrates to 1H relative to the Cp^*Me peak. The original source of the hydrogen atom for the hydride must therefore be the allyl ligand, given that there is no other plausible source of ^1H in the reaction mixture.

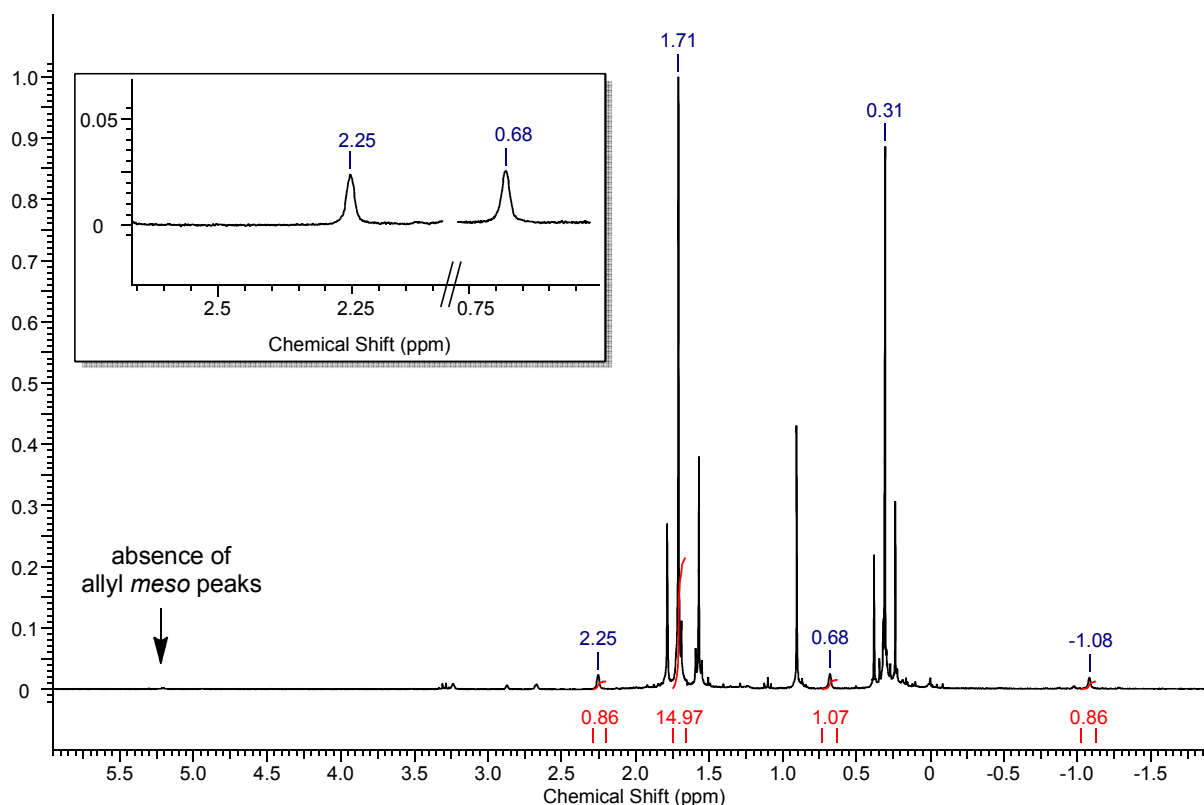


Figure 3.1. ^1H NMR spectrum (300 MHz) of the final reaction mixture of **2.1** thermolyzed in C_6D_6 .

Assignments (ppm): δ -1.08, W-*H*; 0.31, SiMe_3 ; 0.68, CHSiMe_3 ; 1.71, Cp^* Me; 2.25, CHPh . Inset: Magnification of the two signals arising from the non-*meso* protons on the allyl ligand.

Isomerization to the 1,3-disubstituted allyl ligand appears to be very favoured. The phenyl intermediate might be isolable if the Cp^* ligand is replaced with the tetramethyl analogue, $\text{C}_5\text{Me}_4\text{H}$, which has previously been shown to slow the rate of these isomerizations.⁵⁴ Since the ν_{NO} stretching frequencies of the product complexes are quite low, an indication of fairly electron-rich W centres, it is possible that the isomerizations may occur to relieve electron deficiency at the metal centre in the intermediate phenyl complex.

Because C–H activation by **2.1** proceeds through an η^2 -allene intermediate, it is expected that the products of thermolysis in benzene should be similar to those of $\text{Cp}^*\text{W}(\text{NO})(\text{Np})(\eta^3\text{-CH}_2\text{CHCHPh})$. However, as the trimethylsilyl substituent on the allyl ligand causes the resulting 1,3-disubstituted allyl ligand to be non-symmetric, the complex can exist in one of two conformations: the trimethylsilyl substituent can be placed either proximal (**3.1a**) or distal (**3.1b**) to the NO ligand.

Since $\text{Cp}^*\text{W}(\text{NO})(\text{Np})(\eta^3\text{-CH}_2\text{CHCHSiMe}_3)$, **2.1**, exists as a single isomer, with the trimethylsilyl substituent proximal to the NO ligand, the initial product is also expected to be monoisomeric. Monitoring the reaction by ^1H NMR spectroscopy at 75 °C (Figure 3.2) confirms this hypothesis: the isomer with the SiMe_3 proximal to the NO ligand (**3.1a**) is the first hydride product observed. As heating continues, the distal product (**3.1b**) begins to appear in greater quantities, concurrent with further formation of the proximal product. Gradually, the proportion of the **3.1b** increases relative to **3.1a**. Thus, while the proximal product is the kinetic product due to the arrangement of the ligands around the W centre, the distal isomer is the more thermodynamically stable one. Isomerization from the distal back to the proximal isomer has not been observed. The formation of **3.1c** (the complex containing the 1,1-disubstituted allyl ligand) is examined in further detail in Section 3.2.2.2.

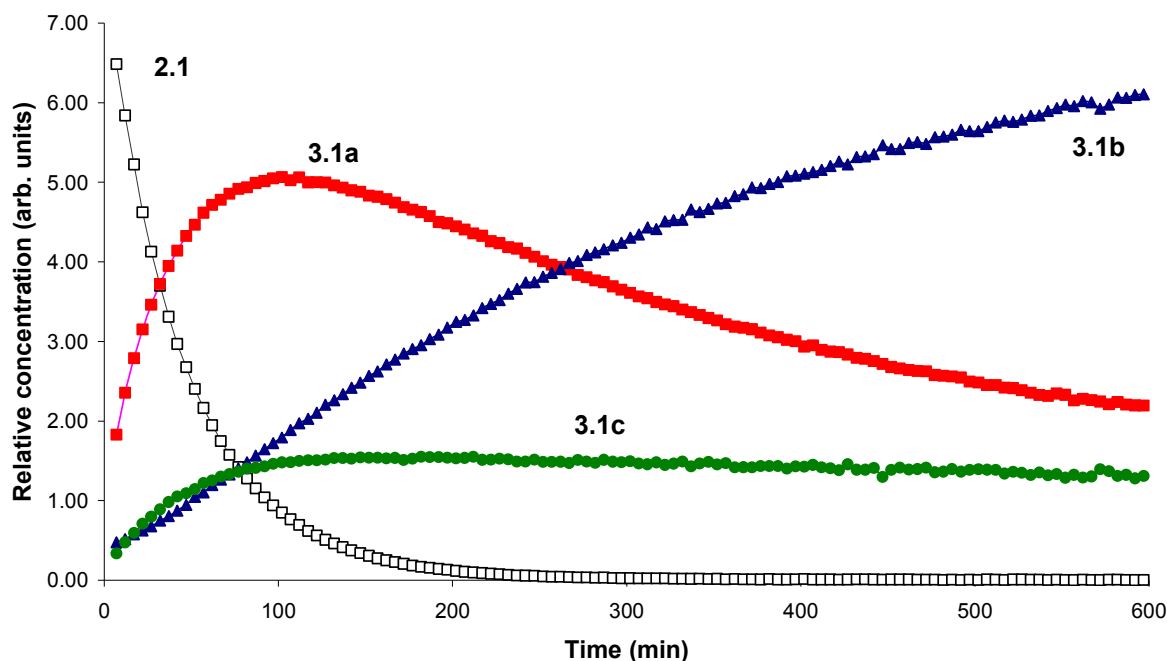


Figure 3.2. Product distribution during the thermolysis of **2.1** in C_6D_6 at 75 °C as monitored by 1H NMR spectroscopy.

These shifts in product distribution appear to be dictated by sterics: The relatively unencumbered $Cp^*W(NO)(Np)(\eta^3-CH_2CHCHMe)$ exists as two isomers in solution, whereas complexes containing bulkier allyl ligands, e.g., **2.1** and $Cp^*W(NO)(Np)(\eta^3-CH_2CHCHPh)$, do not. Therefore, the isomerization from **3.1a** to **3.1b** is probably facilitated by the small size of the hydride ligand, which relieves steric congestion such that the necessary haptotropic shifts for the allyl ligand to rotate about the W–C bond become possible. The stereochemical flexibility of allyls has been implicated in “alkene flipping” mechanisms, which interconvert substituents on metal-coordinated alkenes.⁷⁰

Interestingly, the proximal and distal isomers can be separated by fractional recrystallization from the same solution: the proximal isomer crystallizes as an orange solid, while the crystalline form of the distal isomer is yellow. Single-crystal X-ray diffraction

3.1a and **3.1b** are presented in Figure 3.3 and Figure 3.4, respectively.

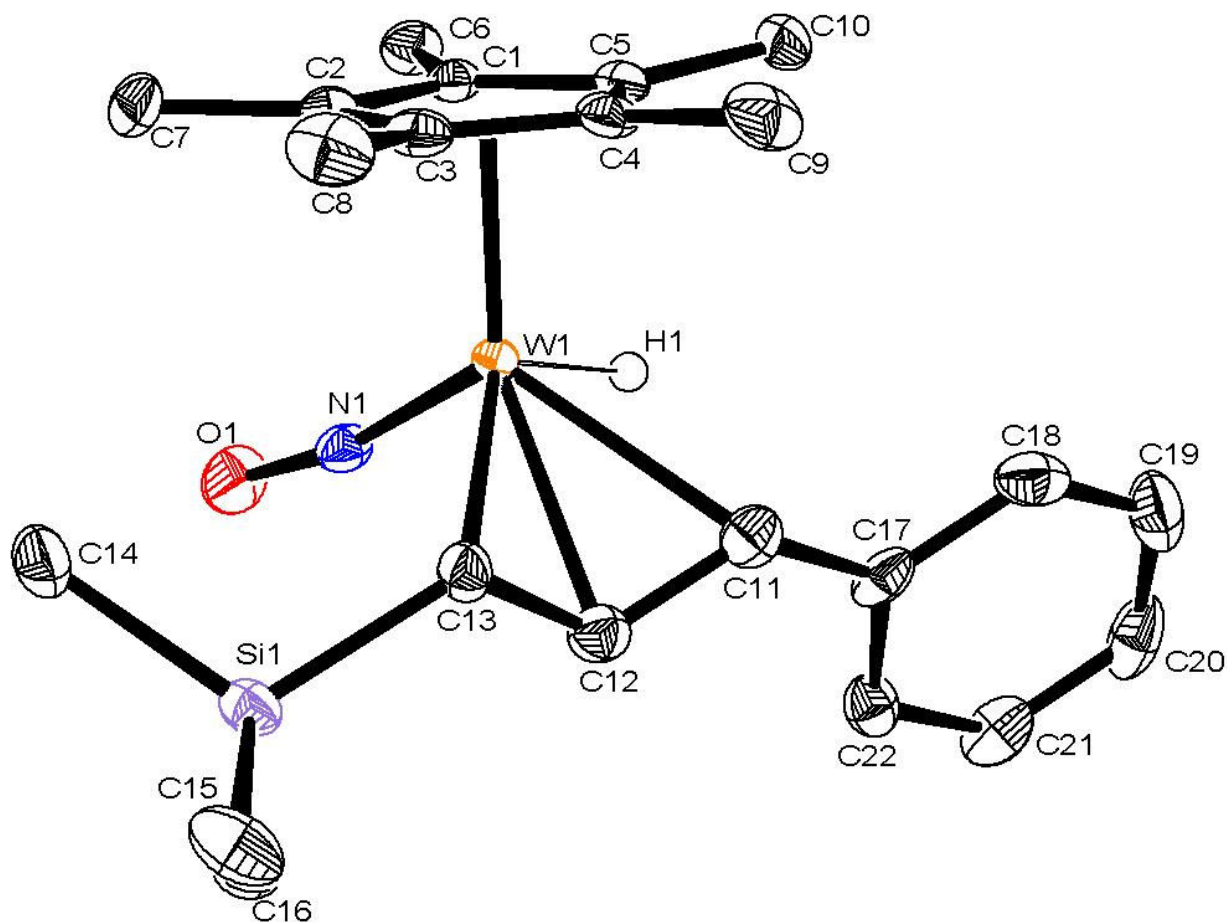


Figure 3.3. Solid-state molecular structure of **3.1a** with 50% probability thermal ellipsoids.

Selected interatomic bond distances (Å) and angles (deg): C(11)–W(1) = 2.420(3); C(12)–W(1) = 2.323(3); C(13)–W(1) = 2.263(3); C(11)–C(12) = 1.384(5); C(12)–C(13) = 1.458(4); N(1)–O(1) = 1.223(3); N(1)–W(1) = 1.779(2); W(1)–H(1) = 1.63(4); C(11)–C(12)–C(13) = 119.1(3); O(1)–N(1)–W(1) = 169.4(2).

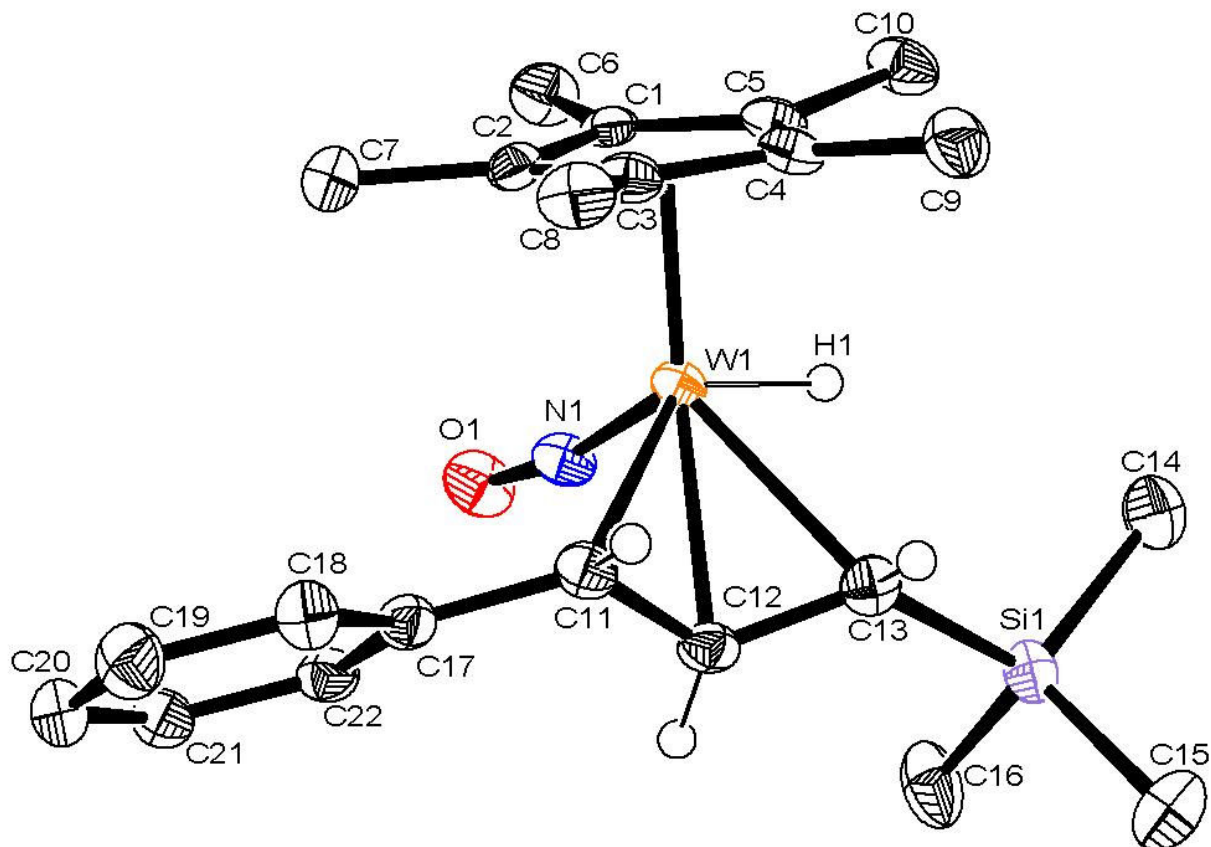


Figure 3.4. Solid-state molecular structure of **3.1b** with 50% probability thermal ellipsoids.

Selected interatomic bond distances (Å) and angles (deg): C(11)–W(1) = 2.302(4); C(12)–W(1) = 2.296(4); C(13)–W(1) = 2.377(4); C(11)–C(12) = 1.411(6); C(12)–C(13) = 1.404(6); N(1)–O(1) = 1.229(4); N(1)–W(1) = 1.783(3); W(1)–H(1) = 1.55(5); C(13)–C(12)–C(11) = 120.2(4); O(1)–N(1)–W(1) = 169.1(3).

The solid-state molecular structures of the isomers present some interesting structural and spectroscopic features, summarized in Table 3.1.

Table 3.1. Comparison of solid-state structural and solution spectroscopic properties of **3.1a** and **3.1b**.

	Proximal isomer	Distal isomer
	3.1a	3.1b
Shorter allyl C–C bond length (Å)	1.384(5)	1.404(6)
Longer allyl C–C bond length (Å)	1.458(4)	1.411(6)
N–O bond length (Å)	1.223(3)	1.229(4)
ν_{NO} (cm ^{−1})	1557	1547
λ_{max} (nm)	244, 296, 355	240, 280, 343
CHSiMe ₃ , ¹³ C NMR chemical shift (ppm)	44.7	61.7
<i>Meso</i> carbon, ¹³ C NMR chemical shift (ppm)	106.4	110.0
CHPh, ¹³ C NMR chemical shift (ppm)	86.7	72.6

The σ - π distortion only exists in the kinetic product, complex **3.1a**: the C–C bond lengths in the allyl ligand are 1.384 and 1.458 Å, while in the thermodynamic product, complex **3.1b**, they are 1.411 and 1.404 Å. Thus, in **3.1b**, the allyl ligand is completely symmetric within the standard deviation. This is likely related to the different electronic effects of the SiMe₃ and Ph substituents. The difference in the N–O bond lengths in the two isomers is not statistically significant.

The coupling constants between the signals arising from the protons on the allyl ligand also appear to reflect a difference in structure. The signal due to the *meso* proton of **3.1a** is an apparent triplet, with a ³*J*_{HH} of 12.4 Hz to both non-*meso* protons. Conversely, the

resonance of the *meso* proton of **3.1b** is a doublet of doublets, with $^3J_{\text{HH}}$ values of 14.6 and 10.1 Hz to the *CHSiMe₃* and *CHPh* protons, respectively. The general magnitudes of these $^3J_{\text{HH}}$ values are consistent with typical values for $^3J_{\text{trans}}$. However, why the *meso* proton in one isomer should have the same coupling constant to both allyl protons, while the other should show distinct coupling constants, is unclear. The *meso* hydrogen in **3.1b** might be expected to have the same coupling to the other allyl hydrogens, which appear to be in similar chemical environments due to the similarity in C–C bond lengths and ^{13}C chemical shifts. Yet, this is the isomer in which the coupling constants are different. Vicinal coupling constants such as these are related to torsion angles through the Karplus relationship. However, analysis of the torsion angles in the solid-state structure of **3.1a** does not resolve this conundrum either, for in this isomer, the torsion angle from the *meso* proton to the *CHSiMe₃* is 163.3°, and the torsion angle to *CHPh* is 171.2°, and yet the coupling constants to these two protons is identical. (Meaningful analysis of the torsion angles in **3.1b** was not possible since the hydrogen atoms in question were included in calculated positions, rather than located from the diffraction map.)

Linkage isomerization is a common rationale for changing colours of transition-metal complexes.⁷¹ In order to gain further insight into how the allyl ligand's coordination mode affects the electronic structure of these complexes, the UV/Vis spectra of these complexes (in acetonitrile solution) have been acquired. For **3.1a**, maxima are observed at 244 ($\epsilon = 1.7 \times 10^4 \text{ L mol}^{-1} \text{ cm}^{-1}$), 296 ($\epsilon = 1.4 \times 10^4 \text{ L mol}^{-1} \text{ cm}^{-1}$), and 355 ($\epsilon = 2.1 \times 10^3 \text{ L mol}^{-1} \text{ cm}^{-1}$) nm, while in **3.1b**, maxima are observed at 243 ($\epsilon = 2.5 \times 10^4 \text{ L mol}^{-1} \text{ cm}^{-1}$), 280 ($\epsilon = 2.3 \times 10^4 \text{ L mol}^{-1} \text{ cm}^{-1}$), and 343 ($\epsilon = 3.5 \times 10^2 \text{ L mol}^{-1} \text{ cm}^{-1}$) nm. Neither **3.1a** nor **3.1b** absorbs strongly in the visible region, so the observed colours are probably due to the tail of the

lowest energy band. The wavelength of the lowest energy band is consistent with the observed colours; the band of **3.1a** at 355 nm might be reasonably expected to extend further into the blue region of the UV/Vis spectrum than the band of **3.1b** at 343 nm, leading to a more orange colour for **3.1a**.

UV/Vis absorption in transition-metal complexes is usually due to either *d-d* transitions, or charge transfer between ligand and metal. The usual criterion for distinguishing between these two possibilities is the magnitude of ϵ , the molar extinction coefficient, since *d-d* transitions are symmetry-forbidden in octahedral complexes. However, given the low symmetry in **3.1a** and **3.1b**, *d-d* transitions would not be expected to be affected by this rule. In addition, the presence of the 1-trimethylsilyl-3-phenylallyl ligand is expected to introduce an additional complication, as the ligand itself is UV active. More tellingly, the different positions of the peaks in the UV/Vis spectra of the two isomers can illuminate the electronic structure of the complexes. In particular, if the lowest energy band in each isomer can be assigned to a *d-d* transition (presumably between the same orbitals given the similarity in their geometric structures), the transition in **3.1b** is of higher energy. This could indicate additional stabilization through lowering the energy of the occupied *d* orbitals of the ground state relative to **3.1a**, which would be consistent with **3.1b** being the thermodynamic product of the reaction.

3.2.2.2 Formation of $\text{Cp}^*\text{W}(\text{NO})(\text{H})(\eta^3\text{-CH}_2\text{CHC}(\text{SiMe}_3)\text{Ph})$

The appearance of $\text{Cp}^*\text{W}(\text{NO})(\text{H})(\eta^3\text{-CH}_2\text{CHC}(\text{SiMe}_3)\text{Ph})$ (**3.1c**) in the final product mixture was unexpected, given that 1,1-disubstituted allyl products had only been observed previously when the substituent on the allyl ligand was the less sterically bulky methyl

group.⁵⁴ The formation of this product is likely assisted by conformational changes in the allyl during the initial C–H activation, but as the formation of this product requires more shifts in the allyl ligand, its rate of formation is slower than for the 1,3-disubstituted isomers. Based on the results in Figure 3.2, the proportion of this product in the reaction mixture remains constant once the majority of the starting material has been consumed. While **3.1c** appears to undergo no significant changes under these conditions, thermolysis of protio-**3.1c** in C₆D₆ leads to D incorporation (Section 3.2.3.3). The temperature of the reaction appears to have only a slight effect on the amount of **3.1c** produced compared to the 1,3-disubstituted isomers; at 75 °C roughly 15% of the product contains the 1,1-disubstituted allyl ligand, while at 65 °C and 55 °C the proportion is closer to 20%.

3.2.2.3 Thermolysis of other Cp*W(NO)(η^3 -CH₂CHCHSiMe₃)(R) complexes

While the majority of the R groups known to migrate onto the allyl ligand are aryl ligands, the possible migration of alkyl ligands onto the allyl ligand has also been investigated. Activation of methylcyclohexane by Cp*W(NO)(Np)(η^3 -CH₂CHCHPh) produced Cp*W(NO)(η^3 -PhCHCHCHCH₂Cy)(H) in small amounts;⁷² however, no such analogous product is seen for the activation of methylcyclohexane by **2.1**. In addition, for the complexes Cp*W(NO)(R)(η^3 -CH₂CHCHSiMe₃), extended thermolyses of **2.6** (R = CH₂-3,5-Me₂C₆H₃) and **2.7** (R = CH₂SiMe₃) do not produce the desired 1,3-disubstituted allyl ligands. The final reaction mixture of the thermolysis of **2.6** yielded predominantly starting material, but also a small amount (approx. 8% by ¹H NMR spectroscopy) of a new Cp*-containing product. Unfortunately, the low conversion does not produce material in sufficient quantity to

be fully characterized. Only starting material can be recovered from the thermolysis of **2.7**. The investigations with fluorinated arenes are reported in Chapter 4.

3.2.3 Reactivity of $\text{Cp}^*\text{W}(\text{NO})(\eta^3\text{-Me}_3\text{SiCHCHCHPh})(\text{H})$

3.2.3.1 Reaction with PMe_3

3.1a and **3.1b** have been thermolyzed in the presence of Lewis bases to ascertain if any 16e intermediates, e.g., through the loss of dihydrogen, can be trapped. After thermolysis of **3.1a** and **3.1b** in neat PMe_3 , the final reaction mixture contains five products containing W–P bonds: this is evident from the $^{31}\text{P}\{^1\text{H}\}$ NMR spectrum, which contains five signals with similar chemical shifts (within 14 ppm of one another). Each of these signals also has the customary ^{183}W satellites indicating a W–P linkage (Table 3.2). The coordination of phosphorus to W was also confirmed by comparing the ^1H and $^1\text{H}\{^{31}\text{P}\}$ NMR spectra, where doublets in the former arising from $^2J_{\text{PH}}$ collapse to singlets upon decoupling. Unfortunately, column chromatography is ineffective in separating these products, and recrystallization by slow evaporation of a pentane solution yielded only **3.1a** and **3.1b**, a testament to the apparent instability of the adduct formed. MS data, however, are consistent with simple adduct formation with PMe_3 . Possible formulations for 18e complexes consistent with this data are the η^1 -allyl PMe_3 adduct or the η^2 -olefin PMe_3 adduct (through hydride migration onto the allyl ligand), and their possible structural isomers (Figure 3.5).

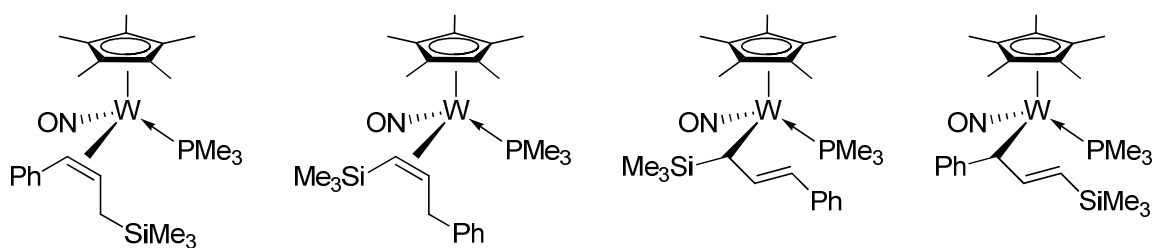


Figure 3.5. Possible products arising from the thermolysis of **3.1** in PMe_3 .

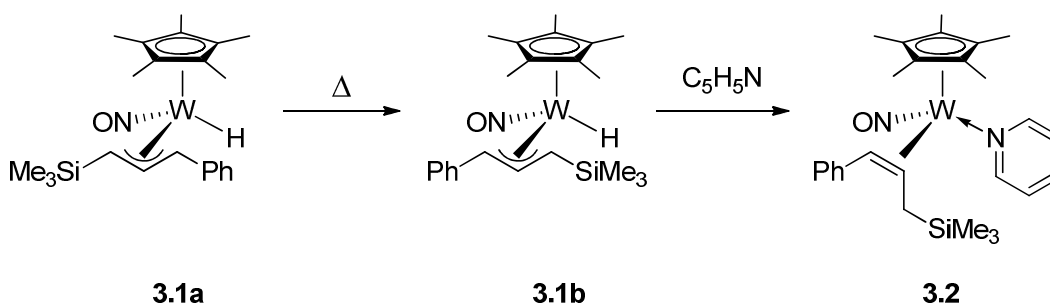
Table 3.2. ^{31}P NMR spectroscopic data for the product mixture arising from thermolysis of **3.1a** and **3.1b** in PMe_3 .

Chemical shift (ppm)	$^1J_{\text{WP}}$ (Hz)
-7.2	373
-9.3	376
-11.0	369
-14.4	357
-21.5	453

3.2.3.2 Reaction with pyridine

Thermolysis in the presence of pyridine also presents an interesting case. When a mixture of **3.1a** and **3.1b** is thermolyzed in neat pyridine, MS and NMR spectroscopic data suggest that an η^2 -olefin pyridine adduct is formed, whose identity is presumed to be $\text{Cp}^*\text{W}(\text{NO})(\eta^2\text{-Me}_3\text{SiCH}_2\text{CH=CHPh})(\text{C}_5\text{H}_5\text{N})$ (**3.2**) by analogy with $\text{Cp}^*\text{Mo}(\text{NO})(\eta^2\text{-CH}_2=\text{CHCH}_2\text{CH}_2t\text{Bu})(\text{C}_5\text{H}_5\text{N})$ ⁵⁶ (Scheme 3.3).

Scheme 3.3. Reaction of **3.1a** and **3.1b** in pyridine.



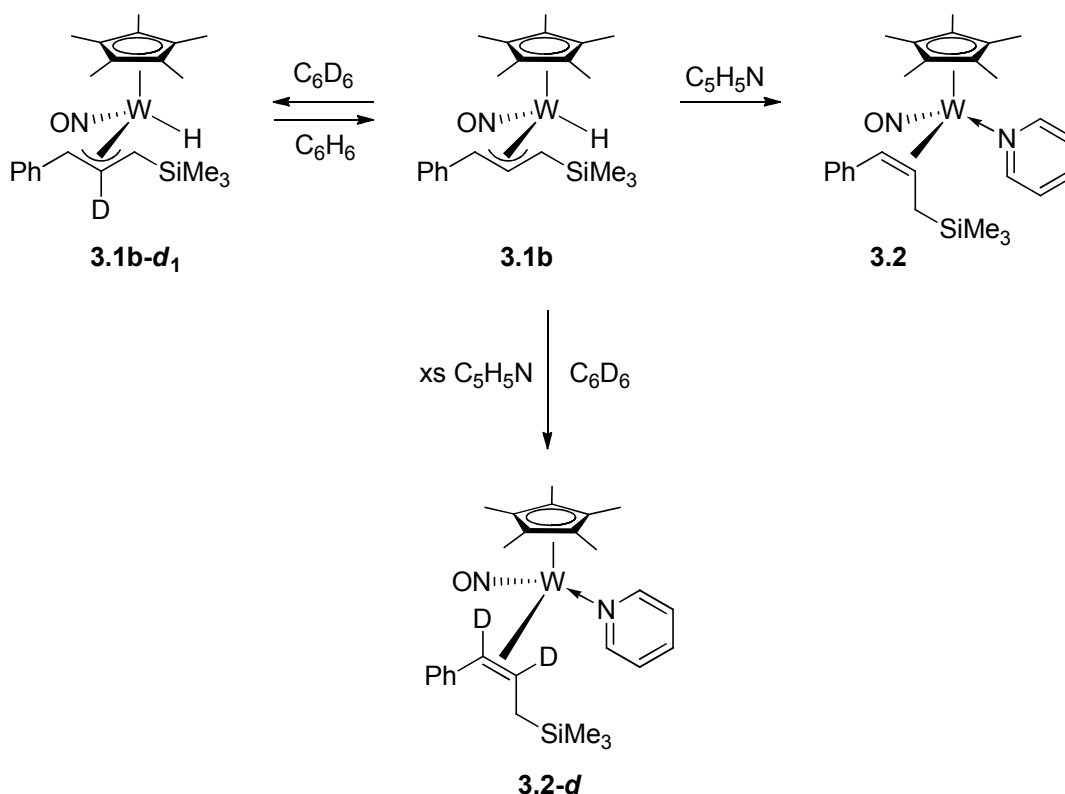
The hydride migrates exclusively onto the SiMe₃-substituted end of the allyl ligand rather than the Ph-substituted end, as evidenced by a correlation in the ¹H-¹³C HMBC spectrum between a methine signal at 2.55 ppm and the *ipso* C signal of the phenyl group at 150.0 ppm. In addition, through monitoring by ¹H NMR spectroscopy, it can be determined that adduct formation only occurs once **3.1a** (kinetic product) has isomerized to **3.1b** (thermodynamic product). This accounts for the regioselectivity of the reaction, since the hydride in **3.1b** is cisoid to the SiMe₃ group. This reaction is formally a reductive coupling of an allyl and a hydride ligand to give an olefin. These couplings require that the two ligands in question have a *cis* orientation. Such behaviour also reveals that the activation energy barrier for allyl isomerization in **3.1a** is lower than that of hydride migration. The preference to migrate onto the SiMe₃-substituted end of the ligand is contrary to what might be expected on the basis of electronics or sterics, as the C bound directly to Si should carry a partial negative charge due to the low electronegativity of silicon, and the SiMe₃ group is more sterically demanding than the Ph group.⁷³ Here, the metrical parameters of the solid-state structure can provide some insight: the W–C bond length of the nearest allyl carbon to the hydride is shorter in **3.1b** than **3.1a** (2.377 Å vs 2.420 Å, respectively). The allyl ligand in **3.1b** is therefore better situated for hydride migration.

The ν_{NO} IR stretching frequency in the pyridine adduct has also decreased by 10 wavenumbers to 1537 cm^{-1} relative to **3.1b**, reflecting a greater degree of backbonding from the W centre to the NO ligand as a result of better σ -donation from the pyridine ligand increasing the electron density at the metal centre.

3.2.3.3 Reaction with deuterobenzene

Yet, when the same reaction is carried out in deuterobenzene with ten equivalents of pyridine, ^1H NMR spectroscopic data suggest that the *meso* hydrogen is exchanged for a deuterium atom before the pyridine trapping occurs, forming **3.2-d** (Scheme 3.4, Figure 3.6). Analysis of the final product mixture, however, shows that the signal from the methine proton α to the Ph group integrates to less than 1H relative to the Cp* peak; therefore, it appears that this position on the allyl ligand also becomes partially deuterated.

Scheme 3.4. Reactivity of **3.1b** with deuterobenzene and pyridine.



After reaction for 2 days at 75 °C, the signal for the *meso* proton of **3.1b** (Figure 3.6c) integrates to 0.5 H against the Cp* Me resonance at 1.65 ppm; however, the signals due to the non-*meso* protons (Figure 3.6a and b) on the allyl ligand still integrate to one hydrogen, though their appearance has changed. Instead of the simple doublets observed in the spectrum of **3.1b**, they both appear to be overlapping with a singlet at the same chemical shift. The singlet is the result of deuterium incorporation at the allyl *meso* position, leading to the loss of $^3J_{\text{HH}}$ coupling, similar to the behaviour exhibited during the synthesis of **3.1a** and **3.1b** from **2.1** (Section 3.2.2.1).

The signal from the hydride at −1.11 ppm also merits consideration since it integrates to one full hydrogen against the Cp* signal. The retention of this signal implies that the

hydride is not involved in the incorporation of deuterium on the allyl ligand. Most notably, it precludes H₂ elimination from the metal's coordination sphere *via* abstraction of the *meso* hydrogen by the hydride. In addition, there has been no evidence for the evolution of either H₂ or HD in the ¹H NMR spectra of these sealed-tube reactions.

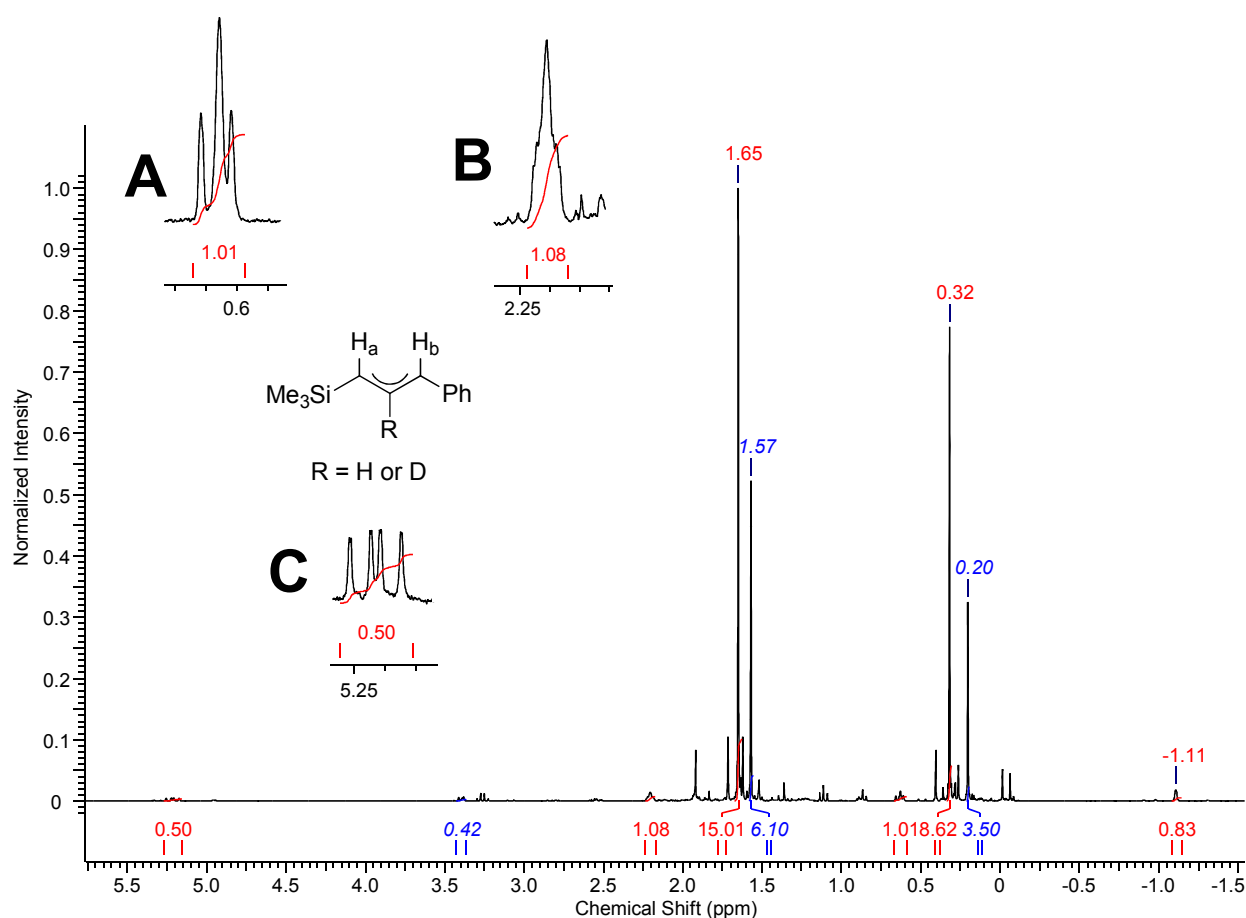


Figure 3.6. Expansion (−1.5 to +6.0 ppm) of the ^1H NMR spectrum (300 MHz) of **3.1** thermolyzed in C_6D_6 (2 d, 75 °C) with ten equivalents of pyridine demonstrating deuterium incorporation on the *meso* proton of the allyl ligand. Inset: Expansions of the signals due to the protons a) CHSiMe_3 , b) CHPh , c) *meso*, on the allyl ligand, showing partial deuteration at the *meso* position. Signals marked by blue italics are due to the formation of **3.2-d**.

MS data (Figure 3.7) of the final reaction mixture suggest that **3.1** has reacted further and has incorporated various numbers of deuterium atoms into the allyl ligand. This is evident from comparing the results of thermolyzing **3.1b** in neat pyridine (Figure 3.7a) with

the results obtained when thermolyzing **3.1b** in pyridine and C₆D₆ (Figure 3.7b). The isotope pattern of the two clusters from the latter reaction at m/z 619 and m/z 540 (corresponding to monodeuterated **3.2** and monodeuterated **3.1**, respectively) is broad and does not show the usual W isotope pattern, implying varying degrees of deuteration. However, the cluster at m/z 428 corresponding to the Cp*W(NO) fragment does display the expected W isotope pattern, implying that deuterium is not incorporated into the Cp* ligand.

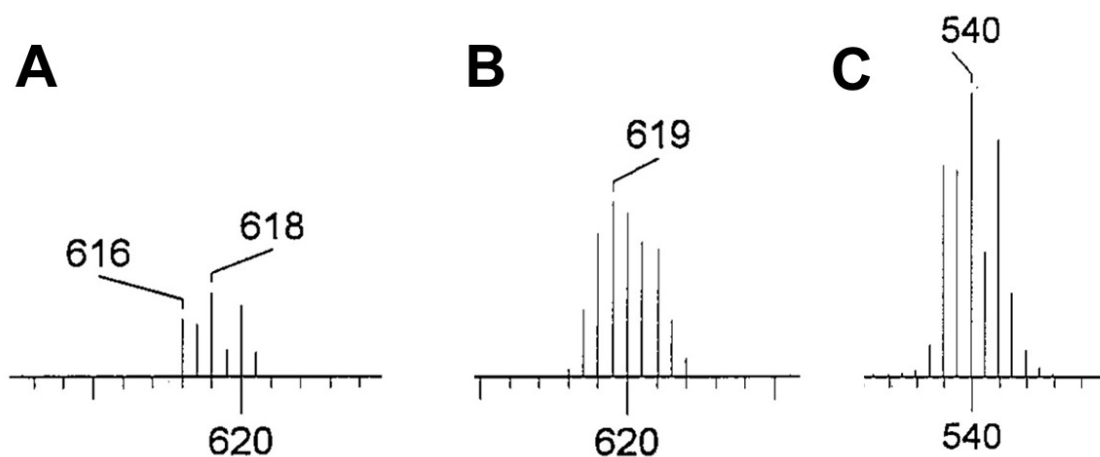


Figure 3.7. Comparison of the M^+ peaks for the product of the reaction of **3.1** in a) neat pyridine; b) pyridine and C₆D₆; c) neat C₆D₆. The M^+ peak of **3.1** is found at m/z 539 (¹⁸⁴W).

Although first observed in the presence of a Lewis base, the H/D exchange is also observed when **3.1** is thermolyzed in neat deuterobenzene, forming **3.1b-d₁**. In this case, however, deuteration at a single site—the *meso* position—is observed, and is upheld both by MS (Figure 3.7c) and NMR data. Deuteration of the allyl ligand is reversible; thermolysis of **3.1b-d₁** in C₆H₆ regenerates **3.1b**.

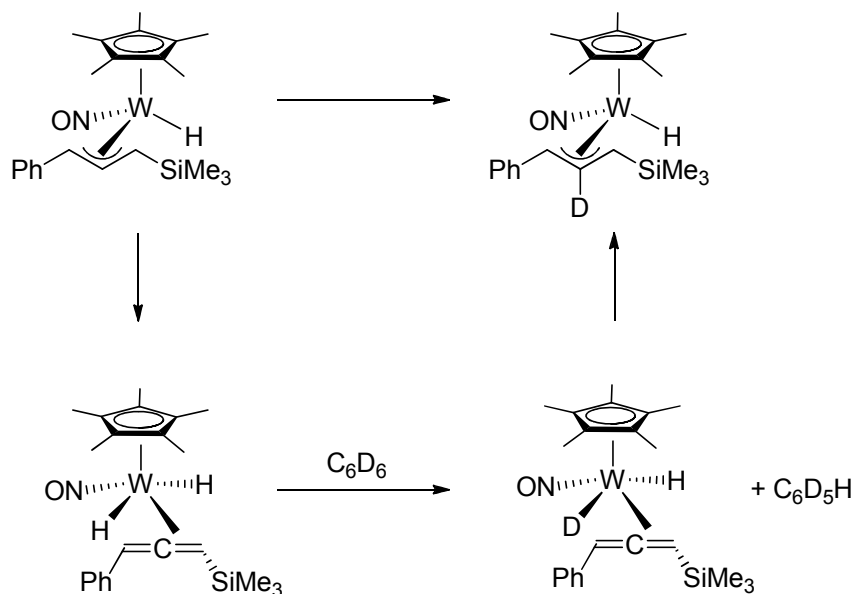
Because this exchange happens even in the presence of a Lewis base, it is unlikely that the mechanism of this transformation involves an open coordination slot on the metal

centre. Additionally, there is neither NMR nor MS evidence for the incorporation of a C₆D₅ group into the metal complex, so any mechanistic speculation must account for the fact that this fragment does not remain in the metal's coordination sphere.

The retention of the hydride is the most surprising feature of this reaction, as H/D exchange on transition metal complexes is usually mediated by a metal-hydride linkage.⁷⁴ This results in replacement of the hydride by deuterium, contrary to what has been observed here. However, in 1999, Jones and co-workers reported that CpRe(PPh₃)₂H₂ catalyzes H/D exchange without deuterium incorporation into the hydride ligands.⁷⁵ It was proposed that the active intermediate in this transformation is (η³-C₅H₇)Re(PPh₃)₂, in which both hydride ligands have migrated onto the Cp ligand. In principle, a similar mechanism could be at work in our system, but hydride migration onto the Cp* ring would open a coordination slot on the W centre, and such an intermediate would likely be trapped by the Lewis base present in the reaction mixture.

An alternative mechanism could involve hydride abstraction from the *meso* position on the allyl ligand to give a dihydride η²-allene intermediate (Scheme 3.5). One of the W–H bonds can then undergo σ-bond metathesis with a C–D bond of C₆D₆ to generate C₆D₅H and a W–D bond. This deuteride could then migrate back to the *meso* position of the allyl, forming the observed **3.1b-d₁** complex. The origin of the reaction's selectivity could be the result of the steric bulk of the allene substituents preventing the original hydride from reacting with the solvent. The intervening allene ligand also prevents reductive elimination of H₂ from the metal's coordination sphere. A similar η³-allyl to η²-allene transformation has been suggested for Cp*Ir(allyl)(alkyl) complexes.⁷⁶

Scheme 3.5. Proposed mechanism for deuterium incorporation into **3.1b**.



It is worth noting that the small amount of **3.1c** present in these reactions also incorporates deuterium into the allyl ligand at the *meso* position to give **3.1c-d**. Unfortunately, it is not clear whether the hydride persists in this complex, as the region around 0.00 ppm where this signal is expected to appear is obscured by other signals.

3.2.3.4 Thermolysis of **3.1** in alkanes

3.1a has also been thermolyzed in C₆D₁₂ to ascertain if deuterium could be incorporated from the activation of *sp*³-hybridized C–H bonds. While isomerization to the thermodynamic product **3.1b** has been observed, no deuterium has been incorporated into the allyl ligand. Thus, this behaviour is unique to arenes.

A sample of **3.1** has been heated in a solution of pentane in order to evaluate its ability to activate alkanes. Despite prolonged heating at 75 °C, no pentane activation is observed, and only **3.1b** can be recovered from the reaction mixture. Taken together, these

experiments show that 1,3-disubstituted allyl hydrides are thermally robust and not likely to perform aliphatic C–H activation in the manner of the monosubstituted complexes.

3.3 Experimental procedures

3.3.1 Preparation of Cp*W(NO)(H)(η^3 -Me₃SiCHCHCHPh) (**3.1**).

Cp*W(NO)(Np)(η^3 -CH₂CHCHSiMe₃) (**2.1**) (146 mg, 0.274 mmol) was dissolved in C₆H₆ (ca. 15 mL) to obtain a orange solution. The reaction mixture was heated at 55 °C for 17 h. The solvent was removed in vacuo, and the solid recrystallized from pentane contained **3.1a**, **3.1b**, and **3.1c** in approximately a 2:2:1 ratio, as judged by ¹H NMR spectroscopy (84 mg, 41% yield). **3.1a** and **3.1b** were recrystallized from a minimal amount of pentane to afford yellow and orange crystals, respectively. **3.1c** was identified from NMR spectroscopic data.

Characterization data for **3.1a**: IR (cm⁻¹) 1557 (s, ν_{NO}), 1933 (m, ν_{WH}). ¹H NMR (300 MHz, C₆D₆): δ -0.97 (s, 1H, $^1J_{\text{WH}} = 119$, W–H), 0.13 (d, 1H, $^3J_{\text{HH}} = 13.2$, CHSiMe₃), 0.41 (s, 9H, SiMe₃), 1.71 (s, 15H, Cp* Me), 2.80 (d, 1H, $^3J_{\text{HH}} = 12.5$, CHPh), 5.34 (t, 1H, $^3J_{\text{HH}} = 12.4$, allyl *meso*), 7.00 (m, 1H, *para* CH), 7.12 (obscured t, $^3J_{\text{HH}} = 7.8$, *meta* CH), 7.28 (d, 2H, $^3J_{\text{HH}} = 7.3$, *ortho* CH). ¹³C NMR (100 MHz, C₆D₆): δ 2.1 (SiMe₃), 11.1 (C₅Me₅), 44.7 (CHSiMe₃), 86.7 (CHPh), 104.3 (C₅Me₅), 106.4 (allyl *meso*), 126.7 (*para* CH), 127.0 (*meta* CH), 129.1 (*ortho* CH), 142.7 (*ipso* C). MS (LREI, *m/z*, probe temperature 120 °C) 539 [M⁺, ¹⁸⁴W]. Anal. Calcd for C₂₂H₃₃NOSiW: C, 48.98; H, 6.17; N, 2.60. Found: C, 49.00; H, 6.24; N, 2.53.

Characterization data for **3.1b**: IR (cm⁻¹) 1547 (s, ν_{NO}), 1926 (m, ν_{WH}). ¹H NMR (400 MHz, C₆D₆): δ -1.10 (s, 1H, $^1J_{\text{WH}} = 122$, W–H), 0.32 (s, 9H, SiMe₃), 0.63 (d, 1H, $^3J_{\text{HH}} =$

14.8, allyl CHSiMe_3), 1.65 (s, 15H, $\text{Cp}^* \text{Me}$), 2.20 (d, 1H, $^3J_{\text{HH}} = 10.1$, allyl CHPh), 5.22 (dd, 1H, $^3J_{\text{HH}} = 14.6$, 10.1, allyl *meso*), 7.08 (m, 1H, *para* CH), 7.28 (t, 2H, $^3J_{\text{HH}} = 7.7$, *meta* CH), 7.49 (d, 2H, $^3J_{\text{HH}} = 7.6$, *ortho* CH). ^{13}C NMR (75 MHz, C_6D_6) δ 0.7 (SiMe_3), 10.7 (C_5Me_5), 61.7 (allyl CHSiMe_3), 72.6 (allyl CHPh), 105.0 (C_5Me_5), 110.0 (allyl *meso*), 125.9 (*para* CH), 127.4 (*ortho* CH), 129.0 (*meta* CH), 142.9 (*ipso* C). MS (LREI, m/z , probe temperature 120 °C) 539 [M^+ , ^{184}W]; (HREI, m/z , ^{182}W) Calcd: 537.18137. Found: 537.18179.

Characterization data for **3.1c**: ^1H NMR (400 MHz, C_6D_6): δ 0.00 (s, 1H, $^1J_{\text{WH}} = 123$, W-H), 0.29 (s, 9H, SiMe_3), 1.52 (s, 15H, $\text{Cp}^* \text{Me}$), 2.66 (ddd, 1H, $^3J_{\text{HH}} = 8.6$, $^2J_{\text{HH}} = 2.8$, 2.05, allyl CH_2), 3.28 (dd, 1H, $^3J_{\text{HH}} = 14.1$, $^2J_{\text{HH}} = 1.5$, allyl CH_2), 3.84 (dd, 1H, $^3J_{\text{HH}} = 13.9$, 8.7, allyl *meso*), 6.94 (m, 1H, *para* CH), 7.11 (obscured t, 2H, $^3J_{\text{HH}} = 8.2$, *meta* CH), 7.57 (d, 2H, $^3J_{\text{HH}} = 6.8$, *ortho* CH). ^{13}C NMR (100 MHz, C_6D_6): δ 2.4 (SiMe_3), 10.5 (C_5Me_5), 50.4 (allyl CH_2), 84.7 ($\text{C}(\text{SiMe}_3)\text{Ph}$), 105.3 (C_5Me_5), 105.5 (allyl *meso*), 125.6 (*para* CH), 128.2 (*meta* CH), 133.4 (*ortho* CH), 147.6 (*ipso* C).

3.3.2 Extended thermolysis of 2.7

The thermolysis of **2.7** in tetramethylsilane as described in Section 2.3.8 was continued at 55 °C, 65 °C, and 75 °C for 2 d at each temperature. Aliquots were removed for analysis after 1 d and 2 d at each temperature. The solvent was removed from the samples in vacuo, and the remaining residue was dissolved in C_6D_6 and analyzed by ^1H NMR spectroscopy. No conversion to other products was noted.

3.3.3 Extended thermolysis of 2.6

2.6 (5 mg, 0.009 mmol) was dissolved in C₆D₆ (ca. 0.7 mL) and transferred to a J. Young NMR tube. The reaction mixture was heated in 10 °C increments from 50 °C to 90 °C for 24 h at each temperature. The ¹H NMR spectrum of the reaction mixture was taken periodically to ascertain the extent of reaction. No signals due to tungsten hydrides could be detected during the course of the reaction.

3.3.4 Thermolysis of 3.1 in PMe₃

3.1 (46 mg, 0.084 mmol) was thermolyzed in neat PMe₃ at 55 °C for 24 h. The volatiles were removed in vacuo to leave an orange oil (47 mg). ¹H and ³¹P{¹H} NMR spectra of this crude reaction mixture indicated the presence of five phosphorus-containing compounds. Separation of these compounds by column chromatography was unsuccessful.

3.3.5 Preparation of Cp*W(NO)(η²-PhCH=CHCH₂SiMe₃)(py) (**3.2**)

3.1 (18 mg, 0.033 mmol) was thermolyzed for 24 h at 85 °C in neat pyridine. Following removal of the volatiles in vacuo, Cp*W(NO)(η²-PhCH=CHCH₂SiMe₃)(C₅H₅N) (**3.2**) was found to be the sole organometallic product (20 mg, 96% yield).

Characterization data for **3.2**: IR (cm⁻¹) 1537 (s, ν_{NO}). ¹H NMR (300 MHz, C₆D₆): δ 0.21 (s, 9H, SiMe₃), 1.57 (s, 15H, Cp* Me), 1.93 (s, 2H, CH₂SiMe₃), 2.55 (td, 1H, ³J_{HH} = 9.9, 3.7, CHPh), 3.40 (d, 1H, ³J_{HH} = 10.0, CH), 6.17 (t, 2H, ³J_{HH} = 6.9, pyridine CH), 6.32 (d, 2H, ³J_{HH} = 7.3, aryl CH), 6.60 (t, 1H, ³J_{HH} = 7.6, pyridine CH), 6.76 (m, 1H, aryl CH), 7.06 (t, 2H, ³J_{HH} = 7.5, aryl CH), 8.53 (m, 2H, pyridine CH). ¹³C NMR (75 MHz, C₆D₆): δ -0.47

(SiMe₃), 9.8 (C₅Me₅), 29.7 (CH₂), 52.7 (CHPh), 62.3 (CH), 105.0 (C₅Me₅), 121.6 (aryl CH), 123.2 (pyridine CH), 124.4 (aryl CH), 128.3 (aryl CH), 135.4 (pyridine CH), 150.0 (ipso C), 153.4 (pyridine CH). MS (LREI, *m/z*, probe temperature 120 °C) 618 [M⁺, ¹⁸⁴W]; (HREI, *m/z*, ¹⁸⁴W) Calcd: 618.22630; Found: 618.22683; (HREI, *m/z*, ¹⁸²W) Calcd: 616.22357; Found: 616.22400.

3.3.6 Thermolysis of **3.1** in C₆D₆

A mixture of the isomers of **3.1** (6 mg, 0.01 mmol) was dissolved in C₆D₆ (ca. 0.7 mL) and transferred to a J. Young NMR tube. The sample was heated at 75 °C, and ¹H NMR spectra were taken periodically to assess the extent of reaction. **3.1a** and **3.1b** were converted exclusively to **3.1b-d₁**. **3.1c** was converted to **3.1c-d**, a partially deuterated product.

Characterization data for **3.1b-d₁**: ¹H NMR (300 MHz, C₆D₆): δ -1.11 (s, 1H, ¹J_{WH} = 121, W-*H*), 0.32 (s, 9H, SiMe₃), 0.63 (s, 1H, allyl CHSiMe₃), 1.65 (s, 15H, Cp* Me), 2.20 (s, 1H, allyl CHPh), 7.08 (m, 1H, *para* CH), 7.28 (t, 2H, ³J_{HH} = 7.7, *meta* CH), 7.49 (d, 2H, ³J_{HH} = 7.6, *ortho* CH). MS (LREI, *m/z*, probe temperature 120 °C) 540 [M⁺, ¹⁸⁴W].

Characterization data for **3.1c-d**: ¹H NMR (300 MHz, C₆D₆): 0.29 (s, 9H, SiMe₃), 1.52 (s, 15H, Cp* Me), 2.66 (s, 1H, allyl CH₂), 3.28 (s, 1H, allyl CH₂).

3.3.7 Thermolysis of **3.1** in C₆D₆ and pyridine

A sample of **3.1a** and **3.1b** (6 mg, 0.01 mmol) and pyridine was dissolved in C₆D₆ (ca. 0.7 mL) and transferred to a J. Young NMR tube. The number of equivalents of pyridine was determined by integration of the upfield hydride signals at -0.98 and -1.11 ppm against the signal due to the hydrogens at the 2 and 6 positions of pyridine at 8.53 ppm.⁷⁷ The sample

was heated in ten-degree increments from 55 °C to 95 °C for 24 h at a time, and ^1H NMR spectra were acquired periodically to assess the extent of reaction. Removal of the volatiles in vacuo yielded **3.2-d**, a partially deuterated product.

Characterization data for **3.2-d**: ^1H NMR (300 MHz, C_6D_6): δ 0.21 (s, 9H, SiMe_3), 1.57 (s, 15H, Cp^*Me), 1.93 (m, 2H, CH_2SiMe_3), 2.55 (m, <1H, CHPh), 3.40 (s, <1H, CH), 6.17 (m, 2H, pyridine CH), 6.32 (d, 2H, $^3J_{\text{HH}} = 7.3$, aryl CH), 6.58 (tt, 1H, $^3J_{\text{HH}} = 7.6$, $^4J_{\text{HH}} = 1.5$, pyridine CH), 6.76 (tt, $^3J_{\text{HH}} = 7.2$, $^4J_{\text{HH}} = 1.2$, 1H, aryl CH), 7.06 (t, 2H, $^3J_{\text{HH}} = 7.5$, aryl CH), 8.53 (br m, 2H, pyridine CH).

3.3.8 Thermolysis of **3.1** in C_6D_{12}

A sample of **3.1a** (11 mg, 0.02 mmol) was dissolved in C_6D_{12} (ca. 0.6 mL) and transferred to a J. Young NMR tube. The sample was heated at 75 °C for 48 h, and a ^1H NMR spectrum was taken every 24 h. At the end of this period only **3.1b** was observed, with no deuterium incorporation into the complex.

3.3.9 X-ray crystallography

Data collection was carried out at $-173 (\pm 1)$ °C on a Bruker X8 diffractometer, using graphite-monochromated $\text{Mo K}\alpha$ radiation.

Data for **3.1a** were collected to a maximum 2θ value of 55.1° in 0.5° oscillations with 60 s exposure times. The structure was solved by direct methods⁵⁹ and expanded using Fourier techniques. All non-hydrogen atoms were refined anisotropically, and hydrogens H1, H11, H12, and H13 were refined isotropically. All other hydrogen atoms were included in

fixed positions. The final cycle of full-matrix least squares analysis was based on 5076 observed reflections and 259 variable parameters.

Data for **3.1b** were collected to a maximum 2θ value of 55.9° in 0.5° oscillations. The structure was solved by direct methods⁵⁹ and expanded using Fourier techniques. The structure was a two-component twin; the two components were related by a 2.2° rotation about the (0.654 0.077 1.000) reciprocal axis. The twin components were separated using Cell_Now,⁷⁸ SAINTPLUS,⁷⁹ and TWINABS.⁸⁰ Refinement was performed on a deconvoluted HKLF4 data set. All non-hydrogen atoms were refined anisotropically, and hydrogen H1 was refined isotropically. All other hydrogen atoms were included in fixed positions. The final cycle of full-matrix least squares analysis was based on 5358 observed reflections and 248 variable parameters.

For each structure, neutral-atom scattering factors were taken from Cromer and Waber.⁶⁰ Anomalous dispersion effects were included in F_{calc} ;⁶¹ the values for $\Delta f'$ and $\Delta f''$ were those of Creagh and McAuley.⁶² The values for mass attenuation coefficients are those of Creagh and Hubbell.⁶³ All calculations were performed using SHELXL-97⁶⁴ via the WinGX interface.⁶⁵ X-ray crystallographic data for both structures are presented in Table A.2.

Chapter 4: Reactivity of Cp*W(NO)(Np)(η^3 -CH₂CHCHSiMe₃) with Fluorobenzenes

4.1 Introduction

Given that the σ - π distortion of the allyl ligand is a key feature of nearly all of the Cp*M(NO)(alkyl)(η^3 -allyl) complexes, further investigation of how the presence or absence of this feature—and by extension the electronics of the allyl ligand—affects their characteristic chemistry seemed like an interesting path to explore. This line of inquiry was pursued through the introduction of fluorinated aryl groups into the complex, either through activation of fluorobenzenes or direct introduction of fluoroaryl groups onto the allyl ligand.

Due to the interest in the introduction of fluorine atoms into molecules in areas such as medicinal chemistry⁸¹ and materials chemistry,⁸² the activation of compounds containing both C–H and C–F bonds is a small but growing field of study, and has been the subject of a recent review article.⁸³ Two questions dominate any discussion of the transition-metal based activation of fluoroarenes: first, are the activations chemoselective for C–H or C–F bonds? Secondly, what selectivity is observed in the activation of these bonds?

4.2 Results and discussion

4.2.1 Introduction of C₆F₅ groups

The trimethylsilylallyl ligand is amenable to substitution both at the unsubstituted end of the allyl ligand as well as on the silicon atom itself. Variations like these have the potential

to modify the properties of the resulting complex, as in the case of charge transfer in a Yb complex containing differently-substituted allyl ligands.⁸⁴ The possibility of changing the electron-withdrawing or -donating nature of the SiMe₃ group on the allyl ligand is very attractive, and one of the simplest methods to do so is to introduce electron-withdrawing groups onto the silicon atom. Unfortunately, while (MeO)₃SiCH₂CH=CH₂ is commercially available, reaction with *n*BuLi would likely lead to nucleophilic attack on silicon rather than the desired deprotonation of the allyl group.⁸⁵ In a similar vein, deprotonation of the allylchlorosilanes Me_xCl_{3-x}SiCH₂CH=CH₂ by *n*BuLi is not possible, since the preferred reactivity would again be nucleophilic attack at the Si atom. On the other hand, the latter materials are excellent starting points from which to modify the substituents on the silicon atom. Thus, the possibility of using C₆F₅ as an electron-withdrawing group to circumvent the limitation of silyl halides was investigated, since this group has been used as a replacement for halogens in other compounds, e.g., the Lewis acids BX₃.⁸⁶ Attempts were first made to derivatize the allyl ligand directly by introducing C₆F₅ onto the silicon atom to generate a Me₂(C₆F₅)SiCHCHCH₂ allyl ligand. Although the organic precursor was successfully synthesized *via* reaction between Me₂ClSiCH₂CHCH₂ and C₆F₅MgBr, its subsequent deprotonation by *n*BuLi and metathesis onto Cp*W(NO)(Np)Cl—the same methodology used to synthesize **2.1**—did not lead to the isolation of the desired product.

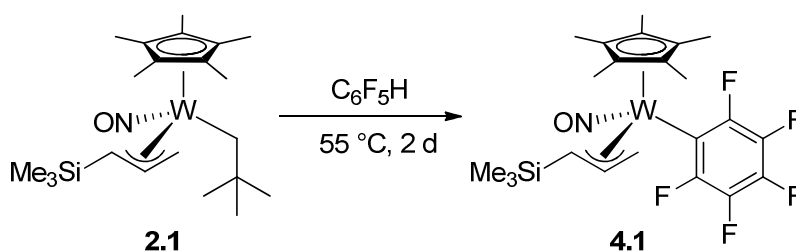
Thus, efforts were focused on the C–H activation of fluorobenzenes, under the hypothesis that the electronic nature of the aryl fluoride ligands would dictate both whether disubstituted allyl ligands could be generated *via* isomerization and, if formed, whether the complexes bearing such ligands would display different chemistry from their non-fluorinated counterparts.

4.2.2 Reactions of Cp*W(NO)(Np)(η^3 -CH₂CHCHSiMe₃) with fluorobenzenes

4.2.2.1 Pentafluorobenzene

The C–H bond of pentafluorobenzene is activated by thermolysis of **2.1** in neat C₆F₅H at 55 °C for 2 days (Scheme 4.1), yielding Cp*W(NO)(C₆F₅)(η^3 -CH₂CHCHSiMe₃) (**4.1**) as the sole product.

Scheme 4.1. Activation of pentafluorobenzene by **2.1**.



No C–F bond activation is observed, since no signals from aromatic protons appear in the ¹H NMR spectrum of **4.1**. Further evidence for exclusive C–H activation is afforded by the ¹⁹F{¹H} NMR spectrum, which shows highly complex signals assignable to C_{aryl}–F, rather than to W–F or C_{allyl}–F. The spectrum is also silent in the upfield region expected for a tungsten fluoride (around –200 ppm).⁸⁷ The solid-state molecular structure of **4.1** is presented in Figure 4.1.

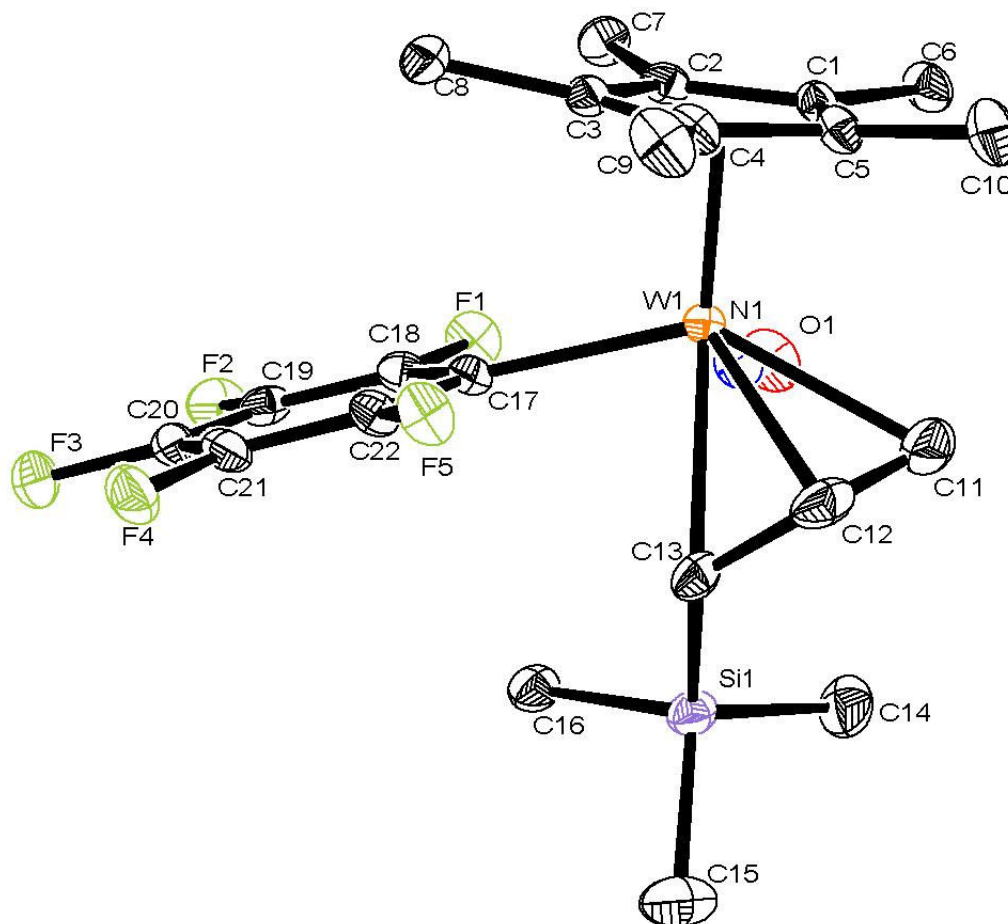


Figure 4.1. Solid-state molecular structure of **4.1** with 50% probability thermal ellipsoids.

Selected interatomic distances (Å) and angles (deg): C(11)–W(1) = 2.345(4); C(12)–W(1) = 2.301(3); C(13)–W(1) = 2.411(3); C(11)–C(12) = 1.391(6); C(12)–C(13) = 1.389(5); C(17)–W(1) = 2.216(3); N(1)–W(1) = 1.781(3); N(1)–O(1) = 1.217(3); C(13)–C(12)–C(11) = 121.3(3); O(1)–N(1)–W(1) = 166.2(3).

The presence of the pentafluorophenyl ligand has a pronounced effect on the allyl ligand. The C–C bond lengths are equal (C(11)–C(12) = 1.391 Å; C(12)–C(13) = 1.389 Å), so it is no longer σ - π distorted, especially when compared to the parent neopentyl complex **2.1**. Therefore, replacing the Np ligand with the C₆F₅ ligand removes the electronic

asymmetry at the metal centre. Both the NO and the C₆F₅ ligands withdraw electron density from the metal centre, but *via* different mechanisms: NO through π backbonding, and C₆F₅ through the inductive effect of the F atoms. The trimethylsilylallyl ligand in **4.1** exists in an *exo, anti* bonding mode with the SiMe₃ group is distal to the NO ligand, rather than proximal as observed in the solid-state molecular structure of **2.1**.

Comparison of the ν_{NO} IR stretching frequencies of **4.1** and **2.1** reveals that **2.1** has a higher ν_{NO} stretching frequency (1589 cm⁻¹) than the pentafluorophenyl compound (1581 cm⁻¹), implying that more W–NO backbonding occurs in **4.1**. Although comparing the NO bond lengths in the solid-state molecular structures of the two complexes (1.217(3) Å for **4.1** vs 1.227(2) Å for **2.1**) may lead one to the opposite conclusion, the difference between these lengths is not statistically significant. This observation could be the result of better σ donation from the undistorted allyl ligand.

The presence of five distinct signals in the ¹⁹F{¹H} spectrum of this complex indicates that the C₆F₅ group is bound fairly statically to the W centre, with minimal bond rotation about the W–C axis. If this were not the case, then only three signals should be observed in the spectrum, one for each set of chemically equivalent fluorine atoms.

Upon heating **4.1** in deuterobenzene, ¹H NMR spectroscopy reveals a second set of signals growing into the spectrum with similar chemical shifts and coupling constants to the initial product, consistent with partial isomerization of the complex, rather than arene migration to form a 1,3-disubstituted allyl ligand. This eventually leads to a thermodynamic distribution of approximately 3:1 between the major (**4.1**) and minor isomers. The minor isomer could have the allyl ligand coordinated in an *endo* fashion through a bond rotation. In addition, there is no evidence for activation of the solvent C–D bonds.

The lack of aryl migration onto the allyl ligand might be expected due to the undistorted allyl ligand being more electron-rich, and therefore less prone to nucleophilic attack than σ - π distorted allyl ligands. This is corroborated by comparing the ^{13}C chemical shifts of the allyl CH_2 carbon of the product of pentafluorobenzene activation, **4.1**, with the parent neopentyl complex, **2.1**. In **2.1**, this value is 84.6 ppm, while in **4.1** it is 56.1 ppm. These observations are consistent with a better-shielded carbon atom in **4.1** that likely also has a greater degree of sp^3 character than the analogous atom in **2.1**. In addition, the electronegativity of the fluorine atoms on the C_6F_5 group also reduces the nucleophilic character of the migrating group, further inhibiting its tendency to migrate.⁷⁰

If migration of the aryl group onto the ligand is prevented in **4.1** by the low nucleophilicity of the pentafluorophenyl group and the lack of σ - π distortion in the allyl ligand, then a less-substituted fluoroarene should somewhat mediate these effects. The first such fluorobenzene investigated was *p*-difluorobenzene, since all the C–H bonds in this substrate are equivalent.

4.2.2.2 *p*-Difluorobenzene

Because the C–H bonds in *p*-difluorobenzene are all chemically equivalent, the thermolysis of **2.1** in this solvent might be expected to lead to a single product from simple activation of the C–H bond. Instead, three major organometallic products are detected by ^1H NMR spectroscopy of the crude reaction mixture after thermolysis at 55 °C in neat *p*- $\text{C}_6\text{H}_4\text{F}_2$, as evidenced by three distinct allyl *meso* signals (Figure 4.2) in the ^1H NMR spectrum. However, there are no signals in the upfield region of the ^1H NMR spectrum, so the formation of hydrides can be excluded from possible reaction pathways.

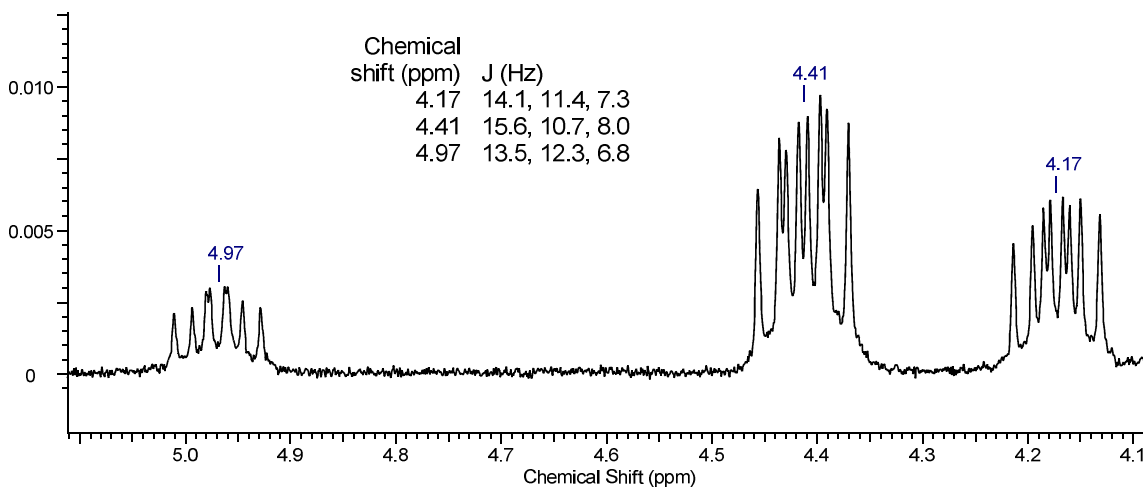
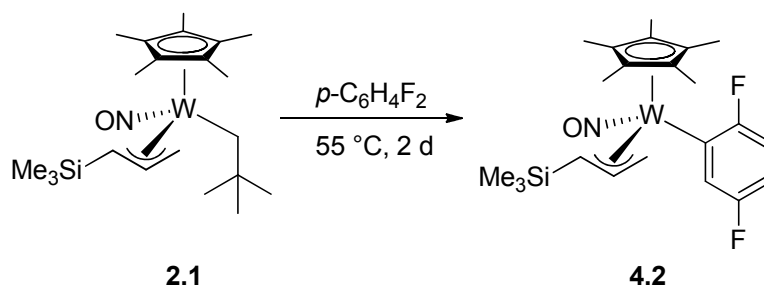


Figure 4.2. Expansion (4.1 to 5.1 ppm) of the ^1H NMR spectrum (300 MHz, C_6D_6) of the products of the thermolysis of **2.1** in *p*-difluorobenzene.

Each signal in Figure 4.2 is split into a doublet of doublets of doublets, implying coupling of the *meso* proton to three other protons in the same spin system. The allyl ligands must therefore still be monosubstituted. Given the splitting pattern of each signal, as well as the similarities in the chemical shifts and the coupling constants of these signals, this seems like a straightforward case of linkage isomerization of the allyl ligand between the various *endo/exo* and *syn/anti* combinations. Thus, the reaction of **2.1** with *p*-difluorobenzene likely proceeds as depicted in Scheme 4.2 to give **4.2**, the product resulting from activation of a single C–H bond:

Scheme 4.2. Activation of $p\text{-C}_6\text{F}_4\text{H}_2$ by **2.1**.



A single crystal suitable for X-ray diffraction analysis was grown and the solid-state molecular structure of one of the isomers of **4.2** is presented in Figure 4.3.

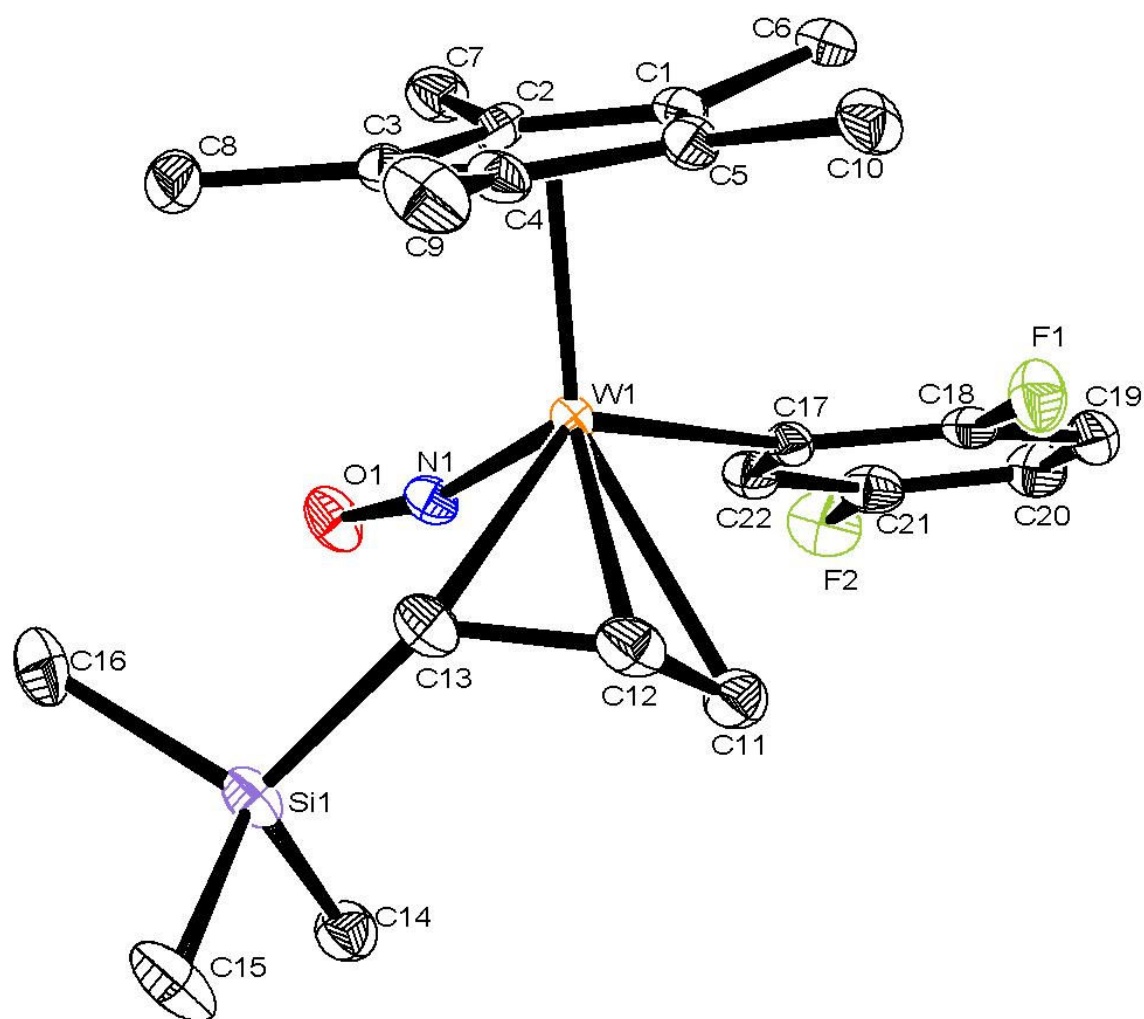


Figure 4.3. Solid-state molecular structure of one of the isomers of complex **4.2** with 50% probability thermal ellipsoids.

Selected interatomic distances (Å) and angles (deg): C(11)–W(1) = 2.400(4); C(12)–W(1) = 2.314(3); C(13)–W(1) = 2.343(3); C(11)–C(12) = 1.381(5); C(12)–C(13) = 1.422(5); C(17)–W(1) = 2.207(3); N(1)–O(1) = 1.226(3); N(1)–W(1) = 1.777(3); C(11)–C(12)–C(13) = 122.1(3); O(1)–N(1)–W(1) = 167.3(3).

The particular isomer represented in the solid state again contains the allyl ligand in the *exo*, *anti* configuration, similar to **4.1**. This may simply be the isomer that crystallizes most readily out of the three present in solution.

The allyl ligand in **4.2** also displays the σ - π distortion characteristic of these complexes ($C(11)-C(12) = 1.381 \text{ \AA}$; $C(12)-C(13) = 1.422 \text{ \AA}$); in fact, the C-C bond lengths are very similar to those in the starting material, **2.1**. Despite the electronegativity of the fluorine atoms, they appear to have only a minor effect on the structure of **4.2**. Consequently, decreasing the number of fluorine atoms on the fluoroaryl ligand relative to **4.1** has succeeded in restoring some of the electronic asymmetry at the metal centre. This is confirmed by comparing the ^{13}C chemical shift of the resonance due to the allyl CH_2 carbon in **2.1**, **4.1**, and **4.2**: the value for **4.2** (80.8 ppm) more closely resembles that of **2.1** (84.6 ppm) than **4.1** (56.1 ppm).

Since the σ - π distortion in the allyl ligand appears to be one factor promoting aryl migration, it might be expected that this complex could form the corresponding hydride under thermolytic conditions. However, thermolysis of a sample of **4.2** enriched in a single isomer in C_6D_6 leads to its partial conversion to one of the isomers found after recrystallization. After prolonged heating at 50 and 60 $^\circ\text{C}$, the system appears to reach equilibrium, with the two products present in about a 5:4 ratio. Hydride formation resulting from migration of the fluoroaryl ligand onto the allyl ligand is not observed. Thus, while a distorted allyl ligand may be a necessary condition for aryl migration, it is not sufficient; the aryl group itself must have also sufficient nucleophilic character.

4.2.2.3 *o*-Difluorobenzene

Continuing the investigation into the reactivity of **2.1** with fluorobenzenes, *o*-difluorobenzene has also been activated in a similar fashion to yield a mixture of products, including two organometallic hydrides.

The ^1H NMR spectrum of the crude reaction mixture arising from the reaction of **2.1** with *o*-difluorobenzene is quite complex, but nevertheless shows the presence of allyl *meso* signals corresponding to both mono- and disubstituted allyl ligands, which can be distinguished on the basis of their splitting patterns. In addition, the upfield region of the ^1H NMR spectrum contains two signals attributable to tungsten hydride species.

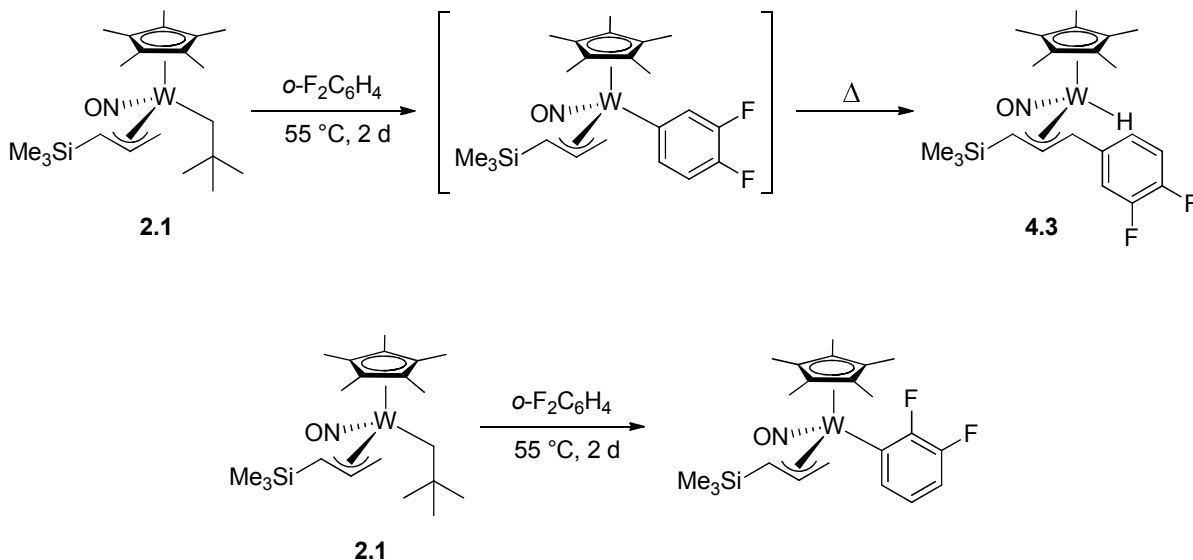
Table 4.1. ^1H NMR chemical shifts and coupling constants of selected signals from the mixture of products arising from the thermolysis of **2.1** in *o*-difluorobenzene.

δ_{Cp^*} (ppm)	δ_{hydride} (ppm)	δ_{meso} (ppm), multiplicity	<i>meso</i> J_{HH} (Hz)
1.59	-1.13	4.99, dd	14.8, 9.8
1.69	-1.24	5.13, t	12.3
1.57	n/a	4.38, ddd	15.6, 10.6, 7.9
1.65	n/a	4.15, ddd	13.9, 11.4, 7.3

Proceeding by analogy from the reaction of **2.1** with benzene, it is reasonable to expect that the two hydrides are the result of aryl migration onto the allyl ligand, since the signals due to the *meso* protons in these products only show coupling to two other protons. In addition, if the reactivity is truly analogous, then these two products are likely isomers differing in the orientation of the allyl ligand. The products which are not hydrides contain

monosubstituted allyl ligands, as evidenced by the ddd splitting pattern of the *meso* resonances. Taken together, these features suggest that two pathways for the C–H activation of *o*-difluorobenzene are available (Scheme 4.3).

Scheme 4.3. C–H activation of *o*-C₆F₂H₄ by **2.1**.



This hypothesis is further supported by the solid-state molecular structure of one of the hydride products (**4.3**), which has been isolated by recrystallization from pentane.

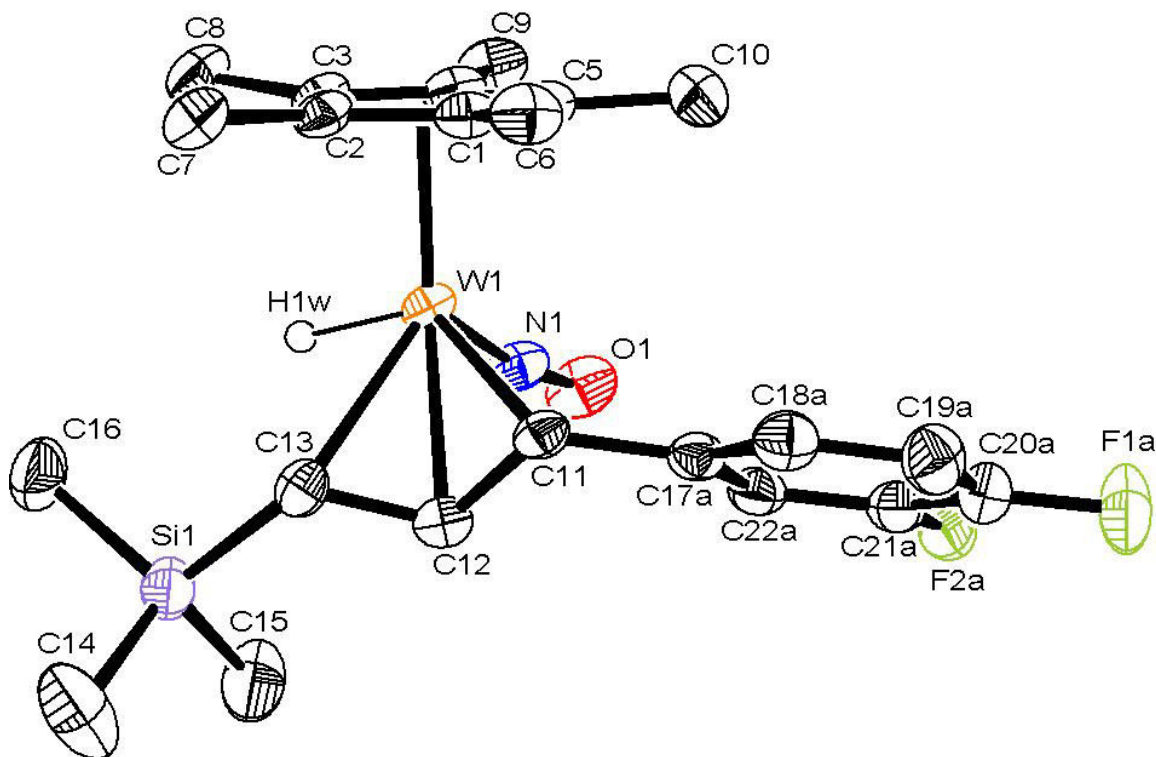


Figure 4.4. Solid-state molecular structure of **4.3** with 50% probability ellipsoids.

F2a is disordered over C21 and C19 in approximately a 3:1 ratio. Selected interatomic distances (Å) and angles (deg): C(11)–W(1) = 2.292(5); C(12)–W(1) = 2.307(5); C(13)–W(1) = 2.372(5); C(11)–C(12) = 1.414(7); C(12)–C(13) = 1.399(7); W(1)–H(1W) = 1.51(4); N(1)–O(1) = 1.238(5); N(1)–W(1) = 1.774(4); C(13)–C(12)–C(11) = 118.9(5); O(1)–N(1)–W(1) = 170.5(4).

In this solid-state molecular structure (Figure 4.4), the SiMe₃ group is distal to the NO ligand, and the complex has similar metrical parameters to complex **3.1b**. In particular, the C–C bond lengths in the allyl ligand are nearly equal (the difference is statistically insignificant). It seems then that the presence of fluorine atoms at the 3 and 4 positions on the aryl ring in **4.3** do not have a significant impact on the structure of the disubstituted allyl ligand when compared to **3.1b**. One might also infer that their effect on the nucleophilicity of

the aryl ligand in the presumed fluoroaryl intermediate is decreased, since migration onto the allyl ligand is observed in this case.

This product is expected to arise from the first reaction sequence in Scheme 4.3. First, the C–H bond at position 4 on *o*-difluorobenzene is activated; then, in a manner that parallels the reactivity of the phenyl ligand, the fluoroaryl group migrates onto the allyl ligand.

Like its unfluorinated counterpart, **3.1b**, the thermolysis of **4.3** in C₆D₆ leads to the incorporation of deuterium into the *meso* position of allyl ligand, while the hydride ligand remains intact. A brief comparison of the extent of D incorporation of these two reactions, as measured by the integration of the signal due to the *meso* proton against that of the Cp* signal, reveals that the incorporation of D into **4.3** occurs more quickly than for **3.1b**.

Up to this point the non-equivalence of the C–H bonds has not been considered, but naturally this is a key factor in resolving the question of the product distribution. Both the chemical shifts and coupling constants of the signals due to the products which are not hydrides are similar to **4.2** (Section 4.2.2.2). It then seems probable that these signals arise from the activation of a C–H bond adjacent to a C–F bond on the benzene ring (Scheme 4.3). Just as in the case of *p*-difluorobenzene, migration onto the allyl is not observed when the activated C–H bond is *ortho* to a fluorine atom. The separate *meso* signals are probably due to the different possible coordination modes of the allyl ligand. By comparing the relative integrations for the signals due to the *meso* protons in each of these complexes, it is clear that the favoured reaction pathway is activation at position 4 on *o*-difluorobenzene; only about 30% of the complexes in the final product mixture contain a monosubstituted allyl ligand.

Activation at position 4 on *o*-difluorobenzene, furthest from the fluorine atoms, is contrary to previous research done in the Legzdins group, where a preference for activation

at the *ortho*-F position was observed in the activation of fluorobenzene by $\text{Cp}^*\text{W}(\text{NO})(\text{Np})_2$.⁸⁸ Indeed, in most cases of C–H activation of fluorobenzenes, the C–H bond *ortho* to a C–F bond is the favoured site for activation.⁸⁹⁻⁹¹ This preference has been attributed to a thermodynamic stabilizing effect by the *ortho*-F, since the resulting M–C bond is strengthened more by the *ortho* C–F bond than the C–H bond in the substrate.⁹²

Therefore, although the preference to activate the C–H bond non-adjacent to the C–F seems at odds with previous research, it is consistent when one considers the aryl migration (which evidently occurs very quickly) to be a method of trapping the kinetically-favoured product. If this is the case then it appears a bit surprising that the ratio between these products so unbalanced, since, after all, the two chemically inequivalent sites are present in equal numbers. Here, however, sterics likely play a role in determining the regioselectivity of the reaction, as a similar preference has been observed for $[\text{TpOs}(\text{CH}_2\text{CH}_2\text{P}i\text{Pr}_3)(\eta^2\text{-CH}_2=\text{CH}_2)_2][\text{BF}_4]$;⁹³ in fact, C–H activation by **2.1** always occurs at the most sterically accessible site (Section 2.2.2).

Interestingly, Harman's investigation of the activation of fluorobenzenes with $\text{TpW}(\text{NO})(\text{PMe}_3)$ shows that both C–H and C–F bond activation can occur, with C–F activation predominating in the case of mono- and di-substituted fluorobenzenes.⁸⁷ DFT calculations have shown that even though the barriers to C–H and C–F activation for his system are similar, the thermodynamic stability of the resultant tungsten fluoride complex leads to it being the sole product observed from the reaction. Here, there is no evidence that C–F activation is a possible mode of reactivity for **2.1**; indeed, it is C–H activation that seems to be irreversible, particularly in the case of **4.3**.

4.3 Experimental procedures

4.3.1 Preparation of $\text{Cp}^*\text{W}(\text{NO})(\text{C}_6\text{F}_5)(\eta^3\text{-CH}_2\text{CHCHSiMe}_3)$ (**4.1**).

2.1 (115 mg, 0.216 mmol) was dissolved in pentafluorobenzene (ca. 5 mL) to obtain an orange solution. The reaction mixture was heated at 55 °C for 48 h. Subsequently, the solvent was removed in vacuo to give a brown oil. Complex **4.1** was recrystallized by slow diffusion of pentane into an Et_2O solution at –30 °C to yield a yellow microcrystalline solid (86 mg, 63% yield).

Characterization data for **4.1**: IR (cm^{-1}) 1507 (m, C_6F_5), 1581 (s, ν_{NO}). ^1H NMR (300 MHz, C_6D_6): δ –0.06 (s, 9H, SiMe_3), 1.34 (s, 15H, $\text{Cp}^* \text{Me}$), 2.23 (ddd, 1H, $^4J_{\text{HH}} = 2.5$, $^3J_{\text{HH}} = 7.3$, $^2J_{\text{HH}} = 1.3$, allyl CH_2), 2.87 (d, 1H, $^3J_{\text{HH}} = 13.5$, allyl CH_2), 3.53 (dd, 1H, $^3J_{\text{HH}} = 11.4$, $^4J_{\text{HH}} = 2.6$, CHSiMe_3), 4.22 (ddd, 1H, $^3J_{\text{HH}} = 13.6$, 11.3, 7.3, allyl *meso*). ^{13}C NMR (75 MHz, C_6D_6) δ 1.9 (SiMe_3), 9.8 (C_5Me_5), 56.1 (allyl CH_2), 72.8 (CHSiMe_3), 107.5 (C_5Me_5), 109.8 (allyl *meso*). Carbon atoms on the C_6F_5 ring were not observed due to the splitting resulting from ^{19}F . $^{19}\text{F}\{^1\text{H}\}$ NMR (282 MHz, C_6D_6) δ –165.5, –162.3, –158.8, –105.7, –105.5. MS (LREI, m/z , probe temperature 120 °C) 629 [M^+ , ^{184}W]; (HREI, m/z , ^{182}W) Calcd: 627.13426. Found: 627.13439.

^1H NMR spectroscopic data for minor isomer (300 MHz, C_6D_6): δ 0.20 (s, 9H, SiMe_3), 1.39 (s, 15H, $\text{Cp}^* \text{Me}$), 1.60 (dd, $^4J_{\text{HH}} = 2.6$, $^3J_{\text{HH}} = 10.6$, allyl CH_2), 3.78 (dd, 1H, $^3J_{\text{HH}} = 8.1$, 2.5, CHSiMe_3), 4.10 (dd, $^3J_{\text{HH}} = 15.3$, $^2J_{\text{HH}} = 1.5$, allyl CH_2), 4.41 (ddd, $^3J_{\text{HH}} = 15.2$, 10.6, 7.9, allyl *meso*).

4.3.2 Preparation of $\text{Cp}^*\text{W}(\text{NO})(2,5\text{-F}_2\text{C}_6\text{H}_3)(\eta^3\text{-CH}_2\text{CHCHSiMe}_3)$ (**4.2**).

2.1 (107 mg, 0.201 mmol) was dissolved in *p*-difluorobenzene (ca. 4 mL) to obtain an orange solution. The reaction mixture was heated at 55 °C for 48 h, and a colour change to yellow was noted at this time. The solvent was then removed in vacuo to give **4.2**. A single isomer of **4.2** was recrystallized from a pentane solution maintained at –30 °C to give a microcrystalline yellow-orange solid (87 mg, 75% yield).

Characterization data for **4.2**: IR (cm^{-1}) 1592 (s, ν_{NO}). ^1H NMR (300 MHz, C_6D_6): δ 0.19 (s, 9H, SiMe_3), 1.43 (s, 15H, $\text{Cp}^* \text{Me}$), 1.70 (dd, 1H, $^3J_{\text{HH}} = 10.7$, $^4J_{\text{HH}} = 2.5$, allyl CHSiMe_3), 3.91 (dd, 1H, $^3J_{\text{HH}} = 15.6$, $^4J_{\text{HH}} = 2.2$, allyl CH_2), 4.05 (dd, 1H, $^3J_{\text{HH}} = 8.1$, $^4J_{\text{HH}} = 2.2$, allyl CH_2), 4.41 (ddd, 1H, $^3J_{\text{HH}} = 15.5$, 10.8, 8.2, allyl *meso*), 6.63 (m, 2H, aryl *CH*), 8.12 (dt, 1H, $J = 9.1$, 2.9, aryl *CH*). ^{13}C NMR (75 MHz, C_6D_6) δ 2.1 (SiMe_3), 9.6 (C_5Me_5), 51.1 (allyl CHSiMe_3), 80.7 (allyl CH_2), 107.3 (C_5Me_5). Due to splitting by F and isomerization of the complex at room temperature, satisfactory spectra for assigning the ^{13}C resonances on the fluoroaryl ligand could not be obtained. MS (LREI, m/z , probe temperature 120 °C) 575 [M^+ , ^{184}W]; (HREI, m/z , ^{182}W) Calcd: 573.16252. Found: 573.16279.

4.3.3 Thermolysis of **4.2**.

A C_6D_6 solution of **4.2** in a J. Young NMR tube was heated at 50 °C and 60 °C for 24 h. The progress of the isomerization was observed by ^1H NMR spectroscopy.

Spectral data for isomer: ^1H NMR (300 MHz, C_6D_6): δ –0.03 (s, 9H, SiMe_3), 1.38 (s, 15H, $\text{Cp}^* \text{Me}$), 2.38 (ddd, 1H, $^3J_{\text{HH}} = 7.3$, $^2J_{\text{HH}} = 2.6$, $^4J_{\text{HH}} = 1.1$, allyl CH_2), 3.13 (d, 1H, $^3J_{\text{HH}} = 14.1$, allyl CHSiMe_3), 3.51 (dd, $^3J_{\text{HH}} = 11.4$, $^2J_{\text{HH}} = 2.6$, allyl CH_2), 4.17 (ddd, 1H, $^3J_{\text{HH}} = 13.9$, 11.4, 7.4, allyl *meso*), 6.66 (m, 2H, aryl *CH*), 8.04 (dt, 1H, $J = 9.2$, 3.4, aryl *CH*).

4.3.4 Thermolysis of 2.1 in *o*-difluorobenzene.

2.1 (110 mg, 0.206 mmol) was thermolyzed in *o*-difluorobenzene for 2 d at 55 °C. Two sets of signals attributable to isomers of Cp*W(NO)(η^3 -3,4-F₂C₆H₃CHCHCHSiMe₃)(H) (**4.3**) and Cp*W(NO)(η^3 -CH₂CHCHSiMe₃)(2,3-F₂C₆H₃) were observed in the ¹H NMR spectrum. Only **4.3** was recrystallized from a pentane solution maintained at –30 °C (31 mg, 26% yield).

Characterization data for **4.3**: IR (cm^{–1}) 1596 (s, ν_{NO}), 1928 (w, ν_{WH}). ¹H NMR (300 MHz, C₆D₆): δ –1.12 (s, 1H, ¹ J_{WH} = 120, W–H), 0.30 (s, 9H, SiMe₃), 0.62 (d, 1H, ³ J_{HH} = 14.7, CHSiMe₃), 1.59 (s, 15H, Cp* Me), 1.90 (d, 1H, ³ J_{HH} = 9.7, CH(3,4-F₂C₆H₃)), 5.00 (dd, 1H, ³ J_{HH} = 14.7, 9.7, allyl *meso*), 6.84 (dd, 1H, ³ J_{HF} = 18.5, ³ J_{HH} = 8.5, aryl CH), 6.96 (m, 1H, aryl CH), 7.18 (obscured, 1H, aryl CH). ¹³C NMR (75 MHz, C₆D₆) δ 0.6 (SiMe₃), 10.6 (C₅Me₅), 62.8 (CHSiMe₃), 69.8 (CH(3,4-F₂C₆H₃)), 105.1 (C₅Me₅), 109.8 (allyl *meso*), 115.8 (aryl CH, ² J_{CF} = 17.9), 117.7 (aryl CH, ² J_{CF} = 16.2), 122.8 (aryl CH, ³ J_{CF} = 5.7), 140.5 (*ipso* C, ³ J_{CF} = 6.3, ⁴ J_{CF} = 4.0), 148.5 (aryl CF, ¹ J_{CF} = 153.7, ² J_{CF} = 12.7), 151.6 (aryl CF, ¹ J_{CF} = 155.5, ² J_{CF} = 12.7). ¹⁹F{¹H} NMR (282 MHz, C₆D₆) δ –143.0 (³ J_{FF} = 22.6), –138.3 (³ J_{FF} = 21.1). MS (LREI, *m/z*, probe temperature 120 °C) 575 [M⁺, ¹⁸⁴W]; (HREI, *m/z*, ¹⁸²W) Calcd: 573.16252. Found: 573.16232.

Minor isomer, selected ¹H NMR signals: δ –1.24 (s, 1H, ¹ J_{WH} = 115, W–H), 0.10, (d, 1H, ³ J_{HH} = 12.1, allyl CHSiMe₃), 0.38 (s, 9H, SiMe₃), 1.69 (s, 15H, Cp* Me), 2.50 (d, 1H, ³ J_{HH} = 12.6, allyl CH(3,4-F₂C₆H₃)), 5.13 (t, 1H, ³ J_{HH} = 12.0, allyl *meso*).

4.3.5 X-ray crystallography

Data collection was carried out at $-173 (\pm 1 \text{ } ^\circ\text{C})$ on a Bruker X8 diffractometer, using graphite-monochromated Mo K α radiation.

Data for **4.1** were collected to a maximum 2θ value of 59.6° in 0.5° oscillations. The structure was solved by direct methods⁵⁹ and expanded using Fourier techniques. All non-hydrogen atoms were refined anisotropically, and hydrogens H11a and H11b were refined isotropically. All other hydrogen atoms were included in fixed positions. The final cycle of full-matrix least squares analysis was based on 6380 observed reflections and 296 variable parameters.

Data for **4.2** were collected to a maximum 2θ value of 62.9° in 0.5° oscillations with 5 s exposures. The structure was solved by direct methods⁵⁹ and expanded using Fourier techniques. All non-hydrogen atoms were refined anisotropically, and hydrogens H11a, H11b, and H13 were refined isotropically. All other hydrogen atoms were included in fixed positions. The final cycle of full-matrix least squares analysis was based on 7395 observed reflections and 273 variable parameters.

Data for **4.3** were collected to a maximum 2θ value of 54.3° in 0.5° oscillations with 60 s exposures. The structure was solved by direct methods⁵⁹ and expanded using Fourier techniques. All non-hydrogen atoms were refined anisotropically, and hydrogens H1w, H11, H12, and H13 were refined isotropically. The thermal parameter of H1w was constrained to be 1.2 times that of the tungsten atom. All other hydrogen atoms were included in fixed positions. Fluorine F2 was disordered over two sites on the aryl ring in approximately a 74/26 ratio. The final cycle of full-matrix least squares analysis was based on 5101 observed reflections and 286 variable parameters.

For each structure, neutral-atom scattering factors were taken from Cromer and Waber.⁶⁰ Anomalous dispersion effects were included in F_{calc} ;⁶¹ the values for $\Delta f'$ and $\Delta f''$ were those of Creagh and McAuley.⁶² The values for mass attenuation coefficients are those of Creagh and Hubbell.⁶³ All calculations were performed using SHELXL-97⁶⁴ *via* the WinGX interface.⁶⁵ X-ray crystallographic data for all structures are presented in Table A.3.

Chapter 5: Conclusion

5.1 Summary of thesis work

At the outset of this research, the goal was to investigate how incorporating a 1,3-disubstituted allyl ligand into the $\text{Cp}^*\text{W}(\text{NO})(\text{alkyl})(\eta^3\text{-allyl})$ complexes would affect these complexes' characteristic chemistry, with the ultimate hope that these allyl ligands would prove more resistant to reaction with external agents than their monosubstituted counterparts. Along the way, the chemistry of the monosubstituted trimethylsilylallyl ligand was also investigated.

Trimethylsilylallyl ligands remain relatively rare in organometallic chemistry. They (or their derivatives) have been studied as stabilizers for homoleptic allyl complexes³¹ and as intermediates in the palladium-catalyzed Tsuji-Trost reaction.⁷³

$\text{Cp}^*\text{W}(\text{NO})(\text{Np})(\eta^3\text{-CH}_2\text{CHCHSiMe}_3)$ (**2.1**) has been shown to selectively activate alkanes at their terminal positions *via* an η^2 -allene intermediate. Sterics are the main determinant of the selectivity of the system. This system is also tolerant of ether functionalities, but decomposes to $\text{Cp}^*\text{W}(\text{O})_2(\text{Np})$ in the presence of aldehyde or alcohol groups. Experiments with PMe_3 and cyclohexene have confirmed the nature of the allene intermediate, and kinetic studies have shown that the consumption of **2.1** follows pseudo-first-order kinetics.

Carbonylation of the neopentyl ligand in **2.1** has also been accomplished. The introduction of the acyl group onto the sterically bulky neopentyl ligand allows for some

flexibility in the metal's coordination sphere, and the slow interconversion of two isomers has been confirmed by a ROESY NMR experiment.

The Mo congener of **2.1**, **2.11**, has also been synthesized and assessed for its C–H activation ability. This complex has a lower thermal stability than its W counterpart. While capable of generating an η^2 -allene intermediate to activate aryl C–H bonds, this complex has a second mode of reactivity, not observed in the W system: coupling of the neopentyl and allyl ligands to form a molybdenum hydride. **2.11**, therefore, is not likely to be of interest as a system for C–H activation.

Instead of affording the expected aryl allyl complex, thermolysis of **2.1** in benzene leads primarily to the formation of isomeric hydride complexes $\text{Cp}^*\text{W}(\text{NO})(\eta^3\text{-Me}_3\text{SiCHCHCHPh})(\text{H})$ (**3.1a** and **3.1b**) containing a disubstituted allyl ligand, along with small amounts of another hydride complex (**3.1c**) containing a 1,1-disubstituted allyl ligand. **3.1a** and **3.1b** showed a high thermal stability in aliphatic solvents. However, when thermolyzed in C_6D_6 , deuterium is selectively incorporated into the *meso* position of the allyl ligand, without any exchange into the hydride itself. This observation suggests that **3.1b** may be able to activate aryl C–H bonds, albeit in a somewhat cursory manner (no additional phenyl groups are observed in the tungsten atom's coordination sphere.)

Finally, preliminary investigations into modifications of the electronic nature of the allyl ligand have been carried out. A disubstituted allyl ligand bearing a fluoroaryl substituent undergoes H/D exchange onto the allyl ligand in the same way as the non-fluorinated complex; indeed, it does so more quickly. This suggests that modifying the electronics of the allyl ligand can have an impact on a complex's reactivity. While the direct introduction of a pentafluorophenyl substituent onto the silicon atom of the allyl ligand has proven

unsuccessful, the C–H activation of *o*-difluorobenzene at position 4 on the benzene ring leads to the formation of a 1,3-disubstituted allyl hydride complex containing a fluoroaryl substituent. The C–H activation of pentafluorobenzene and *p*-fluorobenzene leads to the formation of the expected fluoroaryl complexes, without migration of the fluoroaryl ligands onto the allyl ligand. The products of these reactions contain fluoroaryl ligands with F atoms *ortho* to the activated position, which decreases the nucleophilicity of the fluoroaryl ligand, preventing migration. No C–F activation is observed for any fluorinated substrate.

In summary, this work adds to the existing body of knowledge on C–H activation by the Cp*M(NO)(alkyl)(η^3 -allyl) systems (M = Mo, W), and will aid in the rational design of a system for catalytic alkane functionalization.

5.2 Future work

Although the work presented in this thesis broadens the scope of knowledge about the Cp*W(NO)(alkyl)(η^3 -allyl) systems, further questions have been raised during the course of this research.

First, with regards to **2.1**, and in particular, **2.11**, investigation into possible ways to release the acyl ligand is of paramount importance. Completing the catalytic cycle would represent a great advance in the field of alkane functionalization, particularly if it can be achieved without the use of costly reagents or harsh conditions. A discovery such as this would obviously have far-reaching implications from an industrial point of view, but might also have applications to smaller-scale bench chemistry, due to the selectivity of the transformations facilitated by these complexes.

Secondly, more studies on the mechanism of the deuterium incorporation into **3.1b** should be undertaken, as the hydride's persistence throughout the course of deuterium incorporation is unique. These could include measurement of kinetic isotope effects in order to reveal possible candidates for the rate-determining step of the mechanism, as well as theoretical investigations to devise mechanistic proposals. The reversibility of the deuterium incorporation suggests that **3.1b** can act as a catalyst for H/D exchange, so its activity could be compared to extant systems. In addition, the role of pyridine, and why its presence results in the incorporation of multiple deuterium atoms into the complex, should be elucidated.

Thirdly, given the results of modifying the metal's electronic environment on the structure of the allyl ligand, further modification of ligand electronics seems like a promising line of research. However, these systems have also proven to be quite sensitive to the steric demand of the allyl ligand. As a start, investigating the pentafluorophenylallyl ligand would provide a direct comparison with the properties of the phenylallyl ligand, without an unreasonable increase in steric congestion around the W centre. Modification of the substituents on the silicon atom with less sterically-demanding groups than C₆F₅ might also be possible.

References

- (1) Schrock, R. R. *Proc. Natl. Acad. Sci. U. S. A.* **2006**, *103*, 17087.
- (2) Davies, H. M. L.; Du Bois, J.; Yu, J. *Chem. Soc. Rev.* **2011**, *40*, 1855.
- (3) Crabtree, R. H. *J. Organomet. Chem.* **2004**, *689*, 4083.
- (4) Chen, X.; Engle, K. M.; Wang, D.; Yu, J. *Angew. Chem., Int. Ed.* **2009**, *48*, 5094.
- (5) Haynes, A. *Top. Organomet. Chem.* **2006**, *18*, 179.
- (6) Crabtree, R. H. *J. Chem. Soc., Dalton Trans.* **2001**, (17), 2437.
- (7) Hashiguchi, B. G.; Bischof, S. M.; Konnick, M. M.; Periana, R. A. *Acc. Chem. Res.* **2012**, *45*, 885.
- (8) Holmen, A. *Catalysis Today* **2009**, *142*, 2.
- (9) McMurray, L.; O'Hara, F.; Gaunt, M. J. *Chem. Soc. Rev.* **2011**, *40*, 1885.
- (10) Lewis, J. C.; Coelho, P. S.; Arnold, F. H. *Chem. Soc. Rev.* **2011**, *40*, 2003.
- (11) Crabtree, R. H. *Chem. Rev.* **2010**, *110*, 575.
- (12) Green, M. L.; Knowles, P. J. *J. Chem. Soc. D* **1970**, (24), 1677.
- (13) Chatt, J.; Davidson, J. M. *J. Chem. Soc.* **1965**, 843.
- (14) Janowicz, A. H.; Bergman, R. G. *J. Am. Chem. Soc.* **1982**, *104*, 352.
- (15) Hoyano, J. K.; Graham, W. A. G. *J. Am. Chem. Soc.* **1982**, *104*, 3723.
- (16) Jones, W. D.; Feher, F. J. *Organometallics* **1983**, *2*, 562.
- (17) Coperet, C. *Chem. Rev.* **2010**, *110*, 656.
- (18) Lin, Z. *Coord. Chem. Rev.* **2007**, *251*, 2280.
- (19) Perutz, R.; Sabo-Etienne, S. *Angew. Chem., Int. Ed* **2007**, *46*, 2578.
- (20) Calladine, J. A.; Duckett, S. B.; George, M. W.; Matthews, S. L.; Perutz, R. N.; Torres, O.; Vuong, K. Q. *J. Am. Chem. Soc.* **2011**, *133*, 2303.
- (21) Young, R. D.; Lawes, D. J.; Hill, A. F.; Ball, G. E. *J. Am. Chem. Soc.* **2012**, *134*, 8294.

- (22) Liu, F.; Pak, E. B.; Singh, B.; Jensen, C. M.; Goldman, A. S. *J. Am. Chem. Soc.* **1999**, *121*, 4086.
- (23) Shilov, A. E.; Shul'pin, G. B. *Chem. Rev.* **1997**, *97*, 2879.
- (24) Periana, R. A.; Taube, D. J.; Gamble, S.; Taube, H.; Satoh, T.; Fujii, H. *Science* **1998**, *280*, 560.
- (25) Chen, H.; Schlecht, S.; Semple, T. C.; Hartwig, J. F. *Science* **2000**, *287*, 1995.
- (26) Hartwig, J. F. *Chem. Soc. Rev.* **2011**, *40*, 1992.
- (27) Ng, S. H. K.; Adams, C. S.; Hayton, T. W.; Legzdins, P.; Patrick, B. O. *J. Am. Chem. Soc.* **2003**, *125*, 15210.
- (28) Tsang, J. Y. K.; Buschhaus, M. S. A.; Graham, P. M.; Semiao, C. J.; Semproni, S. P.; Kim, S. J.; Legzdins, P. *J. Am. Chem. Soc.* **2008**, *130*, 3652.
- (29) Baillie, R. A.; Man, R. W. Y.; Shree, M. V.; Chow, C.; Thibault, M. E.; McNeil, W. S.; Legzdins, P. *Organometallics* **2011**, *30*, 6201.
- (30) Semproni, S. P.; Graham, P. M.; Buschhaus, M. S. A.; Patrick, B. O.; Legzdins, P. *Organometallics* **2009**, *28*, 4480.
- (31) Solomon, S. A.; Layfield, R. A. *Dalton Trans.* **2010**, *39*, 2469.
- (32) Faller, J. W.; Chodosh, D. F.; Katahira, D. *J. Organomet. Chem.* **1980**, *187*, 227-31.
- (33) Armarego, W. L. F.; Chai, C. L. L. In *Purification of Laboratory Chemicals (5th Edition)*; Elsevier: Amsterdam, 2003.
- (34) Debad, J. D.; Legzdins, P.; Rettig, S. J.; Veltheer, J. E. *Organometallics* **1993**, *12*, 2714.
- (35) Periana, R. A.; Bhalla, G.; Tenn III, W. J.; Young, K. J. H.; Liu, X. Y.; Mironov, O.; Jones, C. J.; Ziatdinov, V. R. *Journal of Molecular Catalysis A: Chemical* **2004**, *220*, 7.
- (36) Balcells, D.; Clot, E.; Eisenstein, O. *Chem. Rev.* **2010**, *110*, 749.
- (37) Labinger, J. A.; Bercaw, J. E. *Nature* **2002**, *417*, 507.
- (38) Pannell, K. H.; Lappert, M. F.; Stanley, K. *Journal of Organometallic Chemistry* **1976**, *112*, 37.
- (39) Norman, D. W.; Ferguson, M. J.; McDonald, R.; Stryker, J. M. *Organometallics* **2006**, *25*, 2705.

- (40) Tsang, J. Y. K.; Buschhaus, M. S. A.; Fujita-Takayama, C.; Patrick, B. O.; Legzdins, P. *Organometallics* **2008**, *27*, 1634.
- (41) Hoshi, M.; Masuda, Y.; Arase, A. *Chem. Lett.* **1991**, (2), 251-4.
- (42) Julia, M.; Verpeaux, J.; Zahneisen, T. *Bull. Soc. Chim. Fr.* **1994**, *131*, 539.
- (43) Vyas, D. J.; Oestreich, M. *Chem. Commun.* **2010**, *46*, 568.
- (44) Sharp, W. B.; Daff, P. J.; McNeil, W. S.; Legzdins, P. *J. Am. Chem. Soc.* **2001**, *123*, 6272.
- (45) Davidson, G. In *Vibrational Spectra of Some Co-ordinated Ligands*; Spectroscopic Properties of Inorganic and Organometallic Compounds; The Royal Society of Chemistry: Cambridge, 2000; pp 306.
- (46) Greenhough, T. J.; Legzdins, P.; Martin, D. T.; Trotter, J. *Inorg. Chem.* **1979**, *18*, 3268.
- (47) Villanueva, L. A.; Ward, Y. D.; Lachicotte, R.; Liebeskind, L. S. *Organometallics* **1996**, *15*, 4190.
- (48) Bi, S.; Ariaferd, A.; Jia, G.; Lin, Z. *Organometallics* **2005**, *24*, 680.
- (49) Dymond, J. H. *J. Phys. Chem.* **1967**, *71*, 1829.
- (50) Wada, K.; Pamplin, C. B.; Legzdins, P.; Patrick, B. O.; Tsyba, I.; Bau, R. *J. Am. Chem. Soc.* **2003**, *125*, 7035.
- (51) Graham, P. M.; Buschhaus, M. S. A.; Baillie, R. A.; Semproni, S. P.; Legzdins, P. *Organometallics* **2010**, *29*, 5068.
- (52) Bourgeois, P.; Merault, G. *J. Organometal. Chem.* **1972**, *39*, C44.
- (53) Shaw, B. L.; Stringer, A. J. *Inorg. Chim. Acta, Rev.* **1973**, *7*, 1.
- (54) Baillie, R. A.; Tran, T.; Thibault, M. E.; Legzdins, P. *J. Am. Chem. Soc.* **2010**, *132*, 15160.
- (55) Gonsalvi, L.; Adams, H.; Sunley, G. J.; Ditzel, E.; Haynes, A. *J. Am. Chem. Soc.* **1999**, *121*, 11233.
- (56) Tran, T.; Chow, C.; Zimmerman, A. C.; Thibault, M. E.; McNeil, W. S.; Legzdins, P. *Organometallics* **2011**, *30*, 738.
- (57) Fraenkel, G.; Chow, A.; Winchester, W. R. *J. Am. Chem. Soc.* **1990**, *112*, 1382.

- (58) Legzdins, P.; Phillips, E. C.; Sanchez, L. *Organometallics* **1989**, *8*, 940.
- (59) Altomare, A.; Cascarano, G.; Giacovazzo, C.; Guagliardi, A. *J. Appl. C* **1993**, *26*, 343.
- (60) Cromer, D. T.; Waber, J. T. In *Table 2.2A*; International Tables for X-ray Crystallography; Kynoch Press: Birmingham, U.K., 1974; Vol. IV, .
- (61) Ibers, J. A.; Hamilton, W. C. *Acta Crystallogr.* **1964**, *17*, 781.
- (62) Creagh, D. C.; McAuley, W. J. *International Tables for X-ray Crystallography*; Kluwer Academic: Boston, 1992; Vol. C, Table 4.2.6.8.
- (63) Creagh, D. C.; Hubbell, J. H. *International Tables for X-ray Crystallography*; Kluwer Academic: Boston, 1992; Vol. C, Table 4.2.4.3.
- (64) SHELXL-97: Sheldrick, G. M. *Acta Crystallogr.* **2008**, *A64*, 112.
- (65) WinGX – V1.70: Farrugia, L. J. *J. Appl. Crystall* **1999**, *32*, 837.
- (66) Woodman, T. J.; Sarazin, Y.; Garratt, S.; Fink, G.; Bochmann, M. *Journal of Molecular Catalysis A: Chemical* **2005**, *235*, 88.
- (67) Schormann, M.; Garratt, S.; Bochmann, M. *Organometallics* **2005**, *24*, 1718-1724.
- (68) McNeil, W. S. **2011**, Personal communication.
- (69) Dougherty, D. A.; Mislow, K.; Blount, J. F.; Wooten, J. B.; Jacobus, J. *J. Am. Chem. Soc.* **1977**, *99*, 6149.
- (70) Stoeckenius, E. J., III; Jordan, R. F. *J. Am. Chem. Soc.* **2006**, *128*, 8638.
- (71) Mola, J.; Romero, I.; Rodríguez, M.; Bozoglian, F.; Poater, A.; Solà, M.; Parella, T.; Benet-Buchholz, J.; Fontrodona, X.; Llobet, A. *Inorg. Chem.* **2007**, *46*, 10707.
- (72) Baillie, R. A.; Tran, T.; Lalonde, K. M.; Tsang, J. Y. K.; Thibault, M. E.; Patrick, B. O.; Legzdins, P. *Organometallics* **2012**, *31*, 1055.
- (73) Branchadell, V.; Moreno-Manas, M.; Pleixats, R. *Organometallics* **2002**, *21*, 2407.
- (74) Atzrodt, J.; Derdau, V.; Fey, T.; Zimmermann, J. *Angew. Chem., Int. Ed.* **2007**, *46*, 7744.
- (75) Jones, W. D.; Rosini, G. P.; Maguire, J. A. *Organometallics* **1999**, *18*, 1754.
- (76) McGhee, W. D.; Bergman, R. G. *J. Am. Chem. Soc.* **1988**, *110*, 4246.

- (77) Fulmer, G. R.; Miller, A. J. M.; Sherden, N. H.; Gottlieb, H. E.; Nudelman, A.; Stoltz, B. M.; Bercaw, J. E.; Goldberg, K. I. *Organometallics* **2010**, *29*, 2176.
- (78) *Cell_Now 2008/2*; Bruker AXS Inc.: Madison, WI.
- (79) *SAINTPLUS*, Version 7.60A; Bruker AXS Inc.: Madison, WI 1997-2008.
- (80) *TWINABS, V2008/2*; Bruker AXS Inc.: Madison, WI, 2007.
- (81) Purser, S.; Moore, P. R.; Swallow, S.; Gouverneur, V. *Chem. Soc. Rev.* **2008**, *37*, 320.
- (82) Shimizu, M.; Hiyama, T. *Angew. Chem. , Int. Ed.* **2005**, *44*, 214.
- (83) Clot, E.; Eisenstein, O.; Jasim, N.; MacGregor, S. A.; McGrady, J. E.; Perutz, R. N. *Acc. Chem. Res.* **2011**, *44*, 333.
- (84) White, R. E.; Carlson, C. N.; Veauthier, J. M.; Simpson, C. K.; Thompson, J. D.; Scott, B. L.; Hanusa, T. P.; John, K. D. *Inorg. Chem.* **2006**, *45*, 7004.
- (85) Corey, J.; Guerin, C.; Henner, B.; Kolani, B.; Choy, W. W.; Man, W. C.; Corriu, R. C. *R. Acad. Sci. , Ser. 2* **1985**, *300*, 331.
- (86) Erker, G. *Dalton Trans.* **2005**, (11), 1883.
- (87) Liu, W.; Welch, K.; Trindle, C. O.; Sabat, M.; Myers, W. H.; Harman, W. D. *Organometallics* **2007**, *26*, 2589.
- (88) Tsang, J. Y. K.; Buschhaus, M. S. A.; Legzdins, P.; Patrick, B. O. *Organometallics* **2006**, *25*, 4215.
- (89) Lafrance, M.; Rowley, C. N.; Woo, T. K.; Fagnou, K. *J. Am. Chem. Soc.* **2006**, *128*, 8754.
- (90) Nakao, Y.; Kashiwara, N.; Kanyiva, K. S.; Hiyama, T. *J. Am. Chem. Soc.* **2008**, *130*, 16170.
- (91) Selmecky, A. D.; Jones, W. D.; Partridge, M. G.; Perutz, R. N. *Organometallics* **1994**, *13*, 522.
- (92) Clot, E.; Megret, C.; Eisenstein, O.; Perutz, R. N. *J. Am. Chem. Soc.* **2009**, *131*, 7817.
- (93) Bajo, S.; Esteruelas, M. A.; Lopez, A. M.; Onate, E. *Organometallics* **2011**, *30*, 5710.

Appendix

Appendix A X-ray crystallographic data

Table A.1. X-ray crystallographic data for structures presented in Chapter 2.

	2.1	2.9	2.10
	Crystal Data		
empirical formula	C ₂₁ H ₃₉ NOSiW	C ₁₉ H ₃₆ NOPSiW	C ₂₂ H ₃₇ NOSiW
cryst habit, colour	plate, orange	prism, yellow	prism, yellow
crystal size (mm)	0.26 × 0.23 × 0.07	0.12 × 0.10 × 0.08	0.39 × 0.36 × 0.30
cryst system	Monoclinic	Monoclinic	Monoclinic
space group	<i>P</i> 2 ₁ / <i>n</i>	<i>C</i> 2/ <i>c</i>	<i>C</i> 2/ <i>c</i>
volume (Å ³)	2259.06(17)	4501(2)	4626.6(3)
<i>a</i> (Å)	10.9969(5)	15.367(5)	22.9694(8)
<i>b</i> (Å)	14.8174(6)	9.883(3)	9.2914(4)
<i>c</i> (Å)	14.7423(6)	30.526(9)	21.8178(8)
α (°)	90	90	90
β (°)	109.878(2)	103.876(10)	96.480(2)
γ (°)	90	90	90
<i>Z</i>	4	8	8
calcd density (Mg/m ³)	1.569	1.586	1.560
abs coeff (mm ⁻¹)	5.175	5.264	5.056
<i>F</i> ₀₀₀	1072	2144	2176
No. of measd reflns: total	37697	30064	26072
No. of measd reflns: unique	6639	5346	6757
Final <i>R</i> Indices ^a	R1 = 0.0165, wR2 = 0.0372	R1 = 0.0211, wR2 = 0.0416	R1 = 0.0180, wR2 = 0.0365
Goodness-of-fit on <i>F</i> ^{2 b}	1.017	1.039	1.046
Largest diff. peak and hole (e ⁻ Å ⁻³)	0.629 and -0.623	0.663 and -0.840	0.878 and -0.886

Table A.1 (cont). X-ray crystallographic data for structures presented in Chapter 2.

	2.11	2.12	2.13
	Crystal Data		
empirical formula	C ₂₂ H ₃₉ NO ₂ SiW	C ₂₁ H ₃₉ MoNOSi	C ₁₉ H ₃₆ MoNOPSi
cryst habit, colour	prism, yellow	plate, yellow	plate, yellow
crystal size (mm)	0.50 × 0.23 × 0.12	0.60 × 0.10 × 0.05	0.25 × 0.19 × 0.11
cryst system	Monoclinic	Monoclinic	Monoclinic
space group	<i>P</i> 2 ₁ / <i>c</i>	<i>P</i> 2 ₁ / <i>n</i>	<i>C</i> 2/ <i>c</i>
volume (Å ³)	2344.18(13)	2305.6(7)	4563.8(7)
<i>a</i> (Å)	12.1444(3)	11.045(2)	15.4189(13)
<i>b</i> (Å)	11.4950(4)	14.930(3)	9.9407(8)
<i>c</i> (Å)	17.3264(6)	14.878(3)	30.681(3)
α (°)	90	90	90
β (°)	104.2650(10)	109.992(2)	103.953(4)
γ (°)	90	90	90
<i>Z</i>	4	4	8
calcd density (Mg/m ³)	1.591	1.284	1.308
abs coeff (mm ⁻¹)	4.995	0.629	0.703
<i>F</i> ₀₀₀	1128	944	1888
	Data Collection and Refinement		
No. of measd rflns: total	34248	16753	40852
No. of measd rflns: unique	8927	6475	10403
Final <i>R</i> Indices ^a	R1 = 0.0204, wR2 = 0.0521	R1 = 0.0361, wR2 = 0.0724	R1 = 0.0362, wR2 = 0.0669
Goodness-of-fit on <i>F</i> ^{2 b}	1.043	0.991	1.020
Largest diff. peak and hole (e ⁻ Å ⁻³)	2.454 and -1.688	0.363 and -0.328	0.694 and -0.585

^a R1 on *F* = $\Sigma |(|F_o| - |F_c|)| / \Sigma |F_o|$; wR2 = $[\Sigma (F_o^2 - F_c^2)^2 / \Sigma w(F_o^2)^2]^{1/2}$; *w* = $[\sigma^2 F_o^2]^{-1}$; ^b GOF = $[\Sigma (w (|F_o| - |F_c|)^2) / \text{degrees of freedom}]^{1/2}$.

Table A.2. X-ray crystallographic data for structures presented in Chapter 3.

	3.1a	3.1b
	Crystal Data	
empirical formula	C ₂₂ H ₃₃ NOSiW	C ₂₂ H ₃₃ NOSiW
cryst habit, colour	prism, orange	plate, yellow
crystal size (mm)	0.20 × 0.10 × 0.09	0.09 × 0.02 × 0.02
cryst system	Monoclinic	Monoclinic
space group	<i>C2/c</i>	<i>P2₁/n</i>
volume (Å ³)	4402.0(4)	2243.7(3)
<i>a</i> (Å)	29.8232(18)	8.4708(7)
<i>b</i> (Å)	10.1727(6)	13.6779(11)
<i>c</i> (Å)	15.8503(9)	19.5480(18)
α (°)	90	90
β (°)	113.733(2)	97.850(5)
γ (°)	90	90
<i>Z</i>	8	4
calcd density (Mg/m ³)	1.628	1.597
abs coeff (mm ⁻¹)	5.313	5.212
<i>F</i> ₀₀₀	2144	1072
	Data Collection and Refinement	
No. of measd reflns: total	40913	5358
No. of measd reflns: unique	5076	5358
Final <i>R</i> Indices ^a	R1 = 0.0158, wR2 = 0.0458	R1 = 0.0310, wR2 = 0.0636
Goodness-of-fit on <i>F</i> ² ^b	1.353	1.069
Largest diff. peak and hole (e ⁻ Å ⁻³)	1.535 and -0.516	2.082 and -1.502

^a R1 on $F = \sum (|F_o| - |F_c|) / \sum |F_o|$; wR2 = $[(\sum (F_o^2 - F_c^2)^2) / \sum w(F_o^2)^2]^{1/2}$; w = $[\sigma^2 F_o^2]^{-1}$; ^b GOF = $[\sum (w (|F_o| - |F_c|)^2) / \text{degrees of freedom}]^{1/2}$.

Table A.3. X-ray crystallographic data for structures presented in Chapter 4.

	3.1	3.2	3.3
	Crystal Data		
empirical formula	C ₂₂ H ₂₈ F ₅ NOSiW	C ₂₂ H ₃₁ F ₂ NOSiW	C ₂₂ H ₃₁ F ₂ NOSiW
cryst habit, colour	needle, yellow	prism, yellow-orange	prism, yellow
crystal size (mm)	0.40 × 0.10 × 0.04	0.11 × 0.06 × 0.05	0.11 × 0.06 × 0.05
cryst system	Monoclinic	Monoclinic	Monoclinic
space group	<i>P</i> 2 ₁ / <i>n</i>	<i>P</i> 2 ₁ / <i>c</i>	<i>P</i> 2 ₁ / <i>n</i>
volume (Å ³)	2306.14(19)	2235.5(2)	2313.3(3)
<i>a</i> (Å)	8.6761(4)	11.4956(7)	8.5346(7)
<i>b</i> (Å)	16.4535(8)	11.1957(6)	13.7027(11)
<i>c</i> (Å)	16.2203(8)	17.5205(8)	19.8752(16)
α (°)	90	90	90
β (°)	95.150(2)	97.530(4)	95.591(4)
γ (°)	90	90	90
<i>Z</i>	4	4	4
calcd density (Mg/m ³)	1.813	1.710	1.652
abs coeff (mm ⁻¹)	5.115	5.249	5.073
<i>F</i> ₀₀₀	1232	1136	1136
	Data Collection and Refinement		
No. of measd reflns: total	21710	29440	20920
No. of measd reflns: unique	6380	7395	5101
Final <i>R</i> Indices ^a	R1 = 0.0262, wR2 = 0.0562	R1 = 0.0323, wR2 = 0.0508	R1 = 0.0337, wR2 = 0.0745
Goodness-of-fit on <i>F</i> ^{2 b}	1.041	0.997	1.030
Largest diff. peak and hole (e ⁻ Å ⁻³)	2.007 and -1.434	1.156 and -1.394	3.003 and -0.958

^a R1 on *F* = $\Sigma |(|F_o| - |F_c|)| / \Sigma |F_o|$; wR2 = $[\Sigma (F_o^2 - F_c^2)^2 / \Sigma w(F_o^2)^2]^{1/2}$; *w* = $[\sigma^2 F_o^2]^{-1}$; ^b GOF = $[\Sigma (w (|F_o| - |F_c|)^2) / \text{degrees of freedom}]^{1/2}$.